SHAPE AND TOPOLOGY OPTIMIZATION OF INERTIAL AMPLIFICATION INDUCED PHONONIC BAND GAP STRUCTURES

by

Osman Yüksel

B.S., Chemical Engineering, Boğaziçi University, 2008

M.S., Mechanical Engineering, Boğaziçi University, 2012

Submitted to the Institute for Graduate Studies in
Science and Engineering in partial fulfillment of
the requirements for the degree of
Doctor of Philosophy

Graduate Program in Mechanical Engineering

Boğaziçi University

2018

SHAPE AND TOPOLOGY OPTIMIZATION OF INERTIAL AMPLIFICATION INDUCED PHONONIC BAND GAP STRUCTURES

APPROVED BY:

Assoc. Prof. Çetin Yılmaz (Thesis Supervisor)	.....
Prof. Fazıl Önder Sönmez	.....
Assoc. Prof. Serdar Soyöz	.....
Assoc. Prof. Güllü Kızıltaş Şendur	.....
Assist. Prof. Polat Şendur	.....

DATE OF APPROVAL: 3.1.2018

ACKNOWLEDGEMENTS

Above all, I would like to present my great gratitude to my thesis supervisor Assoc. Prof. Çetin Yılmaz for his enthusiastic effort and guidance during this study. He is an excellent scientist, inventor, mentor and employer.

I would like to thank to my thesis monitoring committee members Prof. Fazıl Önder Sönmez and Assoc. Prof. Serdar Soyöz for their precious comments on my progress reports.

I would like to thank to Assoc. Prof. Güllü Kızıltaş Şendur and Assist. Prof. Polat Şendur for their participation in my thesis jury.

I also would like to thank to the colleagues, the professors and the administration of the Department of Mechanical Engineering of Boğaziçi University. It was a great honour to be a part and an employee of this mighty institution.

Finally, I would like to thank to my family for their support.

This work was supported by TÜBİTAK Grant No. 110M663.

This work was supported by Boğaziçi University Research Grant No. 17A06D2.

ABSTRACT

SHAPE AND TOPOLOGY OPTIMIZATION OF INERTIAL AMPLIFICATION INDUCED PHONONIC BAND GAP STRUCTURES

Inertial amplification is a novel phononic band gap generation method in which wide vibration stop bands can be obtained at low frequency regions. The engineering importance for this novelty comes from the fact that the phononic band gap structures can be utilized as passive vibration isolators for the low frequency range. In this thesis, primarily the research is focused on the improvements achieved on stop band widths and depths via employment of structural optimization tools. To that end, size, shape and topology optimization studies are conducted on a compliant inertial amplification mechanism, then with these compliant unit cell mechanisms, one and two dimensional periodic structures are formed. Consequently, by means of these periodic structures, it is demonstrated that the vibration transmission is inhibited for wide ranges at low frequencies. The work comprises analytical and numerical studies and more importantly experimental validation of the results. Moreover, topology optimization studies performed during the thesis lead to the development of a new fast topology optimization algorithm to obtain structures with maximized fundamental frequency, though this was not originally among the research objectives. Finally, explicit problem formulations and a comprehensive review on topology optimization are also presented.

ÖZET

ATALET ARTIRIMI YÖNTEMİ İLE ELDE EDİLEN FONON BANT ARALIĞI GÖSTEREN YAPILARDAKİ ŞEKİL VE TOPOLOJİ ENİYİLEMESİ ÇALIŞMALARI

Atalet artırımı, düşük frekans bölgelerinde yer alan titreşim durdurma bantlarının elde edilebildiği yeni bir fonon bant aralığı oluşturma yöntemidir. Bu yeniliğin mühendislik uygulamaları açısından önemi, fonon bant aralığı gösteren yapıların, düşük frekans bölgelerinde pasif titreşim yalıtıcıları olarak kullanılabilmesinden kaynaklanmaktadır. Bu tezde araştırma, özellikle yapısal eniyilemeler neticesinde titreşim durdurma bantlarının genişliği ve derinliğinde elde edilen gelişmelere odaklanmıştır. Bu amaçla, esnek bağlantılı bir atalet artırımı mekanizmasında, boyut, şekil ve topoloji eniyilemesi çalışmaları yürütülmüş, ardından, bu esnek bağlantılı birim hücre mekanizmaları ile bir ve iki boyutlu periyodik yapılar oluşturulmuştur. Ardından bu periyodik yapılar vasıtasıyla, düşük frekans bölgelerinde yer alan geniş bant aralıklarında titreşim iletiminin engellendiği gösterilmiştir. Bu eserde, analitik ve sayısal çalışmalar sunulmuş, daha da önemlisi, elde edilen sonuçların deneysel doğrulaması gerçekleştirilmiştir. Bunların dışında, başlangıçta araştırma hedefleri arasında olmamasına rağmen, tez süresince gerçekleştirilen topoloji eniyilemesi çalışmaları neticesinde, birinci doğal frekanslarının maksimize edildiği topolojik olarak eniyilenmiş yapıların bulunmasını sağlayan yeni ve hızlı bir algoritma geliştirilmiştir. Son olarak, topoloji eniyilemesi üzerine kapsamlı bir inceleme ve açık problem formulasyonları sunulmuştur.

TABLE OF CONTENTS

ACKNOWLEDGEMENTS . . . iii
ABSTRACT . . . iv
ÖZET . . . v
LIST OF FIGURES . . . ix
LIST OF TABLES . . . xv
LIST OF SYMBOLS . . . xvi
LIST OF ACRONYMS/ABBREVIATIONS . . . xx
1. INTRODUCTION . . . 1
1.1. Phononic Band Gap Structures . . . 1
1.2. Structural Optimization . . . 2
1.3. The Aims of the Current Study . . . 3
2. THE INERTIAL AMPLIFICATION MECHANISM . . . 5
2.1. The Lumped Parameter Model of the Inertial Amplification Mechanism 5
2.2. The Distributed Parameter Model of the Inertial Amplification Mechanism 10
3. SHAPE OPTIMIZATION OF INERTIAL AMPLIFICATION INDUCED PHONONIC BAND GAP STRUCTURES . . . 11
3.1. Building Block Mechanism Design . . . 11
3.1.1. Finite Element Models . . . 11
3.1.2. Size Optimization . . . 11
3.1.3. Shape Optimization . . . 13
3.1.4. Numerical Results . . . 15
3.1.5. Pareto study . . . 20
3.2. Experimental and Numerical Results for the Phononic Band Gap Structure 23
4. AN OVERVIEW ON TOPOLOGY OPTIMIZATION . . . 29
4.1. Topology Optimization Problem . . . 29
4.1.1. Description of Topology . . . 29
4.1.2. Optimization Problem . . . 30
4.1.3. Early Progress . . . 32
4.2. Basic Categories of Modern Topology Optimization Methods . . . 33

4.2.1. Homogenization Methods 33
4.2.2. Density Methods 35
4.2.3. Discrete Methods 35
4.2.4. Boundary Variation Methods 37
4.3. The Topology Optimization Technique of Choice: SIMP Method 38
4.3.1. Microstructure Description 39
4.3.2. Problem Regularization 41
4.3.3. Merits of the SIMP Method 44
5. TOPOLOGY OPTIMIZATION PROBLEM FORMULATIONS 46
5.1. Stiffness Maximization 46
5.2. Natural Frequency Maximization 53
5.3. Frequency Gap Maximization 63
6. TOPOLOGY OPTIMIZATION OF INERTIAL AMPLIFICATION INDUCED PHONONIC BAND GAP STRUCTURES 68
6.1. Structural Optimization Problems 68
6.1.1. Size Optimization Problem 70
6.1.2. Topology Optimization Problem 71
6.2. Numerical Results 73
6.2.1. The Size Optimized Mechanism 73
6.2.2. The Topologically Optimized Mechanism 76
6.2.3. The Influence of Topology Optimization Design Space Volume Fraction on Band Gap Limits 80
7. A NOVEL EFFICIENT TOPOLOGY OPTIMIZATION ALGORITHM FOR FUNDAMENTAL FREQUENCY MAXIMIZATION 85
7.1. The Motivation 85
7.2. The Proposed Method 87
7.2.1. Symmetric Boundary Conditions 92
7.2.2. Asymmetric Boundary Conditions 92
7.3. The Hybrid Method 94
7.4. Numerical Results 95
7.4.1. The Benchmark Problems for Numerical Verification 97

7.4.1.1. Simply Supported Beam 97
7.4.1.2. Fixed-Pinned Beam 104
7.4.1.3. Cantilever Beam 106
7.4.2. Comparison of Design-Dependent Inertial Loading and Fixed Inertial Loading 108
8. NOTES ON TOPOLOGY OPTIMIZATION STUDIES 111
9. CONCLUSIONS 114
REFERENCES 117

LIST OF FIGURES

Figure 2.1. The lumped parameter inertial amplification mechanism. 5

Figure 2.2. Stop band depth and width on a transmissibility plot. 9

Figure 2.3. The distributed parameter inertial amplification mechanism. . . . 10

Figure 3.1. The size optimization problem. 13

Figure 3.2. The shape optimization problem. 14

Figure 3.3. Equilateral triangle unit cell block of the two-dimensional periodic structure. 15

Figure 3.4. (a) Size optimized building block mechanism. (b) Shape optimized building block mechanism. 16

Figure 3.5. First three mode shapes of the (a) size optimized building block mechanism, (b) shape optimized building block mechanism. 16

Figure 3.6. Acceleration transmissibility plots of size and shape optimized building block mechanism designs. 17

Figure 3.7. Acceleration transmissibility plots of one-dimensional finite arrays of shape optimized building block mechanisms. 18

Figure 3.8. Band structure of the shape optimized building block mechanism. 19

Figure 3.9. Shell element model of the shape optimized building block mechanism. 20

Figure 3.10. First two modes of the shell element model of the shape optimized building block mechanism. (a) The first mode (255.7 Hz) (b) The second mode (817.4 Hz). 20

Figure 3.11. Comparison of acceleration transmissibilities of one-dimensional offset beam element and shell element shape optimized building block mechanisms. 21

Figure 3.12. Band width versus band depth of optimized mechanism designs. . 22

Figure 3.13. ω_2/ω_1 ratio versus band depth of optimized mechanism designs. . 22

Figure 3.14. Two-dimensional phononic band gap structure. 23

Figure 3.15. 29th mode shape of the phononic band gap structure (264.5 Hz). . 24

Figure 3.16. 30th mode shape of the phononic band gap structure (829.5 Hz). . 24

Figure 3.17. Manufactured phononic band gap structure. 25

Figure 3.18. Experimental setup. 25

Figure 3.19. Experimental and numerical acceleration transmissibility plots of the phononic band gap structure for the longitudinal direction. . . 26

Figure 3.20. Experimental acceleration transmissibility plots of the phononic band gap structure for longitudinal and transverse directions. . . . 27

Figure 3.21. Experimental acceleration transmissibility plots of the phononic band gap structure for longitudinal and out-of-plane directions. . . 27

Figure 4.1. (a) Topologically equivalent domains. (b) Topological classes of simply, two-fold, three-fold connected domains. 30

Figure 4.2. Effect of penalization on an element's relative stiffness vs density values in the SIMP material model for different penalty numbers. . 40

Figure 4.3. (a) Topology optimization problem. (b) Checkerboard pattern formation when filtering is not employed. (c) Optimized design via filter employment. 42

Figure 6.1. Finite element design space dimensions used in structural optimization studies. 69

Figure 6.2. One quarter of the distributed parameter inertial amplification mechanism. 70

Figure 6.3. Topology optimization design space. 72

Figure 6.4. The size optimized inertial amplification mechanism. 74

Figure 6.5. The first three mode shapes of the size optimized inertial amplification mechanism. 74

Figure 6.6. One dimensional periodic structure that consists of three size optimized inertial amplification mechanisms. 75

Figure 6.7. Vibration transmissibility of periodic structures consisting of several number of size optimized unit cells. 75

Figure 6.8. Band structure of the infinitely periodic size optimized unit cells. . 76

Figure 6.9. The topologically optimized inertial amplification mechanism. . . . 77

Figure 6.10. The first three mode shapes of the topologically optimized inertial amplification mechanism. 78

Figure 6.11. One dimensional periodic structure that consists of three topologically optimized inertial amplification mechanisms. 79

Figure 6.12. Vibration transmissibility of periodic structures consisting of several number of topologically optimized unit cells. 80

Figure 6.13. Band structure of the infinitely periodic topologically optimized unit cells. 81

Figure 6.14. f_2/f_1 ratio vs active volume fraction graph. 82

Figure 6.15. Band gap limits vs active volume fraction graph. 83

Figure 7.1. The flowchart of the proposed method. 93

Figure 7.2. Topology optimization design spaces with symmetric and asymmetric boundary conditions. (a) Fixed-fixed beam, (b) Simply supported beam, (c) Fixed-pinned beam. 94

Figure 7.3. The flowchart of the hybrid method. 96

Figure 7.4. Topology optimization design space of the cantilever beam that has a concentrated mass in the middle of the right end. 97

Figure 7.5. Static topology optimization problem of simply supported beam with a point load in the middle. 98

Figure 7.6. Topologically optimized simply supported beam whose stiffness is maximized for a point load applied at the middle of the structure. 99

Figure 7.7. Topologically optimized simply supported beam whose first natural frequency is maximized by the proposed method. 100

Figure 7.8. Topologically optimized simply supported beam whose first natural frequency is maximized by using the dynamic code. 100

Figure 7.9. Convergence history of the topology optimized simply supported design whose first natural frequency is maximized by using the dynamic code. 101

Figure 7.10. Topologically optimized simply supported beam whose first natural frequency is maximized by using the hybrid method. 103

Figure 7.11. Static topology optimization problem of fixed-pinned beam with a point load at the maximum deflection node of the first eigenvector of the structure that consists of fully solid finite elements. 105

Figure 7.12. Topologically optimized fixed-pinned beam whose stiffness is maximized for a point load applied at the node, which has the maximum deflection according to the first eigenvector of the fully solid beam. 105

Figure 7.13. Topologically optimized beam with fixed-pinned ends whose first natural frequency is maximized by the proposed method. 106

Figure 7.14. Static topology optimization problem of cantilever beam with a point load applied at the middle of the right edge. 107

Figure 7.15. Topologically optimized cantilever beam whose stiffness is maximized for a point load applied at the middle of the right edge. . . . 107

Figure 7.16. Topologically optimized cantilever beam whose first natural frequency is maximized by the proposed method. 107

Figure 7.17. Static topology optimization problem of fixed-fixed beam with a point load in the middle. 109

Figure 7.18. Topologically optimized fixed-fixed beam whose stiffness is maximized for a point load applied at the middle of the structure. 109

Figure 7.19. Topologically optimized beam with fixed-fixed ends whose first natural frequency is maximized under constant inertial loading. . . . 110

Figure 7.20. Topologically optimized beam with fixed-fixed ends whose first natural frequency is maximized under design-dependent inertial loads as suggested in the proposed method. 110

LIST OF TABLES

Table 3.1. Comparison of size and shape optimized building block mechanism designs. 17

Table 6.1. Isotropic material properties used in the numerical studies. 73

Table 6.2. Fixed beam parameters used in the numerical studies. 73

Table 6.3. Comparison of band gap limits of size and topologically optimized mechanisms which have the same mass. 79

Table 7.1. Run time comparison of the proposed method and standard dynamic topology optimization code results obtained for the problem in which simply supported beam's first natural frequency is maximized. 102

Table 7.2. Run time for the hybrid method result in which simply supported beam's first natural frequency is maximized. 103

Table 7.3. First natural frequency comparisons of the beams found in the literature, which have the same topology with the beam obtained by the proposed method. 104

LIST OF SYMBOLS

a	The volume fraction of the topology optimization design space
B_e	The parameter of the element e calculated for the optimality criteria update
BD	Stop band depth
BW	Stop band width
$c(\boldsymbol{x})$	The compliance value
c_a,c_b	The eigenvectors of the sub eigenvalue-eigenvector problem encountered in double eigenvalue issue in topology optimization
d	The mass penalization parameter for the SIMP method
E_0	The elastic modulus of the solid isotropic material
E_e	eth microstructure's (element's) elastic modulus in the SIMP method
E_{min}	The very small stiffness value to prevent stiffness matrix to become singular in modified-SIMP method
$\boldsymbol{f}$	The global load vector
$\boldsymbol{f_d}$	The inertial load vector defined in The Proposed Method in Section 7.2
$\boldsymbol{f_s}$	The static load vector
f_1,f_2,f_3	The first, the second and the third natural frequencies of the inertial amplification mechanism, respectively, in Hz
g_a,g_b	The design sensitivities for the double eigenfrequency
g_{ij}	The ijth generalized gradient for double eigenvalue where $i = 1, 2$ and $j = 1, 2$
G_j	The jth constraint in topology optimization problem
H	The objective function of the topology optimization problem
H_1	H_1 estimate of the experimental frequency response function
$H(o_i)$	The weighing function for sensitivity filtering
k	The spring stiffness of the lumped parameter inertial amplification mechanism

k_{static}	The static stiffness constraint in optimizations
$\boldsymbol{K}$	The global stiffness matrix
$\boldsymbol{K_0}$	The stiffness matrix of an element for unit Young's modulus
KE	The total kinetic energy of the system
L	The Lagrange function for equation of motion
$\mathcal{L}$	The Lagrangian for the optimization problem
l_i	The length of the ith beam of the distributed parameter inertial amplification mechanism
m	The big mass of the lumped parameter inertial amplification mechanism
$\boldsymbol{M}$	The global mass matrix
$\boldsymbol{M_0}$	The mass matrix of an element for unit density
m_a	The small mass of the lumped parameter inertial amplification mechanism
m_d	The dynamic mass of the lumped parameter inertial amplification mechanism
m_s	The static mass of the lumped parameter inertial amplification mechanism
ml	The move limit of a design variable for the optimality criteria update scheme
N	The total number of design variables (structural members) in the topology optimization problem
N_e	The neighbourhood of element e in sensitivity filtering
$nelx$	The total number of finite elements in the horizontal axis in topology optimization design domain
$nely$	The total number of finite elements in the vertical axis in topology optimization design domain
o_i	The center location of element i in sensitivity filtering
p	The stiffness penalization parameter for the SIMP method
P	The total number of constraints in the topology optimization problem
PE	The total potential energy of the system
R	The sensitivity filter radius
$\mathbb{R}^n$	The real coordinate space of n dimensions

$\boldsymbol{s_\gamma}$	The mass normalized global eigenvector for the γth mode
$\boldsymbol{s_e}$	The eth element's contribution to the mass normalized global eigenvector $\boldsymbol{s_\gamma}$
t_i	The thickness of the ith beam of the distributed parameter inertial amplification mechanism
TR	Displacement or acceleration transmissibility
$\boldsymbol{u}$	The state field in topology optimization problem (Depending on the problem type, it can be the global displacement or mode shape vector)
$\boldsymbol{u_d}$	The eigenvector estimate vector defined in The Proposed Method in Section 7.2
$\boldsymbol{u_e}$	Depending on the problem type, the displacement or the mode shape vector of element e
$\boldsymbol{u_n}$	The nodal displacement vector for an eigenvalue problem
$\boldsymbol{u_s}$	The static displacement vector
$\boldsymbol{u_\gamma}$	γth mode shape vector
$\boldsymbol{u_1}$,$\boldsymbol{u_2}$	The first and the second mode shape vectors of the distributed parameter inertial amplification mechanism, respectively
V	The total solid volume of the structure in topology optimization
V_0	The total volume of the topology optimization design domain
$\boldsymbol{v_i}$	The ith mass normalized eigenvector of double eigenfrequency where $i = 1, 2$
x	The output displacement
$\boldsymbol{x}$	The design variable vector in topology optimization problem
x_e	The eth structural member (i.e., eth microstructure's density, or eth element's density) that constitutes the design variable vector $\boldsymbol{x}$
y	The input displacement
z	The iteration number of the optimality criteria update scheme
η	The numerical damping coefficient to stabilize the optimality criteria method iterations

θ	The acute angle between the rigid link that connects m and m_a with the spring that binds the masses m in the lumped parameter inertial amplification mechanism
λ, λ_0	The Lagrange multiplier for the mass constraint in topology optimization problem
$\boldsymbol{\lambda_i}$	The Lagrange multiplier vector for the ith constraint in topology optimization problem
ν	The Poisson's ratio of the isotropic material
ρ_0	The density of the solid isotropic material
ρ_e	The physical density of element e in the SIMP method
ρ_{min}	The very small density value to prevent mass matrix to become singular in modified-SIMP method
ω	The natural frequency in rad/s
ω_e	The excitation frequency for transmissibility calculations
ω_s	The starting frequency of the band gap in rad/s
ω_{z1}	The first antiresonance frequency of the inertial amplification mechanism in rad/s
ω_γ	γth natural frequency of the structure, in rad/s
ω_1,ω_2	The first and the second natural frequencies of a system, respectively, in rad/s

LIST OF ACRONYMS/ABBREVIATIONS

2-D	Two Dimensional
ASME	The American Society of Mechanical Engineers
BC	Boundary Condition
BESO	Bi-directional Evolutionary Structural Optimization
DOF	Degree of Freedom
EDM	Electrical Discharge Machining
ESO	Evolutionary Structural Optimization
FEA	Finite Element Analysis
FRF	Frequency Response Function
MAC	Modal Assurance Criterion
MMA	Method of Moving Asymptotes
OC	Optimality Criteria
RAM	Random Access Memory
SDOF	Single Degree of Freedom
SIMP	Solid Isotropic Microstructure (Material) with Penalization

1. INTRODUCTION

1.1. Phononic Band Gap Structures

Wave propagation in periodic structures has long been studied in the literature [1]. Mechanical waves are classified with respect to the medium in which they propagate. Mechanical waves which pass through fluids are called acoustic waves. If mechanical waves pass through a solid then they are called elastic waves. Phonons are quantized vibrational modes (normal modes) of a lattice structure. Phononic crystals are structures with periodic variations of density and/or elastic constants. These alternations due to periodicity cause transmission and reflection of incoming waves. At some specific frequency range, the interference between incoming and reflected waves cancel each other, thus the wave cannot propagate throughout the structure. This specific frequency range in which wave propagation is inhibited is called "phononic band gap". Phononic band gap structures could be used in applications such as; acoustic filters, vibration isolators and acoustic waveguides [2–5]. Therefore, for a vibration control engineer, phononic band gap structures offer the possibility of designing high performance passive vibration isolators.

There are two common methods to generate phononic band gaps: Bragg scattering and resonance scattering (local resonances). Bragg scattering method utilizes periodically varying mass and stiffness properties within the solid structure to generate band gap [6–20]. The second band gap generation method, resonance scattering utilizes periodic local resonators added to the structure to create phononic band gap [21–32]. Furthermore, there also exist hybrid methods that utilize both Bragg scattering and resonance scattering [33–37].

Recently, inertial amplification [38, 39] is introduced as an alternative phononic band gap generation method. In this method, band gap is created by using periodic embedded amplification mechanisms which increase the effective inertia of the system. Inertial amplification method provides wide phononic band gaps at low frequencies

without employing large mass fractions and sacrificing overall stiffness of the structure. This method is first introduced in [38]. In their study, Yilmaz et al. generate wide band gaps at low frequencies by increasing the effective inertia of the system. They use the method to create band gaps in infinite periodic wave propagation media. In a later study [39], this method is used for a finite periodic structure. It is shown that by utilizing reasonable number of unit cells, wide and deep band gaps at low frequencies are acquired as in the infinite periodic case.

The inertial amplification induced gaps are qualitatively different from the two well-known gap types in terms of wave energy localization characteristics or gap depth profiles in frequency response function (FRF) plots [39]. By just increasing the amplification ratio, the band gap frequency range can be reduced without changing the total mass or stiffness of the structure [38]. This is an advantage when the two common phononic band gap generation methods are considered, since, Bragg scattering requires heavy, low stiffness and large size structures and resonance scattering requires heavy resonators to obtain band gaps at low frequencies [38].

1.2. Structural Optimization

Finding the optimum layout defined as a material distribution problem of structures via a pre-determined objective function and constraints is known as structural optimization. Generally, in structural optimization problems, there exists an objective function, design variables and state variables. Objective function mainly defines the aim of the design. It provides a metric by which designers can evaluate different designs. Generally, the purpose of the optimization is to maximize or minimize this metric. Design variables are scalars or vectors which are updated throughout the optimization procedure. Design variables in topology optimization correspond to the geometry of the structure or equivalently material distribution within the structure. On the other hand, state variables are functions or vectors that correspond to the response of the structure such as displacement, stress, strain or force in the case of mechanical structures. [40]

Three types of structural optimization problems are encountered in the literature. The first one, size optimization can be summarized as finding the optimum dimensions of the structures with predetermined shape and topology. Finding optimum cross-sectional areas of truss members or finding optimum thickness distribution in a thin plate can be given as examples [40]. The second type is shape optimization problem. In shape optimization, aim is to find the optimum shape of the structure for which the requirements for constraints and objective function is satisfied. Third and the most general structural optimization problem is the topology optimization. Here, the aim is to find the optimum topology of the structure, for the best objective function value within the constraints. In general, topology optimization problems are presented as, either finding the optimal topology under the constant volume / material constraint, or finding the optimum material distribution in composite structures [41]. In the literature there exist numerous structural optimization studies which aim to enhance vibration and band gap properties of the structures [42–55].

1.3. The Aims of the Current Study

In the literature, there exist miscellaneous studies that show the effectiveness of the inertial amplification method for phononic band gap generation. In these studies, theoretical aspects [38, 39, 56] are investigated, numerical [57–60] and experimental [61–63] verifications are performed on various inertial amplification mechanisms.

Phononic band gap structures are formed by the periodic inclusion of inertial amplification mechanisms [61–63]. The unit cell mechanisms determine the inertial amplification induced band gap properties of periodic structures [61]. At this point, employment of structural optimization tools on the unit cell can enhance band gap properties, such as band width and depth. Size, shape and topology optimization are the means that serve this purpose.

This thesis presents the structural optimization studies performed on the compliant inertial amplification mechanism to generate wide and deep phononic band gaps. The subject is investigated by analytical, numerical and experimental techniques.

Structural optimization studies cover size, shape and topology optimization efforts and their comparisons. A comprehensive review on topology optimization methods and problem formulations are also introduced. Moreover, a novel fast topology optimization algorithm that finds the optimum topologies with maximized fundamental natural frequency is proposed.

In the following, one can find the contributions of this thesis in comparison to the existing works in the literature:

- Although size optimization was considered for various inertial amplification mechanisms before [61–63], shape and topology optimization studies are conducted on inertial amplification mechanisms for the first time with this thesis.
- Compared to the literature [61], as a result of shape and topology optimization studies, wider and deeper vibration stop bands are obtained in this study.
- The two dimensional shape optimized phononic band gap structure manufactured with this study can be utilized as a passive vibration isolator operating at low frequency range.
- While various structures with simpler design spaces were considered in the literature before [51–55], in this thesis, topology optimization is utilized for frequency gap maximization of complex mechanisms.
- In this study, a novel time efficient topology optimization algorithm is proposed to obtain optimized topologies with maximum fundamental natural frequency. The proposed method provides computational efficiency, when traditional fundamental natural frequency maximization procedure [54, 64–80], which involves computationally costly eigenvalue-eigenvector calculations in every iteration step, is considered.

2. THE INERTIAL AMPLIFICATION MECHANISM

In this chapter, the inertial amplification mechanism, for which, size, shape and topology optimization studies are performed, is presented. First, the lumped parameter model, then the distributed parameter model are introduced. In the forthcoming sections, the structural optimization studies are conducted on the distributed parameter inertial amplification mechanism, while utilizing the relevant formulations obtained from the lumped parameter model.

2.1. The Lumped Parameter Model of the Inertial Amplification Mechanism

The lumped parameter inertial amplification mechanism model is provided in Figure 2.1. In this model, the masses m which reside at the two ends of the mechanism are connected to each other by a spring which has a stiffness of k. The mass m_a, which stays in the middle of the model, is connected to the masses m with rigid links. The angle between the rigid links and the spring is denoted with θ. Moreover, y denotes the input displacement whereas x denotes the output displacement.

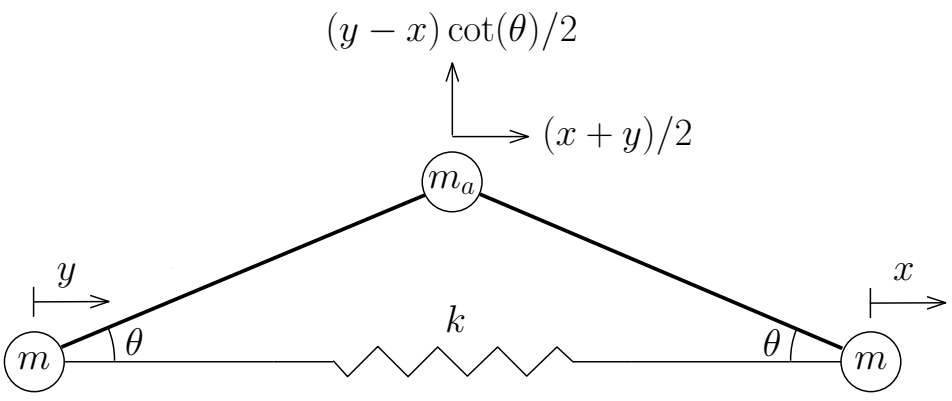


Figure 2.1. The lumped parameter model of the inertial amplification mechanism.

The equation of motion of the mechanism shown in Figure 2.1 can be found by the Lagrange method. To that end, the total kinetic (KE) and the potential (PE)

energies of the system are provided as:

$$KE = \frac{1}{2}m_a\left[\left(\frac{\dot{x}+\dot{y}}{2}\right)^2+\left(\frac{\dot{y}-\dot{x}}{2}\cot\theta\right)^2\right]+\frac{1}{2}m\dot{x}^2+\frac{1}{2}m\dot{y}^2 \tag{2.1}$$

$$PE = \frac{1}{2}k(x-y)^2 \tag{2.2}$$

Using Equations 2.1 and 2.2, the Lagrange function can be defined as:

$$L = KE - PE \tag{2.3}$$

Meanwhile, the Lagrange equation for the x coordinate is:

$$\frac{d}{dt}\left(\frac{\partial L}{\partial \dot{x}}\right)-\frac{\partial L}{\partial x}=0 \tag{2.4}$$

When the Lagrange function obtained in Equation 2.3 is solved for the Equation 2.4, the equation of motion of the lumped parameter inertial amplification mechanism shown in Figure 2.1 is obtained:

$$\left[m_a(cot^2\theta+1)/4+m\right]\ddot{x}+kx=\left[m_a(cot^2\theta-1)/4\right]\ddot{y}+ky \tag{2.5}$$

By using Equation 2.5, the first resonance (ω_1) and antiresonance frequencies (ω_{z1}) are found respectively as:

$$\omega_1=\sqrt{\frac{k}{m_a(cot^2\theta+1)/4+m}} \tag{2.6}$$

$$\omega_{z1} = \sqrt{\frac{k}{m_a(cot^2\theta - 1)/4}} \tag{2.7}$$

The denominator of the Equation 2.6 can be rewritten as the dynamic mass of the structure (m_d) as:

$$m_d = m + \frac{m_a(\cot^2\theta + 1)}{4} \tag{2.8}$$

Then the Equation 2.6 reduces to:

$$\omega_1 = \sqrt{\frac{k}{m_d}} \tag{2.9}$$

Also, it is seen from the Figure 2.1 that the static mass of the structure (m_s) is:

$$m_s = 2m + m_a \tag{2.10}$$

Hence the Equation 2.7 can also be written as:

$$\omega_{z1} = \sqrt{\frac{k}{m_d - m_s/2}} \tag{2.11}$$

Equations 2.9 and 2.11 imply that the lumped parameter system shown in Figure 2.1 is a low pass filter type vibration isolator [81] and its displacement or acceleration transmissibility is given by [81, 82]:

$$TR(\omega_e) = \frac{|x(\omega_e)|}{|y(\omega_e)|} = \frac{|\ddot{x}(\omega_e)|}{|\ddot{y}(\omega_e)|} = \frac{|1 - (\omega_e/\omega_{z1})^2|}{|1 - (\omega_e/\omega_1)^2|} \tag{2.12}$$

where ω_e is the excitation frequency.

Stop bands occur when the transmissibility values given in Equation 2.12 is below 1. Utilizing Equation 2.12, stop band depth (BD) can be defined as [61]:

$$BD = 1 - \frac{\omega_1^2}{\omega_{z1}^2} \tag{2.13}$$

This band depth formulation is utilized in the optimization problems as band depth constraints. The detailed derivation of the Equation 2.13 can be found in [61].

Besides, the band gap starts at the frequency where Equation 2.12 is equal to 1. By equating Equation 2.12 to 1, the lower limit of the band gap (ω_s) can be defined [61]:

$$\omega_s = \sqrt{\frac{2\omega_1^2\omega_{z1}^2}{\omega_1^2 + \omega_{z1}^2}} \tag{2.14}$$

The band gap starts at the frequency ω_s and ends at the frequency ω_2. So, by using this information, the normalized band width can be defined:

$$BW = \frac{\omega_2 - \omega_s}{\sqrt{\omega_2\omega_s}} \tag{2.15}$$

As can be seen from Equations 2.6, 2.7 and 2.14, for small θ values, the effective inertia of the mechanism becomes quite large, thus band gap starting frequency (ω_s) decreases.

In Figure 2.2, stop band depth and width concepts are shown on a transmissibility plot. Here, for a single degree of freedom (SDOF) inertial amplification mechanism, a semi-infinite stop band is achieved, i.e., the stop band starts at the frequency ω_s and continues infinitely without a bound, with a transmissibility value of ω_1^2/ω_{z1}^2 at large frequencies. Whereas for a multi degree of freedom (multi-DOF) system, the stop band is confined between the stop band starting frequency (ω_s) and approximately the second resonance frequency (ω_2) of the structure. Please note that, the stop band

starting frequency (ω_s) can deviate from the first resonance frequency (ω_1) significantly because of the stop band depth achieved (see Equations 2.13 and 2.14). However, for a multi-DOF system, the acceptance of the stop band finishing frequency as the second resonance frequency (ω_2) is a valid assumption. Hence, normalized band width definition provided in Equation 2.15 describes the extent of the stop band in a better way. Nevertheless, for optimization studies in the literature [53, 61], ω_2/ω_1 ratio is utilized to describe the band width, since, when this ratio is maximized the stop band width maximizes, as well.

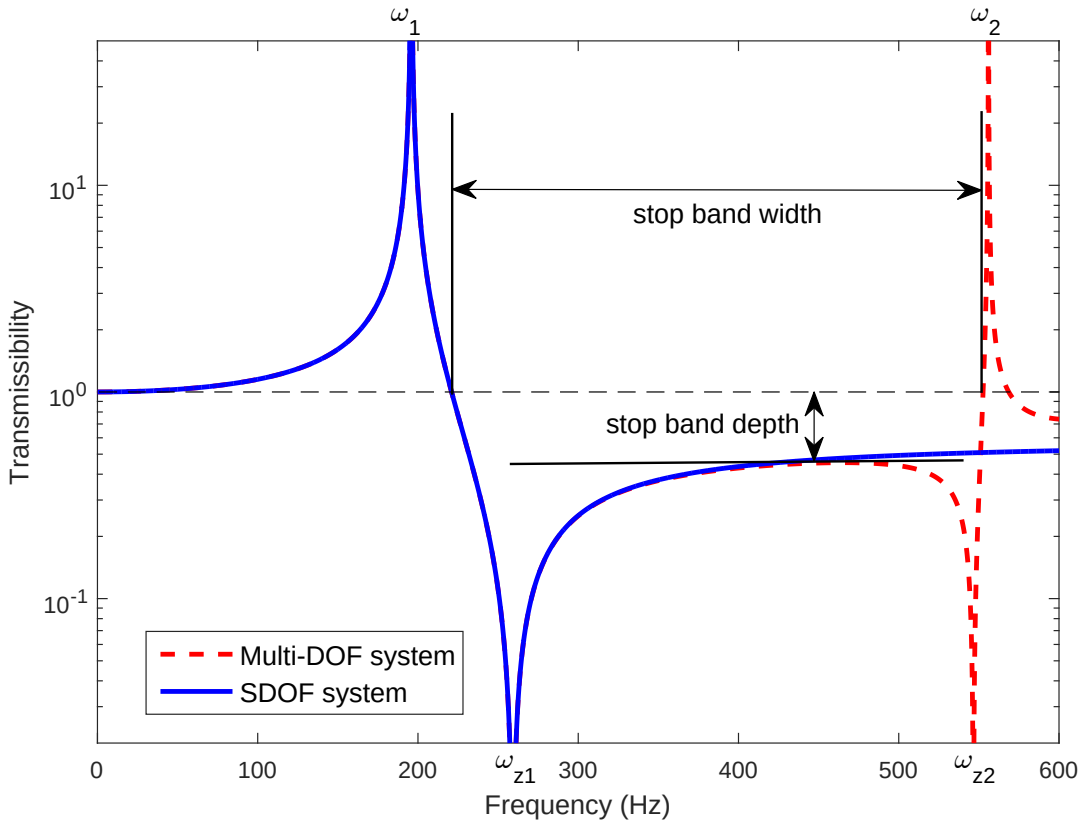


Figure 2.2. Stop band depth and width on a transmissibility plot.

In Figure 2.2, it is seen that stop band depth characteristics of the SDOF system closely resembles the multi-DOF system's. Furthermore, ω_1, ω_{z1} and ω_s frequencies are the same for both of the systems. Therefore, Equations 2.9, 2.11, and 2.13 can be utilized directly for structural optimization studies of distributed parameter inertial

amplification models, which require more involved calculations.

2.2. The Distributed Parameter Model of the Inertial Amplification Mechanism

In Figure 2.3, distributed parameter model of the inertial amplification mechanism is presented. In this two dimensional model; l_1, l_2, l_3 and l_4 denote the corresponding beam lengths, whereas t_1, t_2, t_3 and t_4 denote the corresponding beam thickness values. Inertial amplification is achieved due to flexing of the thin compliant hinges numbered as 2 and 4. Size, shape and topology optimization studies are conducted on the mechanism shown in Figure 2.3.

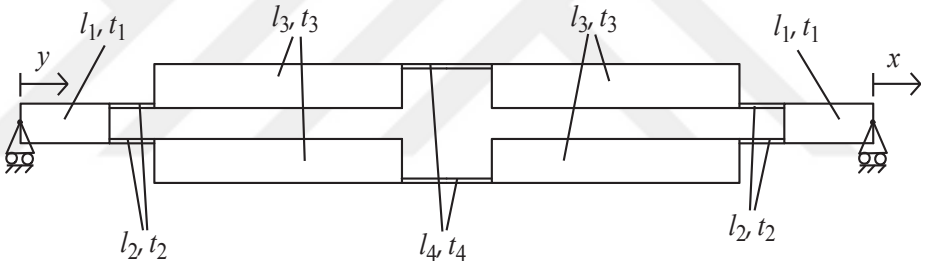


Figure 2.3. The distributed parameter model of the inertial amplification mechanism.

3. SHAPE OPTIMIZATION OF INERTIAL AMPLIFICATION INDUCED PHONONIC BAND GAP STRUCTURES

In this chapter, shape optimization is utilized in two-dimensional distributed parameter systems to generate wider and deeper phononic gaps than that can be obtained by size optimization. By using a finite element model with shell elements, the numerical frequency response of the shape optimized phononic band gap structure with embedded inertial amplification mechanisms is obtained. Moreover, this two-dimensional periodic structure is manufactured and experimental validation of computational results is done.

3.1. Building Block Mechanism Design

3.1.1. Finite Element Models

Size and shape optimization studies are performed on the distributed parameter model of the inertial amplification mechanism seen in Figure 2.3.

In order to perform optimizations, a finite element model of this mechanism is constructed by using one dimensional offset beam elements [83]. After optimization procedure, band gap performances of the resulting designs are validated using a second finite element model based on shell elements [84].

3.1.2. Size Optimization

Size optimization is performed on the compliant mechanism shown in Figure 2.3. The vibration stop band occurs between the first and the second natural frequencies for this inertial amplification mechanism [61]. The aim of the optimization is to achieve vibration isolation for the widest frequency band possible at low frequency region.

Therefore, the objective chosen is the maximization of the ω_2/ω_1 ratio.

In order to obtain a stop band at low frequencies, the the first natural frequency (ω_1), thus overall stiffness of the structure should be decreased. This can be achieved by decreasing thicknesses (t_2 and t_4) or increasing lengths (l_2 and l_4) of thin compliant hinges. The thickness values should be determined by taking into account the manufacturability of design. The phononic band gap structure will be manufactured from a steel plate by wire-EDM (Electrical Discharge Machining) technique. Consequently, the thickness values for t_2 and t_4 are determined as 0.5 mm, which is the smallest thickness that can be produced accurately. On the other hand, increasing the length of thin hinges results in excessive stress formation under bending, in addition to decreased vibration stop band width [61]. To that end, l_2/t_2 ratio is selected as 5 [61]. Besides, in the first mode, the hinges enumerated as 4 bend twice in proportion to the hinges enumerated as 2. Therefore, in order to obtain the same amount of stress in thin compliant hinges, l_4 is selected as twice of l_2 [61].

Phononic band gap structures will be formed by periodically incorporating designed compliant inertial amplification mechanisms. These mechanisms will be merged into each other at beams enumerated as 1. Previously, it was shown that, decreasing length of these beams results in increased stop band width [61]. However, since the manufactured periodic structure will be tested, small length values taken for these beams make it difficult to attach accelerometers and shakers to the structure. Thus, length l_1 is chosen as 10 mm.

The overall stiffness of the structure given in Figure 2.3 can become quite small if t_3 takes large values during the optimization process [61]. In order to prevent this, a static stiffness constraint of 1000 kN/m is taken. At the moment, it should be emphasized that, the rationale mentioned so far about determining the objective function, the constraints and the fixed variables is also valid for shape optimization problem formulation.

Finally, a band depth constraint is given with a value of 0.2, meaning that 20% vibration isolation will be achieved with the optimized mechanism. Consequently, the design variables of the size optimization problem are determined as t_1, l_3 and t_3. The size optimization problem is summarized in Figure 3.1.

Maximize:	ω_2/ω_1
Subject to:	k_{static} = 1000 kN/m
	BD = 0.20
Fixed variables:	$t_2 = t_4$ = 0.5 mm
	$2l_2 = l_4$ = 5 mm
	l_1 = 10 mm
Design variables:	t_1, l_3, t_3

Figure 3.1. The size optimization problem.

As a result of optimization procedure, the design variables are found as follows: $t_1 = 4.1$ mm, $l_3 = 31.9$ mm and $t_3 = 6.3$ mm, as can be seen in Figure 3.4(a). Moreover, the maximum value of ω_2/ω_1 is obtained as 2.79.

3.1.3. Shape Optimization

In order to improve band gap characteristics, more specifically, to widen and deepen the band gap, shape optimization is performed on the mechanism shown in Figure 2.3. The beam with length l_3 is divided into 30 pieces and these pieces are allowed to take different thickness values independent of each other. The same objective function as in the size optimization problem (i.e., maximization of the ω_2/ω_1 ratio) is selected. The same static stiffness constraint as in the size optimization problem (i.e., static stiffness is selected as 1000 kN/m) is also set. Moreover, size optimized mechanism's mass is given as a mass constraint for the shape optimization problem.

As a result of these choices, one can compare the size and shape optimized mechanism with each other since both designs will have the same mass and static stiffness values. In addition, a more challenging band depth constraint is also given ($BD = 0.25$). It is noted that shape optimized mechanism will be used as the building block of the unit cell of the two dimensional phononic band gap structure shown in Figure 3.3. As can be seen from Figure 3.3, in order to prevent touching of the beams with length l_3 to each other an angle constraint should be used. Also, fixed variables are the same as in the size optimized mechanism. Design variables are also the same with the size optimization problem except that the beam with length l_3 is divided into 30 pieces. The summary of the shape optimization problem is given in Figure 3.2.

Maximize:	ω_2/ω_1
Subject to:	k_{static} = 1000 kN/m
	BD = 0.25
	$m_{(shape\ opt.)} = m_{(size\ opt.)}$
	(Upper limit constraint for the 30 thickness values of the segments that form the beam with length l_3 as shown in Figure 3.3)
Fixed variables:	$t_2 = t_4$ = 0.5 mm
	$2l_2 = l_4$ = 5 mm
	l_1 = 10 mm
Design variables:	t_1, l_3 and 30 thickness values of the segments that form the beam with length l_3

Figure 3.2. The shape optimization problem.

As the result of the shape optimization, the thickness t_1 is found as 5.9 mm, the length l_3 is found as 22.4 mm and the resulting thicknesses of the 30 segments of the beam with length l_3 are shown in Figure 3.4(b). Moreover, the maximum value of ω_2/ω_1 is obtained as 3.32.

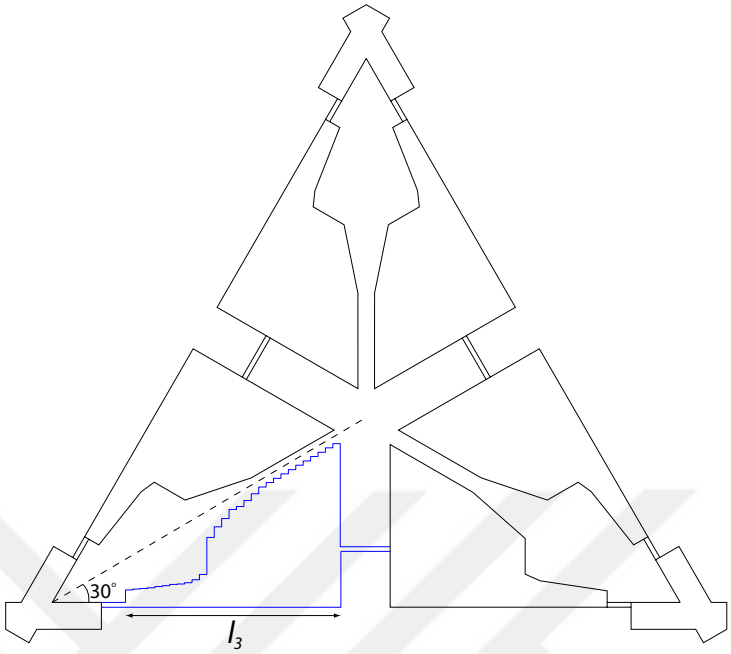


Figure 3.3. Equilateral triangle unit cell block of the two-dimensional periodic structure. The dashed line shows the upper limit constraint for the thicknesses of the 30 segments of the beam with length l_3.

3.1.4. Numerical Results

In Figure 3.4, size and shape optimized mechanisms are shown together to better visualize the relative dimensions of the mechanisms. In Figure 3.5, the first three mode shapes of size and shape optimized building block mechanisms are given. As expected, both designs' first three mode shapes are the same.

In Table 3.1 for comparison purposes, results of size and shape optimized building block mechanisms are listed. It can be seen that, shape optimization provides wider and deeper band gap for the same mass and the static stiffness values.

In Figure 3.6 acceleration transmissibility plots of size and shape optimized designs are given. Results show that shape optimization results in better band gap properties (i.e., wider and deeper band gap).

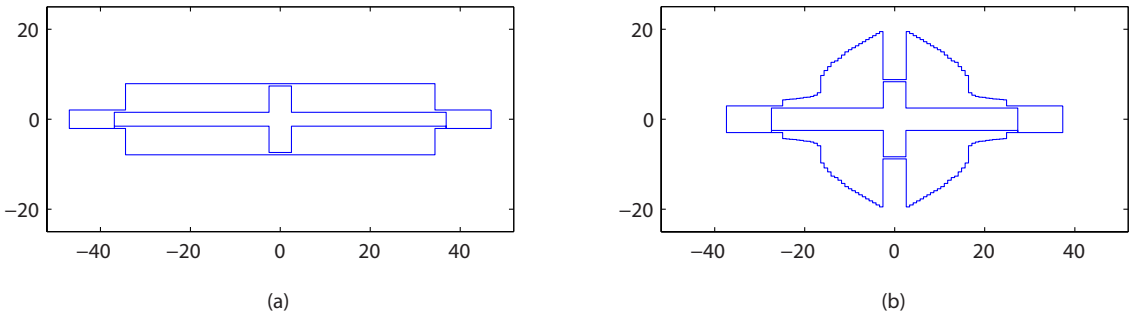


Figure 3.4. (a) Size optimized building block mechanism ($\omega_2/\omega_1 = 2.79$, $BD = 0.20$). (b) Shape optimized building block mechanism ($\omega_2/\omega_1 = 3.32$, $BD = 0.25$).

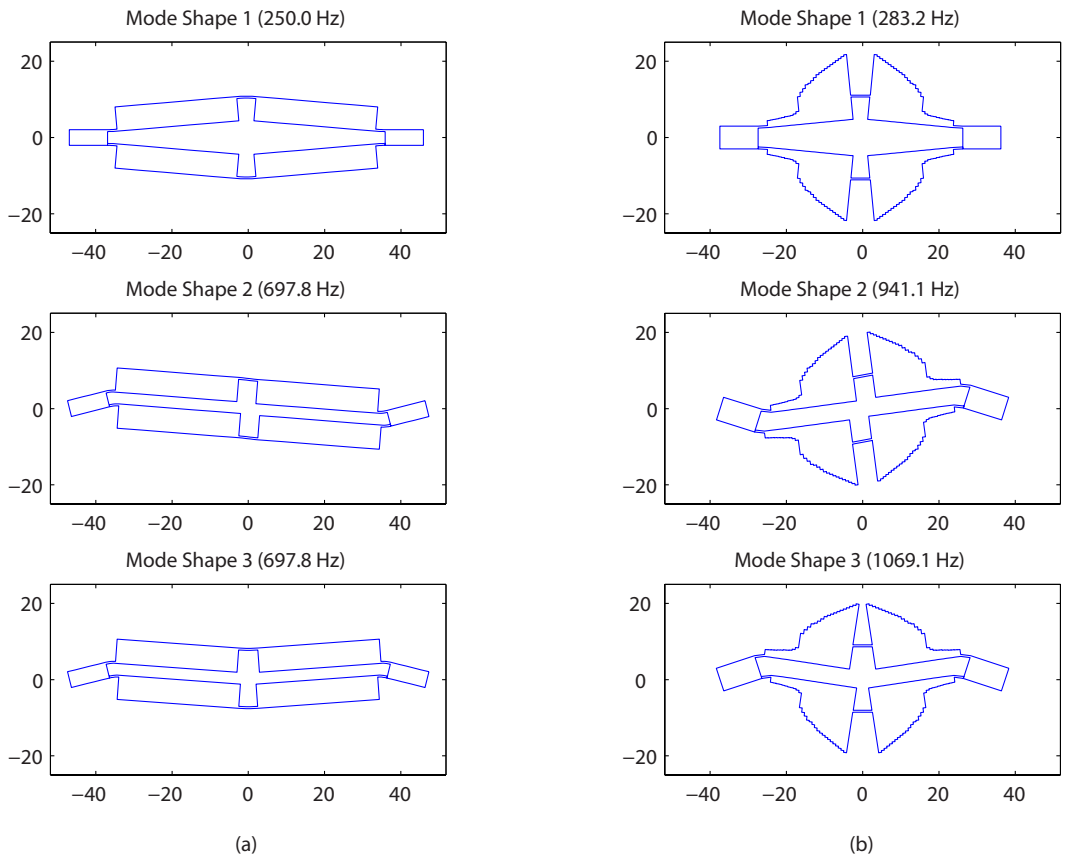


Figure 3.5. First three mode shapes of the (a) size optimized building block mechanism, (b) shape optimized building block mechanism.

Table 3.1. Comparison of size and shape optimized building block mechanism designs.

	Size optimized design	Shape optimized design
ω_2/ω_1 ratio	2.79	3.32
Band depth (BD)	0.20	0.25
Mass	0.143 kg	0.143 kg
Stiffness	1000 kN/m	1000 kN/m

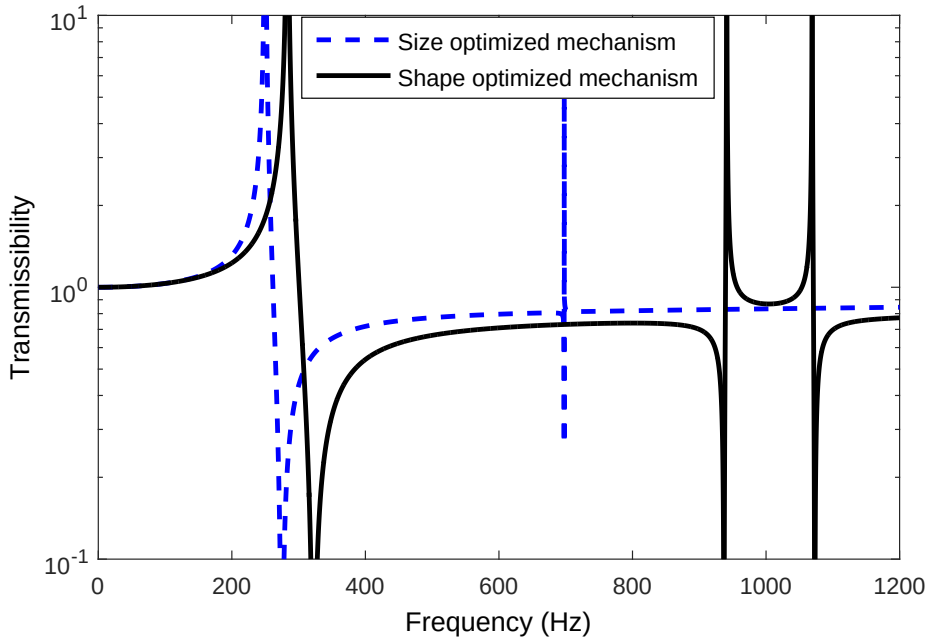


Figure 3.6. Acceleration transmissibility plots of size and shape optimized building block mechanism designs.

A phononic band gap structure comprises periodic involvement of this building block mechanism. In order to see the phononic band gap characteristic of the finite number of shape optimized building block designs, acceleration transmissibility of one-dimensional finite arrays of shape optimized designs are considered in Figure 3.7. As can be seen, band gaps start and end at the same frequencies for all of the three

finite arrays. Yet, band depth characteristics differ such that; array of 2 mechanisms' band depth is 0.61, array of 4 mechanisms' band depth is more than 0.91, and array of 6 mechanisms' band depth is more than 0.98. In other words, just by using 6 mechanisms in one dimensional finite periodic structure, less than 2% of input vibration is transmitted to the other end.

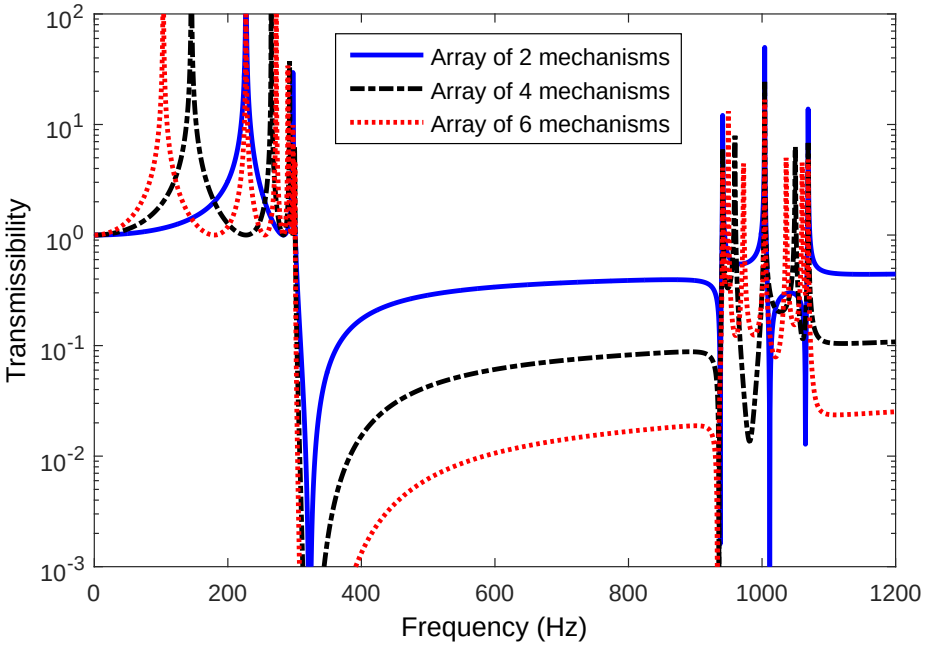


Figure 3.7. Acceleration transmissibility plots of one-dimensional finite arrays of shape optimized building block mechanisms.

In Figure 3.8 band structure of the shape optimized building block mechanism is shown. Referring to this figure, band gap starts at 300.9 Hz and ends at 941.1 Hz. Band gap starting frequency is validated using Equation 2.14 as 300.9 Hz. The formulations given for lumped parameter model works well for the distributed parameter model (Equations 2.13 and 2.14). It can also be observed from Figures 3.7 and 3.8 that the band widths for the finite and infinite periodic one dimensional arrays coincide.

A second finite element model is constructed using shell elements as shown in Figure 3.9. In this model, beams with length l_3 are smoothed for manufacturing pur-

poses. Shell thickness of this model is selected as 55 mm. This choice will be clarified in Section 3.2, which prevents the out-of-plane modes of the two dimensional phononic band gap structure that uses this unit cell mechanism. Poisson ratio is selected as 0.29 for this model. In Figure 3.10 first two mode shapes of this shell element model is shown.

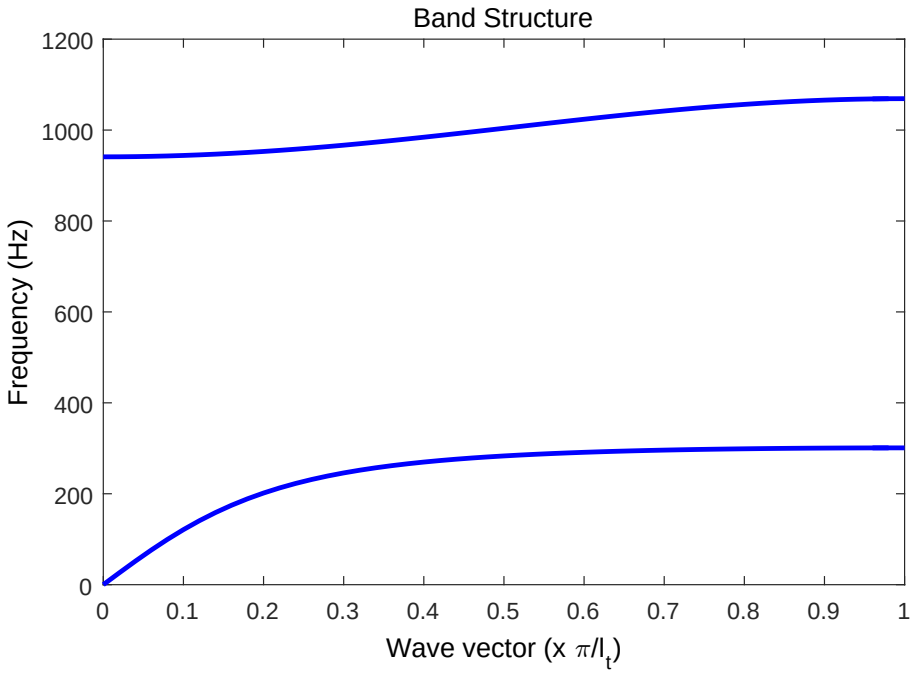


Figure 3.8. Band structure of the shape optimized building block mechanism. Here, l_t represents length of the mechanism.

In order to check the validity of one dimensional shape optimized model, acceleration transmissibilities of one dimensional offset beam element model and shell element models are compared in Figure 3.11. As can be seen, similar band gap characteristics are observed. Band depth is nearly the same (0.25 for the beam element model, 0.24 for the shell element model). On the other hand, band width differs by 3.6% (300.9 Hz - 941.1 Hz giving $\omega_2/\omega_1 = 3.32$ for the beam element model, 271.8 Hz - 817.4 Hz giving $\omega_2/\omega_1 = 3.20$ for the shell element model). These differences stem from element type change and partly due to smoothing of the one dimensional structure. Yet, optimization procedure utilizing one dimensional finite element model is proved to be efficient to

obtain wide and deep band gaps, so that computationally costly shell element models are avoided.

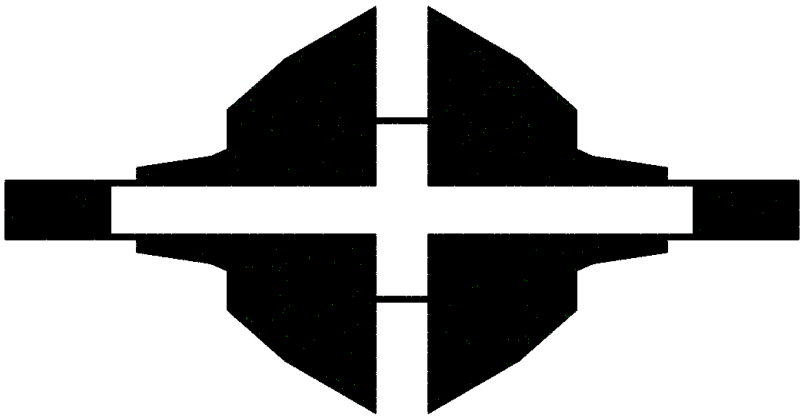
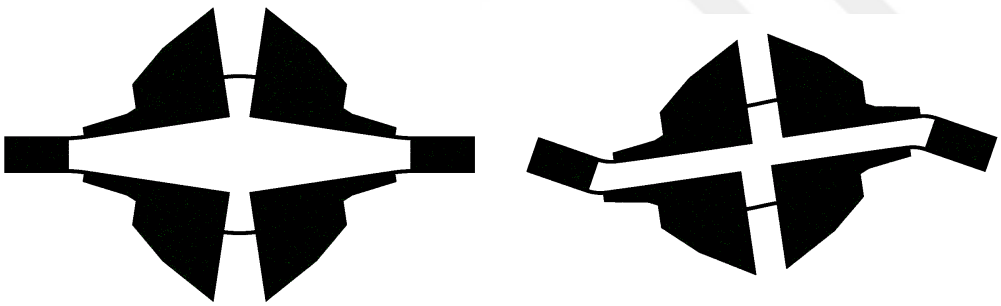


Figure 3.9. Shell element model of the shape optimized building block mechanism.



(a) (b)

Figure 3.10. First two modes of the shell element model of the shape optimized building block mechanism. (a) The first mode (255.7 Hz) (b) The second mode (817.4 Hz).

3.1.5. Pareto study

In order to observe superiority of shape optimization over size optimization, Pareto studies are conducted. In these studies, static stiffness of the mechanisms are taken as 1000 kN/m and mass of the mechanisms are taken as 0.143 kg, which ultimately result in fair comparisons (see Table 3.1).

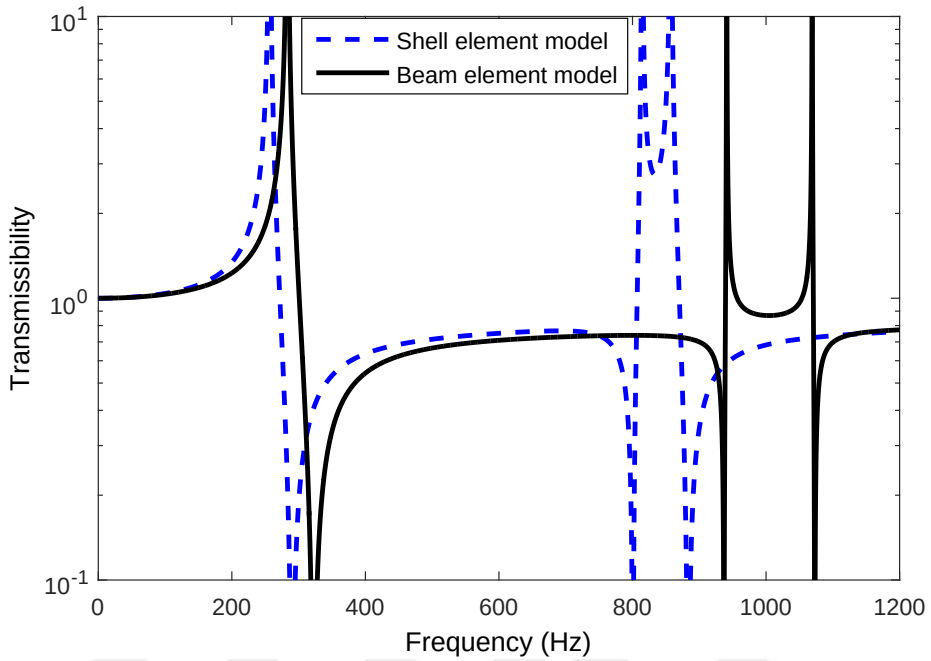


Figure 3.11. Comparison of acceleration transmissibilities of one-dimensional offset beam element and shell element shape optimized building block mechanisms.

In the first Pareto study, normalized band width (Equation 2.15) and band depth (Equation 2.13) relationship is studied. It can be clearly seen from Figure 3.12 that shape optimization provides wider and deeper designs than size optimization. It is also observed from this figure that band width and band depth are inversely proportional.

In the second Pareto study, the relationship of ω_2/ω_1 ratio and band depth (Equation 2.13) is studied (see Figure 3.13). Again, shape optimization offers wider and deeper designs than size optimization. It is also seen that there is an inverse proportional relationship between ω_2/ω_1 ratio and band depth, as expected. To conclude, Pareto study results shown in Figures 3.12 and 3.13 indicate that, shape optimization widens and deepens the band gaps more than size optimization.

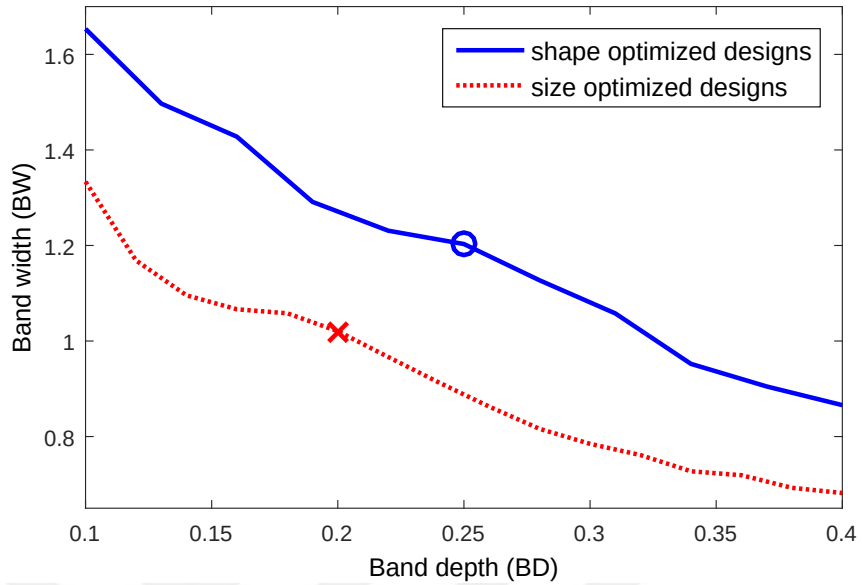


Figure 3.12. Band width versus band depth of optimized mechanism designs. Cross: Selected size optimized design ($BD = 0.20$, $BW = 1.02$), Circle: Selected shape optimized design ($BD = 0.25$, $BW = 1.20$).

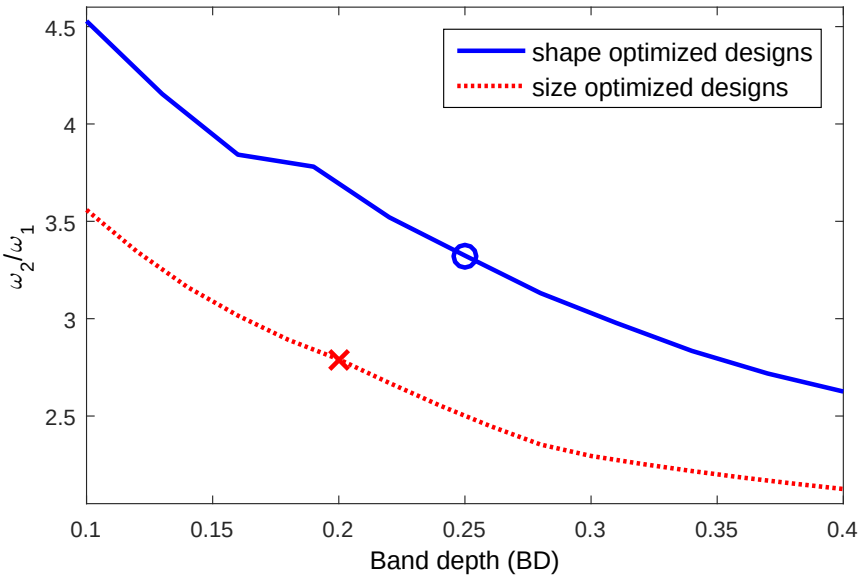


Figure 3.13. ω_2/ω_1 ratio versus band depth of optimized mechanism designs. Cross: Selected size optimized design ($BD = 0.20$, $\omega_2/\omega_1 = 2.79$), Circle: Selected shape optimized design ($BD = 0.25$, $\omega_2/\omega_1 = 3.32$).

3.2. Experimental and Numerical Results for the Phononic Band Gap Structure

A two dimensional phononic band gap structure is formed (see Figure 3.14) by using shape optimized building block mechanisms shown in Figure 3.9. Material properties are the same with the unit cell mechanism, i.e., density is 7800 kg/m^3, modulus of elasticity is 205 GPa, Poisson ratio is 0.29. Shell elements are used for the construction of the phononic band gap structure as shown in Figure 3.14. Shell thickness is taken as 55 mm to prevent out-of-plane modes within the band gap.

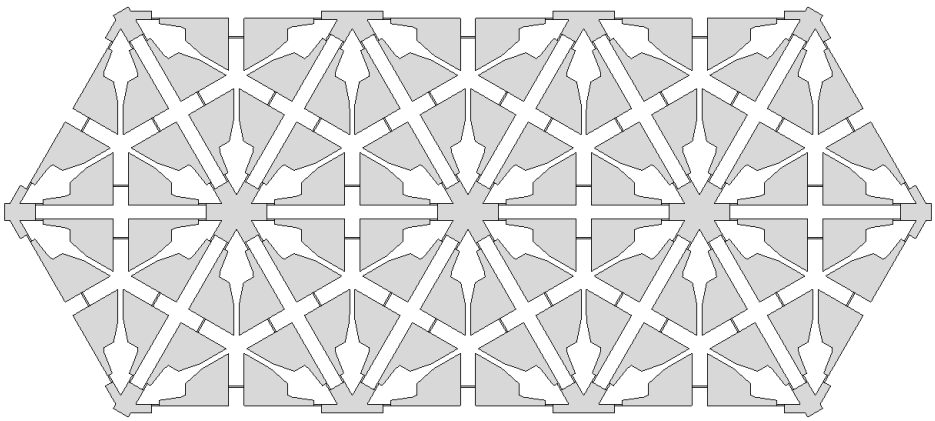


Figure 3.14. Two-dimensional phononic band gap structure.

Phononic band gap occurs between the 29th and 30th modes of the periodic structure shown in Figure 3.14. Band gap starts at 264.5 Hz with 29th mode (Figure 3.15). When Figure 3.15 is investigated, individual building blocks have their 1st mode shapes as in Figure 3.10a, as expected. Band gap ends at 30th mode which is at 829.5 Hz (Figure 3.16). Again as expected, individual building block mode shapes correspond to 2nd modes as shown in Figure 3.10b.

The phononic band gap structure is manufactured from steel by wire EDM method as shown in Figure 3.17. The density of the steel is 7800 kg/m^3, modulus of elasticity is 205 GPa, and Poisson ratio is 0.29. Moreover, thickness of the steel

specimen is 55 mm as in its finite element model.

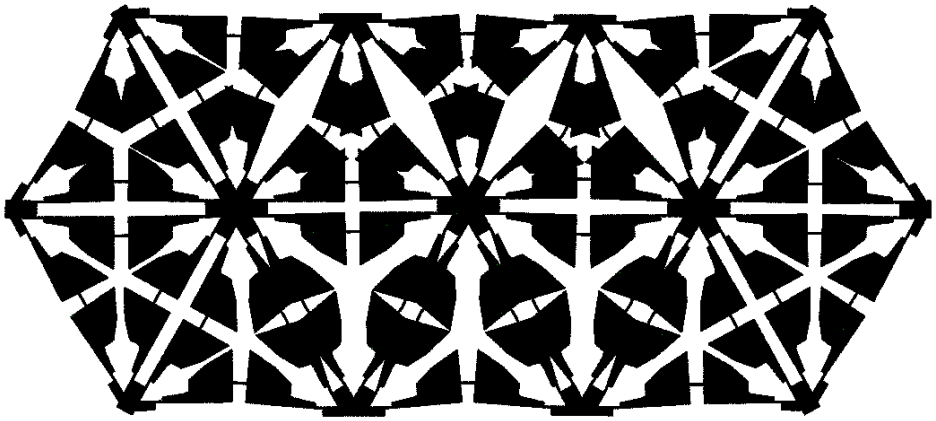


Figure 3.15. 29th mode shape of the phononic band gap structure (264.5 Hz).

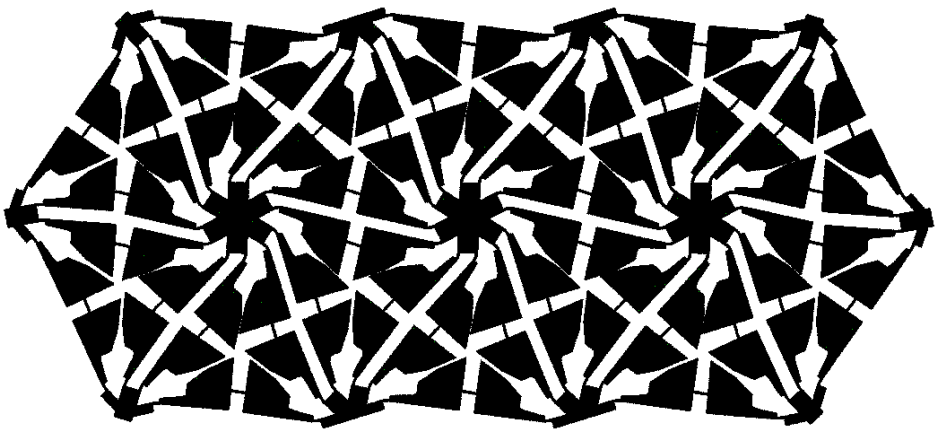


Figure 3.16. 30th mode shape of the phononic band gap structure (829.5 Hz).

The experimental setup is shown in Figure 3.18. The phononic band gap structure is hung by using elastic cords emulating free boundary conditions. The input is given by a modal shaker from one end and the output is taken from the other end with an accelerometer. For the frequency response function of acceleration transmissibilities, H_1 estimate [85] is used.

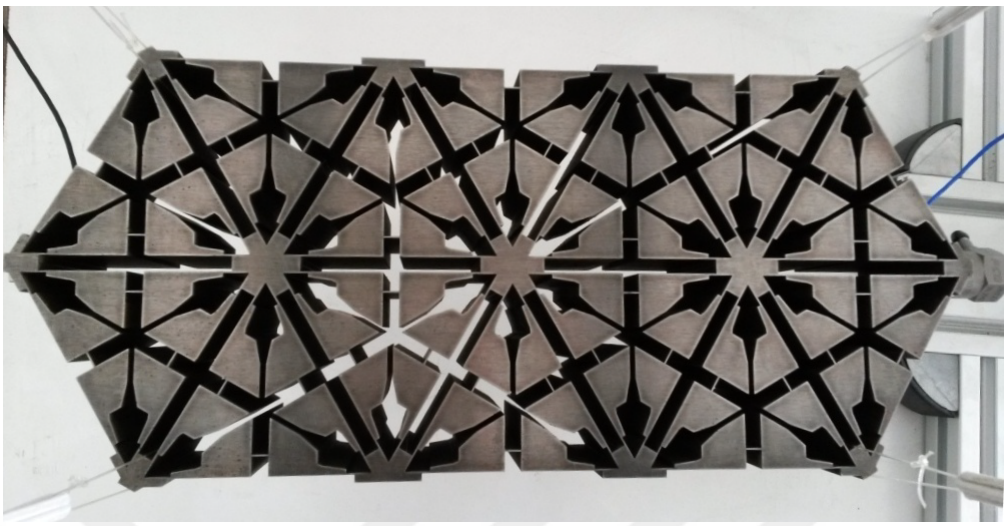


Figure 3.17. Manufactured phononic band gap structure.

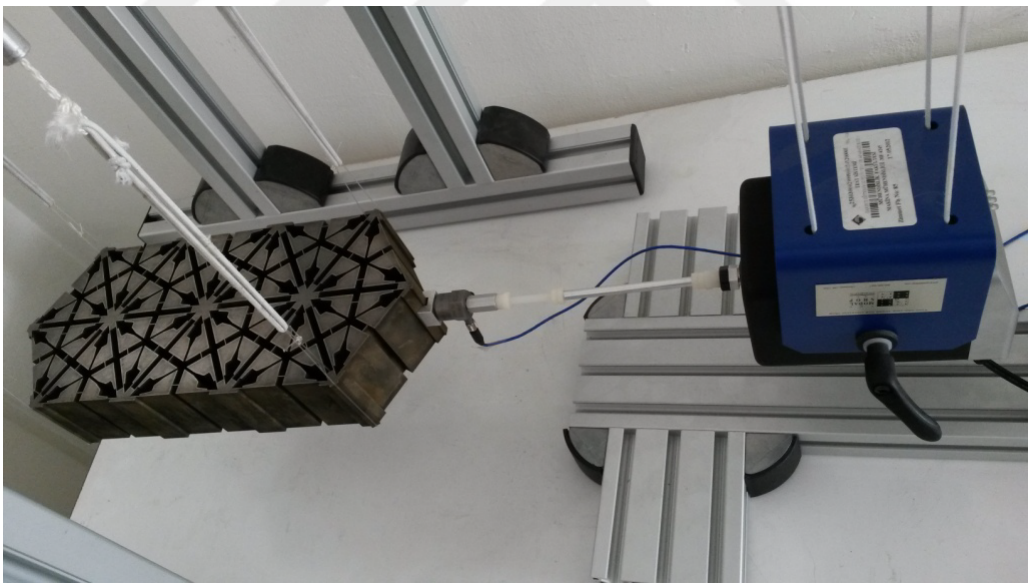


Figure 3.18. Experimental setup.

In Figure 3.19 experimental and numerical acceleration transmissibility plots of the phononic band gap structure are compared in the longitudinal direction. It can be clearly seen that the numerical and experimental results are in a good agreement with each other. Band gap starts and ends at the predicted frequencies. Band width and band depth characteristics are also at the values that are predicted by finite element

analysis.

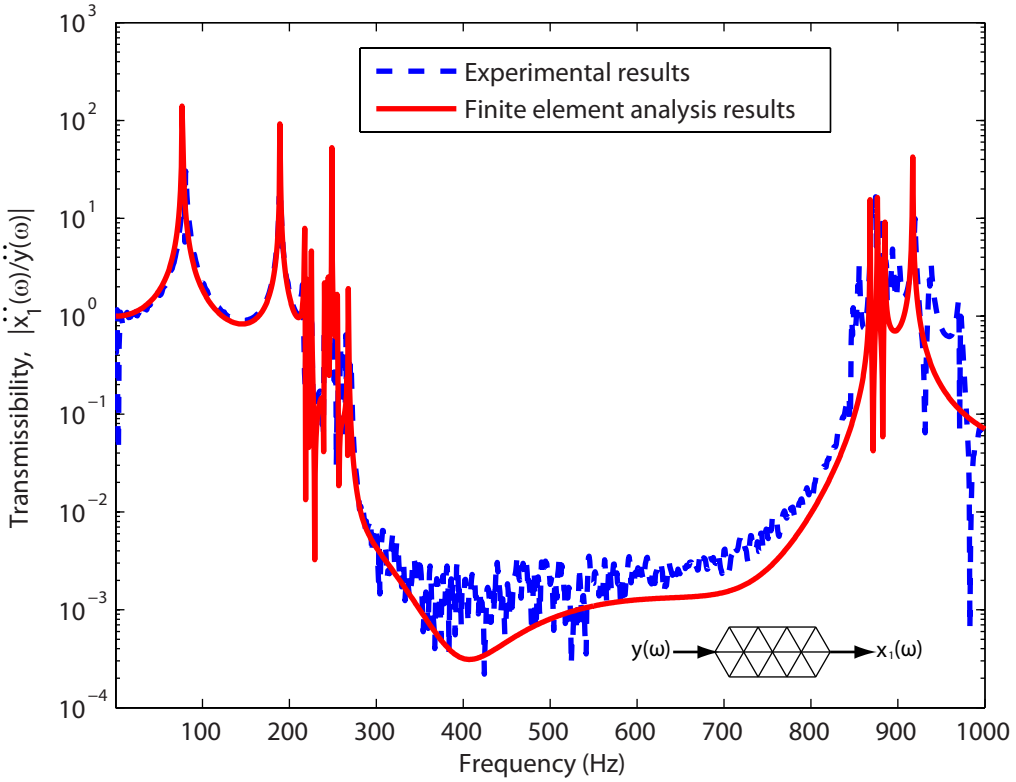


Figure 3.19. Experimental and numerical acceleration transmissibility plots of the phononic band gap structure for the longitudinal direction (x_1).

In Figure 3.20, experimental acceleration transmissibility plots for the phononic band gap structure for longitudinal and transverse directions are given. The in-plane input is provided with a 45°angle to the periodic structure. It is clearly seen from this figure that, predicted wide and deep band gap is formed for the longitudinal (x_1) and transverse (x_2) directions.

In Figure 3.21, experimental acceleration transmissibility plots of the phononic band gap structure for longitudinal and out-of-plane directions are investigated. As can be seen, as a result of the proper selection of structure thickness value, out-of-plane modes do not occur within band gap.

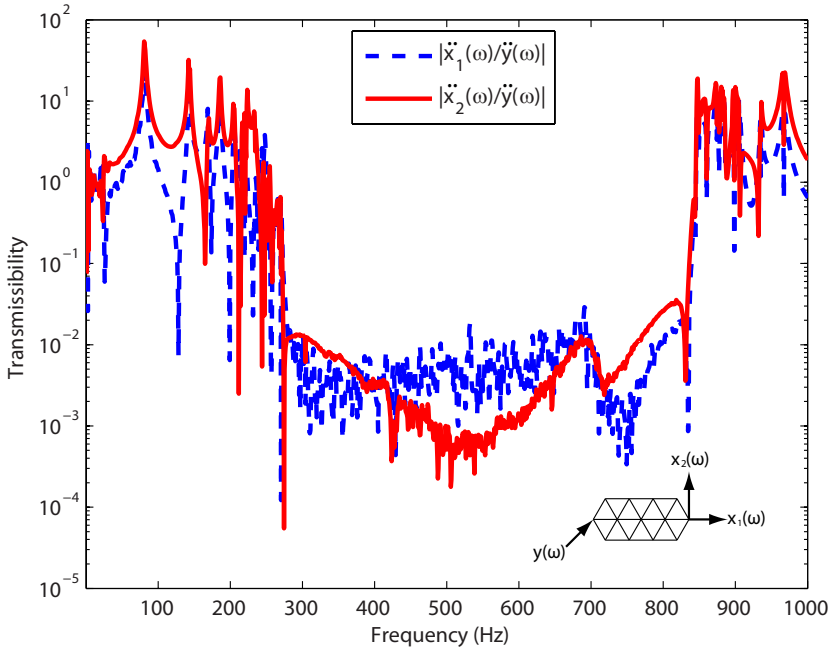


Figure 3.20. Experimental acceleration transmissibility plots of the phononic band gap structure for longitudinal (x_1) and transverse (x_2) directions.

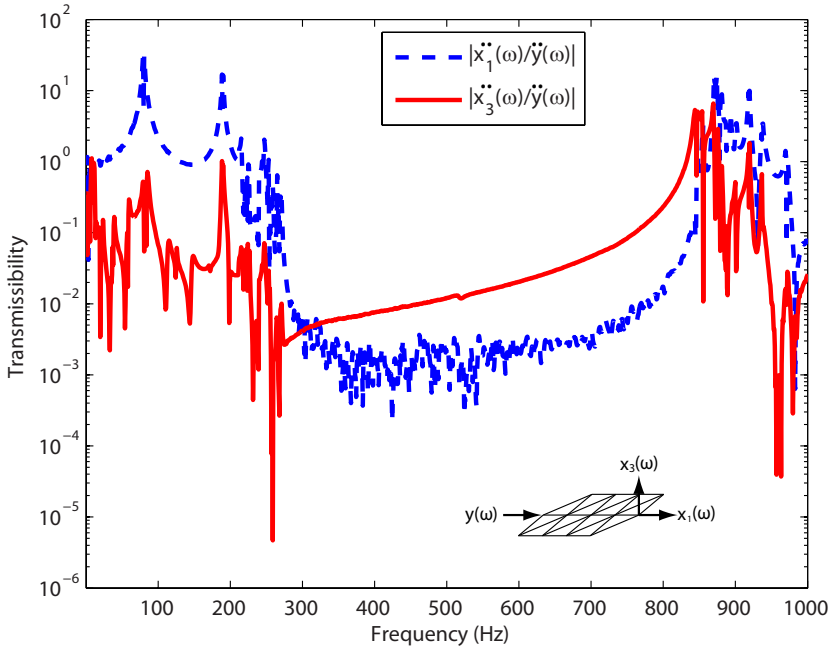


Figure 3.21. Experimental acceleration transmissibility plots of the phononic band gap structure for longitudinal (x_1) and out-of-plane (x_3) directions.

To conclude, overall shape optimization leads to designs with better band gap properties and it is experimentally verified that the proposed periodic structure possesses a wide and deep phononic band gap.

4. AN OVERVIEW ON TOPOLOGY OPTIMIZATION

Any mechanical performance measure of a structure is strongly related with its topology. Size and shape optimization cannot give the best structural performance, since these methods are not able to alter the structure's topology. Hence, topology optimization is needed to obtain the best performance. In this chapter, a review of topology optimization is provided. Firstly, the general topology optimization problem is discussed. Then, modern topology optimization methods are presented. Finally, a unique topology optimization method, which will be utilized in our study, is introduced.

4.1. Topology Optimization Problem

Topology optimization [86,87] is basically the determination of optimum material distribution in a design space which minimizes (or maximizes) an objective function while satisfying some constraints. In this section, topology optimization problem is presented by giving a mathematical description of topology optimization problem formulation and reviewing early historical progress in the field.

4.1.1. Description of Topology

Mathematically, topology is concerned with the deformable objects, and all distortions are considered as transformations or reversibly unique mappings [88]. The topological transformations or topological mappings are the transformations which do not change the neighbourhood relations, in other words, topological transformations cause topologically equivalent domains, therefore, topological property of a domain is invariant for all topological mappings [88].

Topological domains consist of all subsets of $\mathbb{R}^3$. The degree of connection of domains determines its topology class. Domains belonging to the same topology class are considered as topologically equivalent [88] (see Figure 4.1a). Naming of topology classes can be done as follows: n-fold connected domains require (n-1) cuts from one

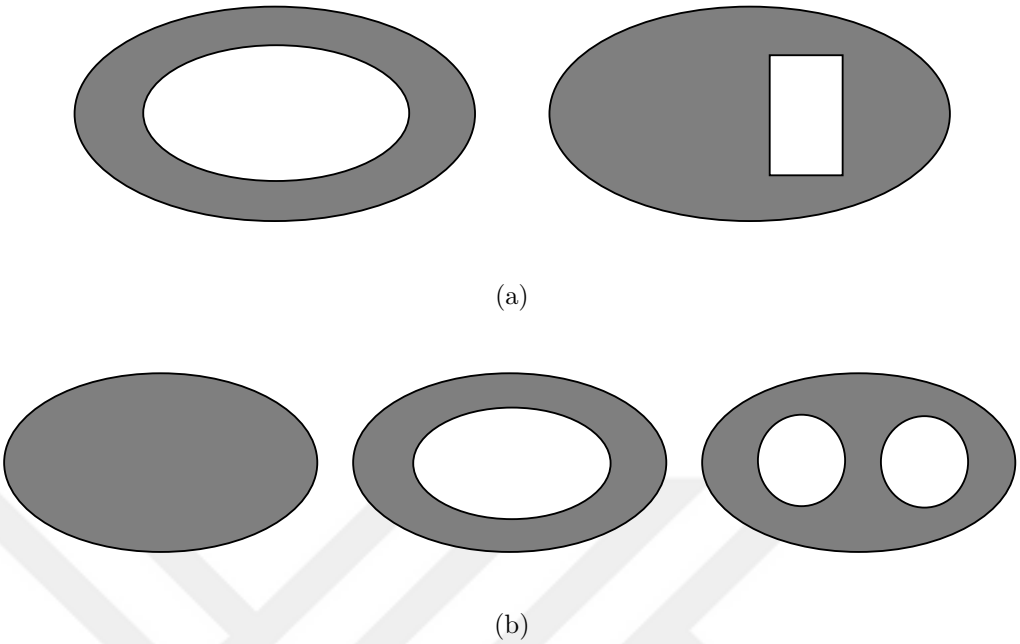


Figure 4.1. (a) Topologically equivalent domains. (b) Topological classes of simply, two-fold, three-fold connected domains.

boundary to another, to convert them into a simply connected domain [88] (see Figure 4.1b).

According to the above definitions, size and shape optimizations cause topological mappings that result in topologically equivalent structures. However, topology optimization transforms the structure from one topology class to another.

4.1.2. Optimization Problem

Although exact analytical solutions of topology optimization problems reveal basic characteristics of optimal designs, they are only capable of solving problems having simple load and support conditions [89]. Therefore, for more realistic problems, it is necessary to use a discretized design domain. Most of the studies in the literature use finite element formulation with a fixed mesh as the discretized model [90]. Here, the general form of topology optimization problem is provided for this model as:

$$
\begin{aligned}
&\text{minimize:} && H(\boldsymbol{u}(\boldsymbol{x}), \boldsymbol{x}) && \\
&\text{subject to:} && G_j(\boldsymbol{u}(\boldsymbol{x}), \boldsymbol{x}) \geq 0 && \text{for } j = 1, 2, ..., P \\
& && x_e = 0 \text{ or } 1 && \text{for } e = 1, 2, ..., N
\end{aligned} \tag{4.1}
$$

where $\boldsymbol{x}$ is the design variable vector, $\boldsymbol{u}$ is the state field, H is the objective function, G_j is the jth constraint, P is the total number of constraints, x_e is the eth structural member that constitutes the design variable vector $\boldsymbol{x}$, N is the total number of design variables (structural members). One of the mostly used constraints above is the so called volume (or mass) constraint [90].

The formulation given in Equation 4.1 most of the time represents a nonlinear topology optimization problem. Here, it should be emphasized that, design variables can only take a value of 0 or 1. In general, topology optimization problems lack solutions (i.e., ill-posed) with this current form [88, 90]. If design variables are defined as continuous, the problem relaxes and efficient gradient-based optimization algorithms can be utilized [90]. Then, the continuous topology optimization problem can be written as:

$$
\begin{aligned}
&\text{minimize:} && H(\boldsymbol{u}(\boldsymbol{x}), \boldsymbol{x}) && \\
&\text{subject to:} && G_j(\boldsymbol{u}(\boldsymbol{x}), \boldsymbol{x}) \geq 0 && \text{for } j = 1, 2, ..., P \\
& && 1 \geq x_e \geq 0 && \text{for } e = 1, 2, ..., N
\end{aligned} \tag{4.2}
$$

The formulation in Equation 4.2 is extensively used in the modern topology optimization literature [90]. Detailed discussions on discrete (Equation 4.1) and continuous (Equation 4.2) formulations are provided in Section 4.2, thus further arguments are omitted here.

4.1.3. Early Progress

Topology optimization studies can be traced back more than a hundred years ago [91]. In that pioneering work, optimal layout of truss structures which minimizes the weight is studied for a single load condition while only stress constraints are being employed. This type of structures are known as Michell trusses to honour their founder. Detailed discussions on Michell trusses can be found in [92]. However, the subject was untouched until 1950s [93]. Between 1950s and 1980s, various analytical and numerical studies on layout optimization are done (for detailed discussion one can refer to [89, 93–95]). In that period, conducted works are referred as layout optimization, since grid-like structures are studied. Here, a valuable definition should be given to clarify the subject. In topology optimization, the ratio of solid structure's volume to total design space volume is referred as the volume fraction. Therefore, layout optimization deals with low volume fraction designs like truss topology optimization [89, 96].

During 1980s, the necessity of studying high volume fraction design spaces emerged. In those years, it was discovered that, for the problems with high volume fractions, it is necessary to consider the microstructure of the system. Related historical advancements can be found in [93]. The so-called microstructure approach is considered under the topic of generalized shape optimization [89, 96]. More clearly, generalized shape optimization is the topology optimization performed for high volume fraction design spaces and it is the most general problem formulation that also covers layout optimization. In this study, "generalized shape optimization" term is omitted. Instead, "topology optimization" is used. So, when the term "topology optimization" is seen in the text, it should be understood that the problem deals with the most general case, i.e., problems with high volume fractions.

The introduction of microstructure approach to topology optimization field leads the modern topology optimization techniques to emerge. In the next section, the basic categories of these techniques are discussed in detail.

4.2. Basic Categories of Modern Topology Optimization Methods

For almost 30 years, numerous topology optimization methods emerged. In a recent study [90], the close relationship among these methods are pointed out. However, a coarse classification of the existing methods is still possible. To that end, in this section, modern topology optimization methods are categorized and the popular ones are introduced within each subsection. One can refer to [88, 90, 96, 97], to extend the idea about the topic.

Here, it should be noted that, it is a tradition to develop and test the topology optimization algorithms on compliance minimization problems with a mass constraint. Unless specified, throughout this chapter, the methods presented are also for that kind of topology optimization problems, as well.

4.2.1. Homogenization Methods

The discrete nature of topology optimization problem formulation given in Equation 4.1 leads lack of existence of solutions even for the simple problems such as minimum compliance case [89]. One way of making the problem formulation relaxed and continuous as given in Equation 4.2 is to introduce composite microstructures to the design domain [98]. To that end, mathematical theory of homogenization (see [99] for a brief review) is used to obtain a homogenized equivalent material model which replaces the composite, in turn, making the optimization problem relaxed and design variables continuous. The usage of homogenization theory is the reason why these techniques are called homogenization methods in the literature [88, 100–102].

In these methods, design domain is considered as being consisted of composite microstructures. These composite microstructures are composed of periodically repeating porous unit cells. These unit cells can be a hole-in-cell type or a layered type [88]. Other unit cell composite types can be found in the literature as well [98]. It is assumed that there exists infinitely many periodically distributed small unit cells within the microstructure. This assumption leads the continuous variation of material

density throughout the microstructure [88]. This periodic microstructure's effective macroscopic properties depend on its unit cell geometry, and homogenization theory is utilized to calculate them at this point [88]. Following this procedure, a well-posed topology optimization problem formulation is obtained, as desired.

There exists mainly two homogenization methods which are classified according to the unit cell type used in the microstructure [96]. One of them uses optimal unit cell structures which are previously found for a certain type of problem. However, that situation brings a disadvantage, since advanced mathematical treatment to obtain optimal unit cells is needed for other problem types [96]. The other method utilizes non optimal unit cells [98]. This type of unit cell consists of a rectangular void inside and isotropic material on the edges. For this type of structure, rectangular void lengths (a and b) and unit cell orientation angle with respect to global coordinate system (θ) are the design variables. Design variables a and b are continuous and they can vary between 0 and 1. By homogenization, mechanical properties of the microstructure which is composed of infinitely many unit cells can be defined in terms of a, b and θ. In other words, when homogenization method is employed, a, b and θ variables actually define the configuration of the microstructure. In discretized domain, a microstructure corresponds to an individual finite element. Easy microstructure definition of this type is used in the first homogenization method topology optimization study in the literature [100] and caused the modern topology optimization field to emerge.

Although, they lead a breakthrough in topology optimization field, homogenization methods bring the following major shortcomings as well:

(i) Number of design variables per a finite element is high (at least 2 in the case of isotropic material with square voids are used) [96].
(ii) Topology optimized structures usually involve large perforated regions which are impractical to manufacture [88].
(iii) Homogenization is required for the determination of the effective macroscopic properties of the microstructure [96].

4.2.2. Density Methods

Density methods [103–105] are introduced after the homogenization methods. In these methods, for an individual finite element (i.e., microstructure) there exists only one design variable which is the element density (x_e). A microstructure's material property contribution to the whole structure depends on this density design variable which can take any value between 0 and 1. With this formulation, various well-known optimization algorithms (see [106]) can be utilized to solve the topology optimization problem. Moreover, density methods involve penalization parameters, which penalize intermediate densities to obtain manufacturable solid-void designs with clear material boundaries instead of the perforated ones acquired with homogenization methods. Various density methods can be reviewed in the literature [90, 97]. However, the argument on density methods is cut here, since a more comprehensive discussion is provided in the whole Section 4.3, in which the most popular and utilized "Solid Isotropic Microstructure with Penalization" (SIMP) method [103, 104] is investigated in detail.

4.2.3. Discrete Methods

Usage of continuous density design variables in the topology optimization problems results in porous or grey regions in the optimized structure if proper penalization or problem regularization is not applied. Discrete methods concern with Equation 4.1 instead of Equation 4.2 in an attempt to obtain directly 0-1 (i.e., void-solid) designs. For this discrete problem, a natural choice is to use non-gradient optimization approaches such as Genetic Algorithms, Simulated Annealing, Particle Swarms, Ant Colonies, etc. However, these methods are inefficient for topology optimization problems in which large number of design variables are involved [107]. They can only solve problems with coarse finite element meshes [107]. Moreover, these algorithms also need some type of problem regularization or filtering to obtain physically reliable designs.

There exists another type of approach so-called evolutionary methods [108]. Inspired from the natural evolutionary process, evolutionary structural optimization (ESO) method [109] is suggested. In the ESO method, the optimum is seeked by

removing some of the inefficient material from the design domain in every iteration step. The determination of inefficient material depends on the type of objective function and constraints. However, as the material can only be removed (not added) during optimization, sometimes non-optimized designs are obtained [93]. To cope with this problem, "bi-directional evolutionary structural optimization" (BESO) method [110] is suggested. In the BESO method, material is being added in the vicinity of overstressed elements while in the inefficient areas, material is being removed.

Despite its conceptual simplicity, ESO/BESO methods are subjected to serious criticism [111–113]. These include, intuitive nature of the procedure, obtaining non-optimal designs at the end of the process and difficulties encountered with multiple constraints [112]. Even, in one study [113], it is shown that these methods fail for a simple test example. As a consequence of these, a new BESO algorithm is suggested recently [114,115]. In the new BESO algorithm, design variable sensitivities are utilized with penalization in order to sort the elements with respect to their efficiency. One further novelty in the method is, none of the elements are completely removed from the design space, instead, inefficient elements get a predetermined minimum value. By this, it is claimed that, void elements can become solid in any iteration step of the algorithm. It is argued in the literature that, the new BESO algorithm can be categorized as a discrete update version of the standard SIMP scheme [90]. However, ESO/BESO methods, together with this new BESO version, still have the following serious shortcomings:

(i) ESO/BESO methods are heuristic methods that lack rational mathematical methodology [90, 111].
(ii) ESO/BESO methods do not have appropriate stopping criteria to end the algorithm [90].
(iii) Because of their discrete or near discrete nature, these methods can lack convergence, thus end up with oscillating, unconverged results [90, 93].
(iv) By using these methods, there exists no guarantee of finding the global solution of the problem [93].

(v) Compared to density methods, ESO/BESO methods have serious problems with multi-objective/multi-constraint problems, thus are not suitable for that kind of problems [90, 97].

4.2.4. Boundary Variation Methods

Boundary variation methods are the recent development in the topology optimization field. They emerged from the need to obtain crisp and smooth edged structures as a result of optimization procedure. These methods have their roots in shape optimization techniques, however, they are fundamentally different, because they allow formation and disappearance of void regions inside the design domain in addition to allowing structural boundary movements [97]. There exist numerous boundary variation methods in the literature, but here, only the most popular level set methods are considered. For other alternative approaches, one can refer to [90, 97].

In the level set approach [116–118], the level set function determines where the boundaries, void and solid sections take place. Material boundaries exist where the level set function takes a certain constant value (usually it is 0). Where the level set function values are below this constant there exist void regions, whereas solid regions take place where the level set function values are greater than that constant. Changes in structure's topology are achieved by level set function updating, and mostly it is performed by solving the augmented Hamilton-Jacobi equation with diffusive and reactive terms [90]. In this manner, the original Hamilton-Jacobi equation is utilized for shape updating, reactive term is used for nucleation of new holes and diffusive term is employed to smooth the level set field [90].

Level set methods are mainly composed of level set function parameterization, mechanical model and optimization parts [119]. Firstly, design variables are parameterized via level set function. Then, geometry described by the level set function is mapped onto the mechanical structural model. Finally, design update is performed [119]. Depending on the level set method type used, in each of these three parts, regularization techniques can be employed to regularize ill-posedness of the topology optimization

problem [119]. Many level set methods utilize the regularization techniques used in density methods. Moreover, similar material interpolation schemes with density methods are utilized in the geometry mapping part of many level set methods, as well. A comprehensive review on the level set methods can be seen in [119].

In the last decade, level set methods gained popularity as a new research direction in the topology optimization field. However, at the current state, these methods are far from being maturized and standardized. Ongoing researches are promising, but in their current form, they are not suitable and reliable for more complex physics problems and engineering applications. In the following, the major shortcomings of the level set methods are presented:

(i) Rather complex mathematics is involved with level set methods [119].

(ii) There exists no commonly accepted level set strategy to solve topology optimization problems. In fact, level set methods show significant differences from each other in topology optimization problem formulations and solution strategies [119].

(iii) The optimized designs obtained by level set methods are strongly dependent on initial guesses [90, 119].

(iv) The problems encountered in the formulation of manufacturing constraints and convergence behaviour limit the applicability of level set methods in engineering design problems [119].

(v) Compared to the density methods, level set methods do not bring any advantage related to the efficiency, convergence and mesh dependency issues [90]. Instead, they often suffer from a poor rate of convergence [119].

4.3. The Topology Optimization Technique of Choice: SIMP Method

"Solid Isotropic Microstructure (Material) with Penalization" (SIMP) method is a density method which is introduced in [103] firstly under the name "the direct approach". Later, with [104], it adopted its current name. In this thesis study, the SIMP method is used as the topology optimization technique. To that end, here, a whole section is devoted to explain the SIMP method, in order to enounce why it was

chosen.

4.3.1. Microstructure Description

In the SIMP method, the mechanical property (for instance, elastic properties as in the case below) of a microstructure is defined as:

$$E_e(x_e) = x_e^p E_0 \qquad \text{for } 0 \leq x_e \leq 1 \tag{4.3}$$

where E_e denotes the microstructure's elastic modulus, x_e denotes the eth microstructure's density, p denotes the penalization parameter, E_0 denotes the elastic modulus of the solid isotropic material.

Furthermore, the total solid structural volume is given below in a finite element formulation scheme as:

$$V(\boldsymbol{x}) = \sum_{e=1}^{N} x_e \qquad \text{for } 0 \leq x_e \leq 1 \tag{4.4}$$

where V is the total solid volume of the structure, $\boldsymbol{x}$ is the vector of design variables consisted of individual element densities (i.e., x_es), x_e is the eth element's (microstructure's) density, N is the total number of elements in the discretized domain.

In Equation 4.3, the continuous variation of the microstructure property of an individual finite element, i.e., density transforms the topology optimization problem into a continuous problem (like Equation 4.2), thus allowing usage of mathematical programming methods based on gradient information. Moreover, in the presence of a volume constraint, the use of penalization parameter values larger than 1 (i.e., $p > 1$) penalizes microstructures with intermediate densities [88]. More clearly, when $p > 1$, the elements (microstructures) with intermediate densities contribute to structure's elasticity (see Equation 4.3) less than the structure's mass (see Equation 4.4). Thus, elements with intermediate densities are penalized and in turn, a solid-void final design

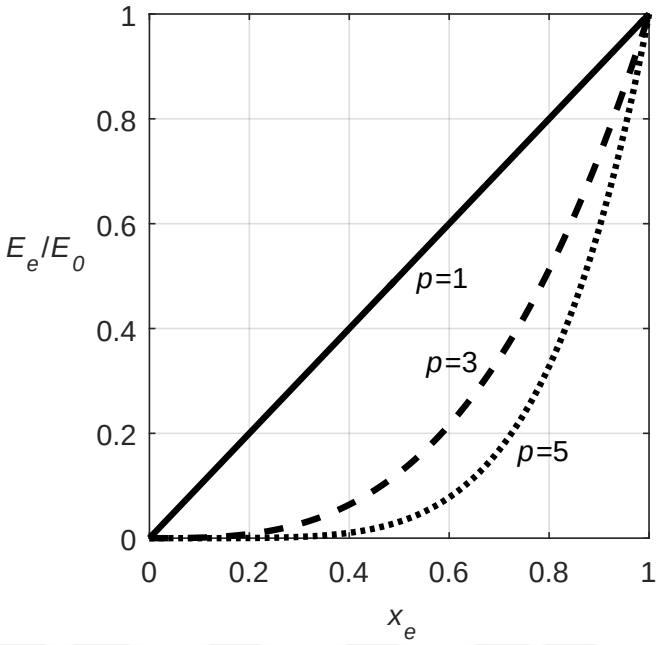


Figure 4.2. Effect of penalization on an element's relative stiffness (E_e/E_0) vs density (x_e) values in the SIMP material model for different penalty numbers (p).

is favored. The effect of penalization on the relationship between an element's relative stiffness and density can be observed in Figure 4.2.

There are two ways to utilize the penalization parameter p in Equation 4.3. The first approach has its roots from compliance minimization problem with a single mass constraint, since for $p = 1$ the problem is convex [111]. Thus, the idea is to start with an initial penalization with $p = 1$ and then gradually increase the penalization during the optimization, in turn not altering the convexity nature of the original problem at the initial stages of the optimization process [90, 96, 111]. On the other hand, it is reported in the literature that, this approach might not work well [90].

An alternative way is to utilize a fixed penalty number p. In the early years of the SIMP method, it was criticized that there exists no material with penalized density. However, in [120], it is demonstrated that, for simple conditions on penalization number p, the SIMP model's microstructures can be realized as composite microstruc-

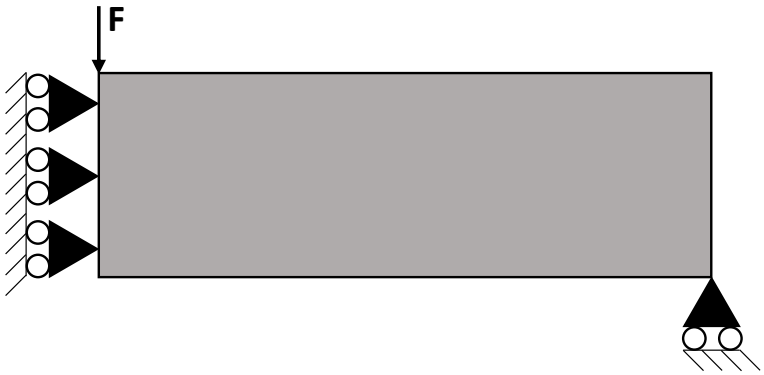
tures which are composed of periodic inclusion of solid and void regions like the ones encountered in the homogenization approach. For the two dimensional (2-D) space these conditions on penalization are given as [120]:

$$p \geq max\{\frac{2}{1-\nu}, \frac{4}{1+\nu}\} \tag{4.5}$$

where ν is the Poisson's ratio of the isotropic material. Therefore, for common engineering metals, penalty number p varies between 3 and 4. Hence, SIMP model becomes a microstructured material model if proper penalty number is chosen [88]. Choosing $p \geq 3$ as a constant penalization number during the optimization process is common in the literature [86]. Besides, the magic number that results with good convergence characteristics to 0-1 (void-solid) designs is $p = 3$ [90]. On the other hand, beyond the physical meaning associated with penalty number, the penalization is a standard technique that is already utilized in nonlinear optimization problems [96, 111]. However, in order to see the benefits of penalization in topology optimization, the volume constraint or another constraint which indirectly limits the volume, should be employed as well [90].

4.3.2. Problem Regularization

The common numerical instabilities in topology optimization problems can also occur in the SIMP method with its current formulation. The encountered difficulties are local minima problem, checkerboard pattern formation and more importantly, mesh dependency issues [121]. Convergence to local minima in gradient based mathematical programming methods are common for non-convex nonlinear optimization problems. Hence, it is not a special issue related to topology optimization itself. On the other hand, checkerboard pattern formation (i.e., formation of alternating solid and void elements successively, see Figure 4.3) in the final design is merely a finite element discretization error, which falsely makes the structure artificially efficient [122]. This problem does not also stem from the topology optimization itself, but in order to obtain manufacturable designs, it should be addressed.



(a)



(b)



(c)

Figure 4.3. (a) Topology optimization problem. There are 150 by 50 elements in the design domain. (b) Checkerboard pattern formation when filtering is not employed. (c) Optimized design via filter employment.

In Section 4.1.2, the need to transform the original problem in Equation 4.1 to Equation 4.2 was mentioned. One way to successfully achieve this is the homogenization approach (see Section 4.2.1). On the other hand, the relaxation attained by the SIMP method with its current form is not satisfactory enough to make the problem well-posed [88]. The nonexistence of solutions forces the optimization to converge to different results for different finite element mesh discretizations. This phenomenon is known as the mesh dependency of solutions in the literature [121]. To close the design space in an appropriate sense, i.e., to make the optimization problem well-posed, prob-

lem regularization is needed [88]. Thus, lack of convergence related with mesh dependency can be discarded. There exist many problem regularization techniques in the literature and some of them were proposed recently [123–127]. However, in this section, the mostly utilized methods, namely, sensitivity filtering, density filtering and projection filtering are discussed to give the fundamental idea on the subject.

The most popular regularization technique used in the topology optimization field is the "sensitivity filtering" [128] which is originally inspired by the image processing methods. In this technique, an element's sensitivity value is modified by taking into account its neighbour element sensitivities. In this manner, a filter radius that describes an element's neighbourhood is defined, and new sensitivity value of the corresponding element is calculated via weighted averages of its neighbours accordingly. Similar concepts are used to stabilize convergence characteristics of the general optimization problems in other physical disciplines, as well [90]. In [129], it is shown that, for the compliance minimization problem, sensitivity filtering has a physical meaning. Moreover, the sensitivity filter does not change the objective function but the descent direction in compliance minimization problem, thereby stabilizes and speeds up the convergence [129]. It is claimed in [129] that the concept of invariance of objective function in the presence of sensitivity filtering may hold for other problems (for instance, compliant mechanism design), as well. The sensitivity filter is very easy to implement in finite element codes [88, 129] and it puts no extra constraints in the optimization problem [88]. Furthermore, at the end of the topology optimization process, the grey transition zones that remains between solid and void regions because of the filter radius can be eliminated by a simple volume preserving post processing step provided in [90].

In the other regularization method called "density filtering" [130] so-called physical density of an element is defined by taking the weighted averages of neighbouring design variables. Again, neighbourhood is described by some filter radius, such that the design variables outside that radius do not effect the physical density of the corresponding element. By using this method, at the end of the optimization, grey transition regions occur in the solid-void interface. A continuation approach in which the filter ra-

dius is reduced gradually, may overcome this issue. The continuation approach may be used for sensitivity filtering as well. However, for the problems in which more complex objective functions or constraints are involved, this strategy may fail [90]. to get rid of the grey zones in the final design, the "projection filtering" [131] is proposed as an alternative regularization scheme, in which a smoothed Heaviside projection is used to make the filtered densities discrete valued, i.e., 0 or 1. This filter provides discrete solutions if the grey zones are caused by insufficiency of the density filter, otherwise it may fail to provide discrete solutions [90]. On the other hand, while the usage of sensitivity filtering has a continuum mechanics motivation, the density filtering [129] and the projection filtering do not have such relations with continuum mechanics. Moreover, finite element implementations of density and projection filters are more involved compared to the sensitivity filter [132].

Apart from the SIMP method (or, in general, the density approaches), filtering is also required for the discrete (such as BESO approach) and the boundary variation (such as level set approach) methods, to obtain well-posed optimization problems with mesh independent results [90]. Although being well-posed, the homogenization methods also suffer from the checkerboard pattern formation, and the proposed cure for this problem is to employ higher order finite elements with much greater number of nodes than the ones that are usually employed [122]. In turn, extra computational cost is added to the homogenization approach which is readily computationally costly, thus with respect to computational efficiency, it results in a situation that is worse than utilizing filtering. Besides from the problem regularization, the filtering techniques prevent checkerboard pattern formation in the SIMP method, as well [121]. Moreover, by adjusting the filter radius, manufacturable designs can be obtained [132].

4.3.3. Merits of the SIMP Method

The main features of the SIMP method can be summarized as follows:

(i) It is the most widely used method in the topology optimization field [97].

(ii) It is used extensively in the commercial finite element analysis (FEA) softwares such as Genesis, MSc Nastran, OptiStruct, Abaqus, Tosca, Ansys, Comsol [97].

(iii) It is used in free source codes such as educational codes [132–134], a web-based program [135], a mobile application for iPhone and Android [136] and an application for Windows and OSX [137].

(iv) It does not involve advanced mathematical formalism, i.e., it is conceptually simple [96, 97, 138].

(v) It is suitable to be used with wide range of constraints and it is computationally efficient to be used for problems in which large number of design variables are involved [90, 96, 111].

(vi) It allows the well-proven gradient based optimization algorithms to be used as optimizers in solving topology optimization problems [90, 97, 139].

(vii) It is utilized for wide range of problems including statics, dynamics, fluid flow, heat transfer, thermoelasticity, aeroelasticity, biomedical, acoustics, wave propagation, etc. [97, 140].

(viii) It is the most utilized method to solve topology optimization problems for vibrations [138].

5. TOPOLOGY OPTIMIZATION PROBLEM FORMULATIONS

In this section, the topology optimization problem formulations that are used in this thesis are presented along with their explicit derivations. Stiffness, natural frequency and frequency gap maximization problems are investigated in detail.

5.1. Stiffness Maximization

Solid isotropic material with penalization (SIMP) [103,104] material interpolation scheme is a rigorous gradient based method implemented to solve topology optimization problems in commercial softwares such as OptiStruct, Genesis, MSC/Nastran, Ansys and Tosca [111]. In the SIMP material interpolation scheme, an element's stiffness value depends on some power of its "density". The element density can take any value between 0 and 1. By taking the power of densities it is aimed that elements with lower density values have less contribution to the overall stiffness of the structure as compared to their mass. Thus, it becomes uneconomical for the structure to have grey elements and therefore these elements are penalized. Eventually, elements with low stiffness contribution with respect to their mass will vanish. On the contrary, elements with higher density values are favored. Eventually, a solid-void design is obtained. A more detailed discussion is given in [86].

Here, to solve topology optimization problems a slightly modified newer version of this material interpolation scheme named "modified SIMP" [131] is used:

$$E_e(x_e) = E_{min} + x_e^p(E_0 - E_{min}) \qquad x_e \in [0,1] \tag{5.1}$$

where x_e denotes the element's density which can take any value between 0 and 1, E_e denotes element's Young's modulus, E_{min} denotes the very small stiffness value to prevent stiffness matrix to become singular, E_0 denotes the elastic modulus of the

material, p denotes the penalization factor for stiffness. For the problems in which the volume constraint is active, in order to obtain solutions consisting of only solid or void elements, the stiffness penalization factor should be chosen as $p \geq 3$ [86].

The material volume is defined as:

$$V(\boldsymbol{x}) = \sum_{e=1}^{N} x_e \tag{5.2}$$

Using the material interpolation scheme shown in Equation 5.1 and the material volume definition given in Equation 5.2, the stiffness maximization, i.e., compliance minimization problem is formulated as:

$$\begin{aligned}
\text{minimize:} \quad & c(\boldsymbol{x}) = \boldsymbol{u}^T \boldsymbol{K} \boldsymbol{u} = \textstyle\sum_{e=1}^{N} E_e(x_e) \boldsymbol{u_e}^T \boldsymbol{K_0} \boldsymbol{u_e} \\
\text{subject to:} \quad & \boldsymbol{K}\boldsymbol{u} - \boldsymbol{f} = \boldsymbol{0} \\
& aV_0 - V(\boldsymbol{x}) \geq 0 \\
& x_e \geq 0 \qquad \text{for } e\text{=1,2,.....,}N \\
& 1 - x_e \geq 0 \qquad \text{for } e\text{=1,2,.....,}N
\end{aligned} \tag{5.3}$$

where; $c(\boldsymbol{x})$ is the compliance value (i.e., two times the total strain energy [111]), $\boldsymbol{u}$ is the global displacement vector, $\boldsymbol{K}$ is the global stiffness matrix, $\boldsymbol{u_e}$ is the displacement vector of element e, $\boldsymbol{K_0}$ is the stiffness matrix of an element for unit Young's modulus, $\boldsymbol{x}$ is the vector of element densities (i.e., vector of design variables), N is the total number of finite elements used, $\boldsymbol{f}$ is the global load vector, a is the volume fraction that indicates the ratio between the material volume over design domain volume, V_0 is the design domain volume.

Defining Lagrangian for this optimization problem [102, 141]:

$$\mathcal{L} = \boldsymbol{u}^T \boldsymbol{K} \boldsymbol{u} - \lambda_0 (aV_0 - V(\boldsymbol{x})) - \boldsymbol{\lambda_1}^T (\boldsymbol{K}\boldsymbol{u} - \boldsymbol{f}) - \boldsymbol{\lambda_2}^T (\boldsymbol{x}) - \boldsymbol{\lambda_3}^T (\boldsymbol{1} - \boldsymbol{x}) \tag{5.4}$$

where; λ_0, $\boldsymbol{\lambda_1^T}$, $\boldsymbol{\lambda_2^T}$, $\boldsymbol{\lambda_3^T}$ are corresponding Lagrange multipliers. Writing necessary conditions for optimality for an element:

$$\frac{\partial \mathcal{L}}{\partial x_e} = 0 \qquad \text{for } e=1,2,\ldots..,N \tag{5.5}$$

Derivative of the lagrangian with respect to design variable x_e:

$$\begin{aligned}\frac{\partial \mathcal{L}}{\partial x_e} = \frac{\partial}{\partial x_e}(\boldsymbol{u}^T \boldsymbol{K} \boldsymbol{u}) - \lambda_0 \frac{\partial}{\partial x_e}(aV_0 - \sum_{e=1}^{N} x_e) - \boldsymbol{\lambda_1^T} \frac{\partial}{\partial x_e}(\boldsymbol{K}\boldsymbol{u} - \boldsymbol{f}) \\ -\boldsymbol{\lambda_2^T} \frac{\partial}{\partial x_e}(\boldsymbol{x}) - \boldsymbol{\lambda_3^T} \frac{\partial}{\partial x_e}(\boldsymbol{1} - \boldsymbol{x})\end{aligned} \tag{5.6}$$

Taking the derivatives we get:

$$\frac{\partial \mathcal{L}}{\partial x_e} = \frac{\partial}{\partial x_e}(\boldsymbol{u}^T \boldsymbol{K} \boldsymbol{u}) + \lambda_0 - \boldsymbol{\lambda_1^T} \frac{\partial}{\partial x_e}(\boldsymbol{K}\boldsymbol{u} - \boldsymbol{f}) - \lambda_{2e} + \lambda_{3e} \tag{5.7}$$

where; λ_{2e} and λ_{3e} are the corresponding Lagrange multipliers of vectors $\boldsymbol{\lambda_2^T}$ and $\boldsymbol{\lambda_3^T}$, respectively. Assume that the lower and upper bound constraints for x_e are not active [141]:

$$\lambda_{2e} = 0 \qquad \text{and} \qquad \lambda_{3e} = 0 \tag{5.8}$$

Then:

$$\frac{\partial \mathcal{L}}{\partial x_e} = \frac{\partial}{\partial x_e}(\boldsymbol{u}^T \boldsymbol{K} \boldsymbol{u}) + \lambda_0 - \boldsymbol{\lambda_1^T} \frac{\partial}{\partial x_e}(\boldsymbol{K}\boldsymbol{u} - \boldsymbol{f}) \tag{5.9}$$

Expanding and remembering that the load vector $\boldsymbol{f}$ is a constant vector (in other words, $\partial \boldsymbol{f}/\partial x_e = 0$):

$$\frac{\partial \mathcal{L}}{\partial x_e} = \frac{\partial \boldsymbol{u}^T}{\partial x_e}\boldsymbol{K}\boldsymbol{u} + \boldsymbol{u}^T \frac{\partial \boldsymbol{K}}{\partial x_e}\boldsymbol{u} + \boldsymbol{u}^T \boldsymbol{K} \frac{\partial \boldsymbol{u}}{\partial x_e} + \lambda_0 - \boldsymbol{\lambda_1^T}(\frac{\partial \boldsymbol{K}}{\partial x_e}\boldsymbol{u} + \boldsymbol{K}\frac{\partial \boldsymbol{u}}{\partial x_e}) \tag{5.10}$$

Since $\boldsymbol{K}$ is real and symmetric:

$$\frac{\partial \boldsymbol{u}^T}{\partial x_e}\boldsymbol{K}\boldsymbol{u} = \boldsymbol{u}^T\boldsymbol{K}\frac{\partial \boldsymbol{u}}{\partial x_e}$$

Then Equation 5.10 becomes:

$$\frac{\partial \mathcal{L}}{\partial x_e} = 2\boldsymbol{u}^T\boldsymbol{K}\frac{\partial \boldsymbol{u}}{\partial x_e} + \boldsymbol{u}^T\frac{\partial \boldsymbol{K}}{\partial x_e}\boldsymbol{u} + \lambda_0 - \boldsymbol{\lambda_1}^T\frac{\partial \boldsymbol{K}}{\partial x_e}\boldsymbol{u} - \boldsymbol{\lambda_1}^T\boldsymbol{K}\frac{\partial \boldsymbol{u}}{\partial x_e} \tag{5.11}$$

Rearranging:

$$\frac{\partial \mathcal{L}}{\partial x_e} = \boldsymbol{u}^T\frac{\partial \boldsymbol{K}}{\partial x_e}\boldsymbol{u} - \boldsymbol{\lambda_1}^T\frac{\partial \boldsymbol{K}}{\partial x_e}\boldsymbol{u} + \lambda_0 + (2\boldsymbol{u}^T - \boldsymbol{\lambda_1}^T)\boldsymbol{K}\frac{\partial \boldsymbol{u}}{\partial x_e} \tag{5.12}$$

Since $\boldsymbol{Ku - f = 0}$ constraint is satisfied, then $\boldsymbol{\lambda_1}^T$ could be selected arbitrarily. Select $\boldsymbol{\lambda_1}^T$ to eliminate $\partial \boldsymbol{u}/\partial x_e$ term (the adjoint method [142]):

$$\boldsymbol{\lambda_1}^T = 2\boldsymbol{u}^T \tag{5.13}$$

Then Equation 5.12 becomes:

$$\frac{\partial \mathcal{L}}{\partial x_e} = \boldsymbol{u}^T\frac{\partial \boldsymbol{K}}{\partial x_e}\boldsymbol{u} - 2\boldsymbol{u}^T\frac{\partial \boldsymbol{K}}{\partial x_e}\boldsymbol{u} + \lambda_0 \tag{5.14}$$

Combining with Equation 5.5:

$$\frac{\partial \mathcal{L}}{\partial x_e} = -\boldsymbol{u}^T\frac{\partial \boldsymbol{K}}{\partial x_e}\boldsymbol{u} + \lambda_0 = 0 \tag{5.15}$$

Expanding the first term in Equation 5.15 results in:

$$\frac{\partial \mathcal{L}}{\partial x_e} = -\boldsymbol{u_e}^T\frac{\partial}{\partial x_e}(E_e(x_e)\boldsymbol{K_0})\boldsymbol{u_e} + \lambda_0 = 0 \tag{5.16}$$

Employing the modified SIMP material interpolation scheme given in Equation 5.1:

$$\frac{\partial \mathcal{L}}{\partial x_e} = -\boldsymbol{u_e}^T \frac{\partial}{\partial x_e}((E_{min} + x_e^p(E_0 - E_{min}))\boldsymbol{K_0})\boldsymbol{u_e} + \lambda_0 = 0 \tag{5.17}$$

Finally, the necessary conditions for optimality are obtained as [132]:

$$\frac{\partial \mathcal{L}}{\partial x_e} = -px_e^{p-1}(E_0 - E_{min})\boldsymbol{u_e}^T \boldsymbol{K_0} \boldsymbol{u_e} + \lambda_0 = 0 \qquad \text{for } e=1,2,.....,N \tag{5.18}$$

The topology optimization problem can be solved by using necessary optimality conditions given in Equation 5.18 by using Optimality Criteria (OC) [74,78,102,132,143–150] methods.

In order to employ OC methods a new parameter (B_e) is defined for each element. These parameters are defined using the optimality conditions given in Equation 5.18:

$$B_e = \frac{px_e^{p-1}(E_0 - E_{min})\boldsymbol{u_e}^T \boldsymbol{K_0} \boldsymbol{u_e}}{\lambda_0} \tag{5.19}$$

The objective function sensitivity for the OC method ($\partial c/\partial x_e$) is defined by using the numerator of Equation 5.19:

$$\frac{\partial c}{\partial x_e} = px_e^{p-1}(E_0 - E_{min})\boldsymbol{u_e}^T \boldsymbol{K_0} \boldsymbol{u_e} \tag{5.20}$$

So by combining Equation 5.19 and Equation 5.20 B_e can also be written as:

$$B_e = \frac{\partial c/\partial x_e}{\lambda_0} \tag{5.21}$$

By using the parameters given in Equation 5.19 which are defined independently for each element, design variables (x_es) are updated with a resizing formula. The heur-

istic resizing formula [145] is derived as follows. For an element, optimality condition is satisfied when $\partial\mathcal{L}/\partial x_e = 0$ or, equivalently it can be stated as:

$$1 = B_e \tag{5.22}$$

Multiplying both sides with x_e^α results in:

$$x_e^\alpha = B_e x_e^\alpha \tag{5.23}$$

where α is a number greater than 1. Taking the αth root of both sides yields:

$$x_e = B_e^{1/\alpha} x_e \tag{5.24}$$

Then, the resizing formula for an element e can be written as:

$$x_e^{new} = B_e^\eta x_e^{current} \tag{5.25}$$

where $\eta = 1/\alpha$ is the numerical damping coefficient ($\eta < 1$, usually $\eta = 1/2$ is taken [86, 132, 145, 147, 151, 152]) to stabilize the iteration.

For a computer implementation of this method, a heuristic updating scheme [132] given below can be used:

$$x_e^{z+1} = \begin{cases} \max(0, x_e^z - ml) & \text{if } x_e^z (B_e^z)^\eta \leq \max(0, x_e^z - ml) \\ \min(1, x_e^z + ml) & \text{if } x_e^z (B_e^z)^\eta \geq \min(1, x_e^z + ml) \\ x_e^z (B_e^z)^\eta & \text{otherwise} \end{cases} \tag{5.26}$$

where; z is the iteration number, ml is the move limit which determines the maximum variation of a design variable in one iteration.

By using optimality criteria method, in each iteration step, it is provided that the design variables are updated independent of each other [141]. Optimality criteria based optimizer is a heuristic updating scheme [133] and its computational efficiency for large scale structural optimization problems is known [153]. Since the search for optimum does not progress from point to point [145], OC methods are more efficient computational tools compared to mathematical programming methods when large number design variables are considered [141].

In the current topology optimization problem, single mass constraint, which is a linear and monotonic function of design variables, is included so that the easy solution by OC method applies [131]. The rate of change of the upper limit on the volume of the solid material with respect to the Lagrange multiplier is less than zero [141]. Or to be more clear, the material volume is a monotonously decreasing function of the Lagrange multiplier [133]. Thus, the Lagrange multiplier λ_0 given in Equation 5.19 can be found by using bisection method [141]. Computer program applications of this approach are provided in [132, 133].

The standard formulation of the topology optimization is promising but suffers from numerical problems such as mesh dependency and checkerboard pattern formation. However, these problems can be overcome by implementing sensitivity filtering technique [128, 129] (see Section 4.3.2). Towards that goal, sensitivity filter formulations are reviewed. First of all, the neighbourhood of element e, (N_e), is defined:

$$N_e = \{i \mid \|o_i - o_e\| \leq R\} \tag{5.27}$$

where R is the filter radius, o_i is the center location of element i, o_e is the center location of element e. Then linearly decaying weighing function, $H(o_i)$, is defined:

$$H(o_i) = R - \|o_i - o_e\| \tag{5.28}$$

Finally, the element sensitivities given in Equation 5.20 are modified according to the following:

$$\left(\frac{\partial c}{\partial x_e}\right)^{new} = \frac{\sum_{i \in N_e} H(o_i) x_i \left(\frac{\partial c}{\partial x_i}\right)}{x_e \sum_{i \in N_e} H(o_i)} \tag{5.29}$$

where x_i is the ith element density and x_e is the eth element density.

Therefore, instead of the original sensitivities provided in Equation 5.20, the modified sensitivities given in Equation 5.29 are used in the optimization process. Application of this filter into computer programming is straightforward and can be found in the literature [132, 133].

5.2. Natural Frequency Maximization

The dynamic topology optimization problems require mass matrix in addition to stiffness matrix. In addition they are computationally costly since they involve eigenvalue and eigenvector calculations. In this section, a dynamic topology optimization problem formulation is derived with a mass constraint employed in which γth natural frequency of the structure is maximized.

Here, again the modified SIMP [131] material interpolation scheme is used. In addition to element stiffness interpolation scheme given in Equation 5.1, an interpolation scheme for the physical density of an element is defined as:

$$\rho_e(x_e) = \rho_{min} + x_e^d(\rho_0 - \rho_{min}) \qquad\qquad x_e \in [0, 1] \tag{5.30}$$

where x_e is the density of element e, ρ_e is the physical density of element e, ρ_{min} is very small density value to prevent mass matrix singularity, ρ_0 is the density of the material, d is the penalization factor for mass. The material volume is defined as in Equation 5.2.

The γth natural frequency maximization problem can be represented as ω_γ^2 maximization. Equivalently, this can be expressed as $-\omega_\gamma^2$ minimization, as well. So, the γth natural frequency maximization (i.e., $-\omega_\gamma^2$ minimization) problem with mass constraint is written as [86]:

$$\begin{aligned} \text{minimize:} \quad & -\omega_\gamma^2(\boldsymbol{x}) = -\frac{\boldsymbol{u_\gamma^T K u_\gamma}}{\boldsymbol{u_\gamma^T M u_\gamma}} \\ \text{subject to:} \quad & \boldsymbol{K u_\gamma} - \omega_\gamma^2 \boldsymbol{M u_\gamma} = \boldsymbol{0} \\ & aV_0 - V(\boldsymbol{x}) \geq 0 \\ & x_e \geq 0 \qquad \text{for } e\text{=}1,2,\ldots..,N \\ & 1 - x_e \geq 0 \qquad \text{for } e\text{=}1,2,\ldots..,N \end{aligned} \tag{5.31}$$

where; $\omega_\gamma^2(\boldsymbol{x})$ is the square of γth natural frequency of the structure, $\boldsymbol{u_\gamma}$ is the γth global eigenvector, $\boldsymbol{K}$ is the global stiffness matrix, $\boldsymbol{M}$ is the global mass matrix, $\boldsymbol{x}$ is the vector of element densities (i.e., vector of design variables), N is the total number of finite elements used, a is the volume fraction that indicates the ratio between the material volume over design domain volume, and V_0 is the design domain volume.

Using Equation 5.1 the global stiffness matrix $\boldsymbol{K}$ is defined as:

$$\boldsymbol{K} = \sum_{e=1}^{N} E_e(x_e) \boldsymbol{K_0} \tag{5.32}$$

where $\boldsymbol{K_0}$ is the stiffness matrix of an element for unit Young's modulus, and the summation notation indicates the usual finite element notation to form global matrices from local matrices.

Similarly, using Equation 5.30 the global mass matrix $\boldsymbol{M}$ is defined as:

$$\boldsymbol{M} = \sum_{e=1}^{N} \rho_e(x_e) \boldsymbol{M_0} \tag{5.33}$$

where $\boldsymbol{M_0}$ is the mass matrix of an element for unit density, and the summation notation indicates the usual finite element notation to form global matrices from local matrices.

Defining Lagrangian for this optimization problem [102]:

$$\mathcal{L} = -\left(\frac{\boldsymbol{u_\gamma^T K u_\gamma}}{\boldsymbol{u_\gamma^T M u_\gamma}}\right) - \lambda_0(aV_0 - V(\boldsymbol{x})) - \boldsymbol{\lambda_1^T}(\boldsymbol{K u_\gamma} - \omega_\gamma^2 \boldsymbol{M u_\gamma}) - \boldsymbol{\lambda_2^T x} - \boldsymbol{\lambda_3^T}(\boldsymbol{1} - \boldsymbol{x}) \quad (5.34)$$

where; λ_0, $\boldsymbol{\lambda_1^T}$, $\boldsymbol{\lambda_2^T}$, $\boldsymbol{\lambda_3^T}$ are corresponding Lagrange multipliers. Writing necessary conditions for optimality for an element:

$$\frac{\partial \mathcal{L}}{\partial x_e} = 0 \qquad \text{for } e=1,2,\ldots..,N \quad (5.35)$$

Derivative of the lagrangian with respect to design variable x_e is:

$$\begin{aligned}\frac{\partial \mathcal{L}}{\partial x_e} = -\frac{\partial}{\partial x_e}\left(\frac{\boldsymbol{u_\gamma^T K u_\gamma}}{\boldsymbol{u_\gamma^T M u_\gamma}}\right) - \lambda_0 \frac{\partial}{\partial x_e}(aV_0 - V(\boldsymbol{x})) - \boldsymbol{\lambda_1^T}\frac{\partial}{\partial x_e}(\boldsymbol{K u_\gamma} - \omega_\gamma^2 \boldsymbol{M u_\gamma}) \\ -\boldsymbol{\lambda_2^T}\frac{\partial}{\partial x_e}(\boldsymbol{x}) - \boldsymbol{\lambda_3^T}\frac{\partial}{\partial x_e}(\boldsymbol{1} - \boldsymbol{x})\end{aligned} \quad (5.36)$$

As for the compliance minimization case, in order to derive the necessary optimality conditions from Equation 5.36, the adjoint method [142] is utilized here, as well.

Evaluating the derivatives in Equation 5.36 term by term:

$$-\boldsymbol{\lambda_2^T}\frac{\partial}{\partial x_e}(\boldsymbol{x}) = -\lambda_{2e} \quad (5.37)$$

$$-\boldsymbol{\lambda_3^T}\frac{\partial}{\partial x_e}(\boldsymbol{1} - \boldsymbol{x}) = \lambda_{3e} \quad (5.38)$$

where; λ_{2e} and λ_{3e} are the corresponding Lagrange multipliers of vectors $\boldsymbol{\lambda_2^T}$ and $\boldsymbol{\lambda_3^T}$, respectively. Assuming that the lower and upper bound constraints for x_e are not

active as for the case in compliance minimization problem [141], then:

$$\lambda_{2e} = 0 \qquad \text{and} \qquad \lambda_{3e} = 0 \tag{5.39}$$

Continuing with the evaluation of the derivative for the mass constraint in Equation 5.36:

$$-\lambda_0 \frac{\partial}{\partial x_e}(aV_0 - V(\boldsymbol{x})) = -\lambda_0 \frac{\partial}{\partial x_e}\left(aV_0 - \sum_{e=1}^{N} x_e\right) = \lambda_0 \tag{5.40}$$

The derivative of the left side term in Equation 5.36 is provided as:

$$-\frac{\partial}{\partial x_e}\left(\frac{\boldsymbol{u}_{\boldsymbol{\gamma}}^T \boldsymbol{K} \boldsymbol{u}_{\boldsymbol{\gamma}}}{\boldsymbol{u}_{\boldsymbol{\gamma}}^T \boldsymbol{M} \boldsymbol{u}_{\boldsymbol{\gamma}}}\right) = \frac{-2\boldsymbol{u}_{\boldsymbol{\gamma}}^T(\boldsymbol{K} - \omega_\gamma^2 \boldsymbol{M})\frac{\partial \boldsymbol{u}_{\boldsymbol{\gamma}}}{\partial x_e} - \boldsymbol{u}_{\boldsymbol{\gamma}}^T(\frac{\partial \boldsymbol{K}}{\partial x_e} - \omega_\gamma^2 \frac{\partial \boldsymbol{M}}{\partial x_e})\boldsymbol{u}_{\boldsymbol{\gamma}}}{(\boldsymbol{u}_{\boldsymbol{\gamma}}^T \boldsymbol{M} \boldsymbol{u}_{\boldsymbol{\gamma}})} \tag{5.41}$$

Since $\boldsymbol{K}$ and $\boldsymbol{M}$ matrices are both real and symmetric, to obtain the right side of the Eq.5.41 following relationships are used:

$$\frac{\partial \boldsymbol{u}_{\boldsymbol{\gamma}}^T}{\partial x_e} \boldsymbol{K} \boldsymbol{u}_{\boldsymbol{\gamma}} = \boldsymbol{u}_{\boldsymbol{\gamma}}^T \boldsymbol{K} \frac{\partial \boldsymbol{u}_{\boldsymbol{\gamma}}}{\partial x_e} \tag{5.42}$$

$$\frac{\partial \boldsymbol{u}_{\boldsymbol{\gamma}}^T}{\partial x_e} \boldsymbol{M} \boldsymbol{u}_{\boldsymbol{\gamma}} = \boldsymbol{u}_{\boldsymbol{\gamma}}^T \boldsymbol{M} \frac{\partial \boldsymbol{u}_{\boldsymbol{\gamma}}}{\partial x_e} \tag{5.43}$$

Moreover, according to the adjoint method [142] the free vibration equation is already satisfied, thus the following relationships are valid:

$$(\boldsymbol{K} - \omega_\gamma^2 \boldsymbol{M})\boldsymbol{u}_{\boldsymbol{\gamma}} = \boldsymbol{0} \tag{5.44}$$

$$\boldsymbol{u}_{\boldsymbol{\gamma}}^T(\boldsymbol{K} - \omega_\gamma^2 \boldsymbol{M}) = \boldsymbol{0}^T \tag{5.45}$$

where $\mathbf{0}^T$ denotes the transpose of a column vector whose elements are all 0 (zero).

Putting, Equation 5.45 in Equation 5.41 results in:

$$-\frac{\partial}{\partial x_e}\left(\frac{\boldsymbol{u_\gamma^T K u_\gamma}}{\boldsymbol{u_\gamma^T M u_\gamma}}\right) = \frac{-2(\mathbf{0}^T \frac{\partial \boldsymbol{u_\gamma}}{\partial x_e}) - \boldsymbol{u_\gamma^T}(\frac{\partial \boldsymbol{K}}{\partial x_e} - \omega_\gamma^2 \frac{\partial \boldsymbol{M}}{\partial x_e})\boldsymbol{u_\gamma}}{(\boldsymbol{u_\gamma^T M u_\gamma})} \tag{5.46}$$

Simplifying Equation 5.46 to get:

$$-\frac{\partial}{\partial x_e}\left(\frac{\boldsymbol{u_\gamma^T K u_\gamma}}{\boldsymbol{u_\gamma^T M u_\gamma}}\right) = -\frac{\boldsymbol{u_\gamma^T}(\frac{\partial \boldsymbol{K}}{\partial x_e} - \omega_\gamma^2 \frac{\partial \boldsymbol{M}}{\partial x_e})\boldsymbol{u_\gamma}}{(\boldsymbol{u_\gamma^T M u_\gamma})} \tag{5.47}$$

The Equation 5.47 is nothing but the non-repeated eigenvalue sensitivity that already exists in the literature [53,54,86,154], which is provided for the mass normalized eigenvector by the following formula:

$$\frac{\partial \omega_\gamma^2}{\partial x_e} = \boldsymbol{s_\gamma^T}\left(\frac{\partial \boldsymbol{K}}{\partial x_e} - \omega_\gamma^2 \frac{\partial \boldsymbol{M}}{\partial x_e}\right)\boldsymbol{s_\gamma} \tag{5.48}$$

where $\boldsymbol{s_\gamma}$ is the mass normalized eigenvector defined with the following equation:

$$\boldsymbol{s_\gamma} = \frac{\boldsymbol{u_\gamma}}{\sqrt{(\boldsymbol{u_\gamma^T M u_\gamma})}} \tag{5.49}$$

Then Equation 5.47 can be simplified by using Equations 5.48 and 5.49 as:

$$-\frac{\partial}{\partial x_e}\left(\frac{\boldsymbol{u_\gamma^T K u_\gamma}}{\boldsymbol{u_\gamma^T M u_\gamma}}\right) = -\frac{\partial \omega_\gamma^2}{\partial x_e} \tag{5.50}$$

Please note that, in the compliance minimization problem (see in Section 5.1), evaluation of the Lagrange multiplier $\boldsymbol{\lambda_1}$ is necessary since the $\partial \boldsymbol{u}/\partial x_e$ term still exists

for the objective function sensitivity expression (see Equation 5.11). However, in Equation 5.47, the $\partial \boldsymbol{u_\gamma}/\partial x_e$ term is already vanished. Therefore, the following statement can be directly used in Equation 5.36, since the free vibration equation is already satisfied and the Lagrange multiplier $\boldsymbol{\lambda_1}$ can be selected arbitrarily (via adjoint method [142]):

$$-\boldsymbol{\lambda_1}^T \frac{\partial}{\partial x_e}(\boldsymbol{K}\boldsymbol{u_\gamma} - \omega_\gamma^2 \boldsymbol{M}\boldsymbol{u_\gamma}) = 0 \tag{5.51}$$

Finally, putting the derivatives obtained in Equations 5.37, 5.38, 5.40, 5.50, 5.51 in Equation 5.36 and considering the Equation 5.35 and the result given in Equation 5.39, the necessary conditions for optimality are obtained as:

$$\frac{\partial \mathcal{L}}{\partial x_e} = 0 = -\frac{\partial \omega_\gamma^2}{\partial x_e} + \lambda_0 \qquad \text{for } e\text{=}1,2,\ldots..,N \tag{5.52}$$

Replacing Equation 5.48 in Equation 5.52 results in [54]:

$$\frac{\partial \mathcal{L}}{\partial x_e} = 0 = -\boldsymbol{s}_\gamma^T \left(\frac{\partial \boldsymbol{K}}{\partial x_e} - \omega_\gamma^2 \frac{\partial \boldsymbol{M}}{\partial x_e} \right) \boldsymbol{s_\gamma} + \lambda_0 \tag{5.53}$$

The derivative of the global stiffness matrix $\boldsymbol{K}$ is obtained by using the modified SIMP interpolation scheme given in Equation 5.1:

$$\frac{\partial \boldsymbol{K}}{\partial x_e} = \frac{\partial}{\partial x_e}(E_e(x_e)\boldsymbol{K_0}) \tag{5.54}$$

$$\frac{\partial \boldsymbol{K}}{\partial x_e} = \frac{\partial}{\partial x_e}\left((E_{min} + x_e^p(E_0 - E_{min}))\boldsymbol{K_0}\right) \tag{5.55}$$

$$\frac{\partial \boldsymbol{K}}{\partial x_e} = p x_e^{p-1}(E_0 - E_{min})\boldsymbol{K_0} \tag{5.56}$$

Similarly the derivative of the global mass matrix $\boldsymbol{M}$ is obtained by using the modified SIMP interpolation scheme given in Equation 5.30:

$$\frac{\partial \boldsymbol{M}}{\partial x_e} = \frac{\partial}{\partial x_e}(\rho_e(x_e)\boldsymbol{M_0}) \tag{5.57}$$

$$\frac{\partial \boldsymbol{M}}{\partial x_e} = \frac{\partial}{\partial x_e}\left((\rho_{min} + x_e^d(\rho_0 - \rho_{min}))\boldsymbol{M_0}\right) \tag{5.58}$$

$$\frac{\partial \boldsymbol{M}}{\partial x_e} = dx_e^{d-1}(\rho_0 - \rho_{min})\boldsymbol{M_0} \tag{5.59}$$

Putting Equations 5.56 and 5.59 into Equation 5.53 and taking into consideration that only the corresponding parts of the mass normalized eigenvector of $\boldsymbol{s_\gamma}$ do not vanish in the Equation 5.53 (as such in compliance minimization problem) then the necessary conditions for optimality are obtained finally in the explicit form as:

$$\frac{\partial \mathcal{L}}{\partial x_e} = 0 = -\boldsymbol{s_e}^T\left(px_e^{p-1}(E_0 - E_{min})\boldsymbol{K_0} - \omega_\gamma^2 dx_e^{d-1}(\rho_0 - \rho_{min})\boldsymbol{M_0}\right)\boldsymbol{s_e} + \lambda_0 \tag{5.60}$$

where $\boldsymbol{s_e}$ is the eth element's corresponding part of the mass normalized global eigenvector $\boldsymbol{s_\gamma}$.

As mentioned for the stiffness maximization (compliance minimization) problem, the dynamic topology optimization problem given in Equation 5.31 can be solved by using the optimality criteria method, as well. To that end, in order to employ OC method a new parameter (B_e) is defined for each element using the optimality conditions given in Equation 5.60:

$$B_e = \frac{\boldsymbol{s_e}^T\left(px_e^{p-1}(E_0 - E_{min})\boldsymbol{K_0} - \omega_\gamma^2 dx_e^{d-1}(\rho_0 - \rho_{min})\boldsymbol{M_0}\right)\boldsymbol{s_e}}{\lambda_0} \tag{5.61}$$

The parameter B_e can also be represented as the following when considering Equation 5.53 and Equation 5.48:

$$B_e = \frac{\partial \omega_\gamma^2 / \partial x_e}{\lambda_0} \tag{5.62}$$

The sensitivities in Equation 5.62 (or equivalently in Equation 5.61) can take negative as well as positive values [86, 155]. Since the Lagrange multiplier of the mass constraint (λ_0) is positive, negative sensitivities result in negative B_e values. When using negative B_e values in the resizing formula mentioned in Equation 5.25, updated design values could be either negative or complex. And this case is not valid since x_e values are allowed to take values between 0 and 1. Thus, in order to prevent this numerical error scheme a slight modification on B_e values shown in Equation 5.62 (or equivalently in Equation 5.61) is performed following the work in [86], to ensure that the B_e values are always positive:

$$B_e = \frac{max\left(0, \partial \omega_\gamma^2 / \partial x_e\right)}{\lambda_0} \tag{5.63}$$

This topology optimization problem can readily be solved by the procedure mentioned previously in Section 5.1. Detailed formulations and derivations can be found in that section. Here, procedure will be just briefly explained: Using the parameter B_e given in Equation 5.63, design variables are updated using the resizing formula given in Equation 5.25. For the computer implementation, a heuristic updating scheme given in Equation 5.26 can be used. In order to prevent numerical instabilities to occur, sensitivity filtering formulation given in Equation 5.29 can be utilized. Moreover, the Lagrange multiplier λ_0 in Equation 5.63 can be found by the bisection algorithm as discussed in Section 5.1.

Similar to the compliance minimization topology optimization problems, the eigenvalue maximization problems also suffer from mesh dependency, checkerboard pattern formation and local minima. However, as in the compliance minimization case,

usage of mesh independent filters, such as sensitivity filtering, prevent the numerical problems mentioned in Section 5.1 to occur in dynamic topology optimization problems. But, eigenvalue topology optimization problems are still prone to two more important problems namely "localized modes" and "repeated eigenvalues".

Localized modes are the artificial modes that occur in design domain where element densities are at minimum or close to minimum [156]. In the SIMP model, if the penalization factors for stiffness and mass are chosen such that for the elements with low densities have relatively large mass to stiffness ratios, then localized modes occur [86, 157]. To get rid of these artificial modes, a high penalization factor for mass is employed for elements with low densities [54, 156, 157]. On the other hand, employment of high mass penalization for the elements with intermediate densities results in wrong resonance frequency values of the structure [156]. The localized modes can be discarded by employing a high mass penalization to low density elements. In order to prevent localized modes while avoiding wrong calculations, a physical density modification derived from [54] is used as follows:

$$\rho_e(x_e) = \begin{cases} \rho_{min} + x_e(\rho_0 - \rho_{min}) & \text{if } x_e > 0.1 \\ \rho_{min} + x_e^d(\rho_0 - \rho_{min}) & \text{if } x_e \leq 0.1 \end{cases} \tag{5.64}$$

The other problematic issue with eigenvalue (eigenfrequency) topology optimization problems is the repeated (multiple) eigenvalues. It is a problem since sensitivities of the repeated eigenvalues cannot be obtained by using Equation 5.48. The reason for that is the non-differentiability of repeated eigenvalues [54, 158]. The non-differentiability of the repeated eigenvalues stem from the fact that they have at least two distinct eigenvectors [142]. Although, at the initial stages of the optimization procedure eigenvalues are distinct, they coincide with the nearest eigenvalue(s) as iterations proceeds. Thus, creation of repeated eigenvalues is a rule rather than an

exception [54]. So taking into account the repeated eigenvalues are inevitable in the dynamic topology optimization process. To that end, it is necessary to formulate the correct sensitivities for repeated eigenvalues.

Eigenvectors of multiple eigenvalues are not unique. Besides, any linear combination of these eigenvectors is also an eigenvector. Considering this, a general method is suggested in [158] to find the repeated eigenvalue sensitivities. In that method, for each design variable (x_e), a subeigenvalue problem is formed utilizing linear combination of eigenvectors that correspond to the repeated eigenvalue. The solution of this mini eigenvalue-eigenvector problem provides the correct sensitivities, together with the proper eigenvector combinations. Following the most general case in [158], a procedure, which finds the sensitivities of multiple eigenvalues with two distinct eigenvectors, is provided in [53]. Here, the procedure given in [53] is shown:

The eigenvectors of double eigenfrequency are mass orthonormalized as such:

$$\boldsymbol{v_1}^T \boldsymbol{M} \boldsymbol{v_1} = 1 \tag{5.65}$$

$$\boldsymbol{v_2}^T \boldsymbol{M} \boldsymbol{v_2} = 1 \tag{5.66}$$

$$\boldsymbol{v_1}^T \boldsymbol{M} \boldsymbol{v_2} = 0 \tag{5.67}$$

Defining generalized gradients for double eigenvalue:

$$g_{\alpha\beta} = \boldsymbol{v_\alpha}^T \left(\frac{\partial \boldsymbol{K}}{\partial x_e} - \omega_\gamma^2 \frac{\partial \boldsymbol{M}}{\partial x_e} \right) \boldsymbol{v_\beta} \qquad \text{for } \alpha = 1,2 \text{ and } \beta = 1,2 \tag{5.68}$$

Obtaining a new 2×2 eigenvalue problem as such:

$$\begin{bmatrix} g_{11} & g_{12} \\ g_{21} & g_{22} \end{bmatrix} \begin{bmatrix} c_1 \\ c_2 \end{bmatrix} = \begin{bmatrix} 0 \\ 0 \end{bmatrix} \tag{5.69}$$

Solving Equation 5.69 for the eigenvalues (g_a,g_b) and the eigenvectors ($\boldsymbol{c_a}$,$\boldsymbol{c_b}$) where $\boldsymbol{c_a}$ and $\boldsymbol{c_b}$ are given as:

$$\boldsymbol{c_a}^T = (c_{a1}, c_{a2}) \tag{5.70}$$

$$\boldsymbol{c_b}^T = (c_{b1}, c_{b2}) \tag{5.71}$$

Finally sensitivities for the double eigenfrequency are obtained as:

$$\frac{\partial \omega_\gamma^2}{\partial x_e} = \begin{cases} g_a & \text{with eigenvector } \boldsymbol{v_a} = c_{a1}\boldsymbol{v_1} + c_{a2}\boldsymbol{v_2} \\ g_b & \text{with eigenvector } \boldsymbol{v_b} = c_{b1}\boldsymbol{v_1} + c_{b2}\boldsymbol{v_2} \end{cases} \tag{5.72}$$

In the optimality criteria method design sensitivities should be positive, thus greater sensitivity value in Equation 5.72 (i.e., $\max(g_a,g_b)$) can be chosen as the desired design sensitivity. Numerical studies performed so far also confirm this procedure. In numerical computations, when the difference between the successive eigenfrequencies are less than a predefined small tolerance value then these eigenfrequencies are considered as multiple [54, 158]. In the numerical studies, it was observed that the optimality criteria method is prone to this repeated eigenvalue problem. Thus, in order to formulate the optimization process considering the multiple eigenfrequencies, repeated eigenvalue definition is updated such that the structure's $(\gamma+1)$th resonance frequency would be some percentage higher than the structure's γth resonance frequency [86].

5.3. Frequency Gap Maximization

The topology optimization problem for frequency gap maximization is stated as the maximization of the ratio between any of the two sequential natural frequencies (ω_γ and $\omega_{\gamma+1}$) of the structure [53]:

$$
\begin{aligned}
\text{minimize:} \quad & -\frac{\omega_{\gamma+1}^2(\boldsymbol{x})}{\omega_{\gamma}^2(\boldsymbol{x})} \\
\text{subject to:} \quad & \boldsymbol{K}\boldsymbol{u_\gamma} - \omega_\gamma^2 \boldsymbol{M}\boldsymbol{u_\gamma} = \boldsymbol{0} \\
& \boldsymbol{K}\boldsymbol{u_{\gamma+1}} - \omega_{\gamma+1}^2 \boldsymbol{M}\boldsymbol{u_{\gamma+1}} = \boldsymbol{0} \\
& aV_0 - V(\boldsymbol{x}) \geq 0 \\
& x_e \geq 0 \qquad \text{for } e\text{=1,2,.....,}N \\
& 1 - x_e \geq 0 \qquad \text{for } e\text{=1,2,.....,}N
\end{aligned}
\tag{5.73}
$$

where; $\omega_\gamma^2(\boldsymbol{x})$ is the square of γth natural frequency of the structure, $\omega_{\gamma+1}^2(\boldsymbol{x})$ is the square of $(\gamma+1)$th natural frequency of the structure, $\boldsymbol{u_\gamma}$ is the γth global eigenvector, $\boldsymbol{u_{\gamma+1}}$ is the $(\gamma+1)$th global eigenvector, $\boldsymbol{K}$ is the global stiffness matrix, $\boldsymbol{M}$ is the global mass matrix, $\boldsymbol{x}$ is the vector of element densities (i.e., vector of design variables), N is the total number of finite elements used, a is the volume fraction that indicates the ratio between the material volume over design domain volume, V_0 is the design domain volume.

Again, modified SIMP material interpolation schemes for element stiffness (see Equation 5.1) and physical density (see Equation 5.64) are used. The global stiffness matrix $\boldsymbol{K}$ is constructed via Equation 5.32 and the global mass matrix $\boldsymbol{M}$ is constructed via Equation 5.33. Additionally, total solid material volume is described with Equation 5.2.

The Lagrangian for this optimization problem is written as [102]:

$$
\begin{aligned}
\mathcal{L} = -\frac{\omega_{\gamma+1}^2(\boldsymbol{x})}{\omega_\gamma^2(\boldsymbol{x})} - \lambda_0(aV_0 - V(\boldsymbol{x})) - \boldsymbol{\lambda_1}^T(\boldsymbol{K}\boldsymbol{u_\gamma} - \omega_\gamma^2\boldsymbol{M}\boldsymbol{u_\gamma}) - \boldsymbol{\lambda_2}^T\boldsymbol{x} \\
-\boldsymbol{\lambda_3}^T(\boldsymbol{1} - \boldsymbol{x}) - \boldsymbol{\lambda_4}^T(\boldsymbol{K}\boldsymbol{u_{\gamma+1}} - \omega_{\gamma+1}^2\boldsymbol{M}\boldsymbol{u_{\gamma+1}})
\end{aligned}
\tag{5.74}
$$

where; λ_0, $\boldsymbol{\lambda_1}^T$, $\boldsymbol{\lambda_2}^T$, $\boldsymbol{\lambda_3}^T$, $\boldsymbol{\lambda_4}^T$ are corresponding Lagrange multipliers.

The necessary conditions for optimality are:

$$\frac{\partial \mathcal{L}}{\partial x_e} = 0 \qquad \text{for } e=1,2,\ldots..,N \tag{5.75}$$

The derivative of the Lagrangian in Equation 5.74 with respect to design variable x_e is:

$$\begin{aligned}\frac{\partial \mathcal{L}}{\partial x_e} = -\frac{\partial}{\partial x_e}\left(\frac{\omega_{\gamma+1}^2(\boldsymbol{x})}{\omega_\gamma^2(\boldsymbol{x})}\right) - \lambda_0 \frac{\partial}{\partial x_e}(aV_0 - V(\boldsymbol{x})) - \boldsymbol{\lambda_1}^T \frac{\partial}{\partial x_e}(\boldsymbol{K u_\gamma} - \omega_\gamma^2 \boldsymbol{M u_\gamma}) \\ -\boldsymbol{\lambda_2}^T \frac{\partial}{\partial x_e}(\boldsymbol{x}) - \boldsymbol{\lambda_3}^T \frac{\partial}{\partial x_e}(\boldsymbol{1} - \boldsymbol{x}) - \boldsymbol{\lambda_4}^T \frac{\partial}{\partial x_e}(\boldsymbol{K u_{\gamma+1}} - \omega_{\gamma+1}^2 \boldsymbol{M u_{\gamma+1}})\end{aligned} \tag{5.76}$$

Considering Equation 5.76, the objective function sensitivity is given by the following expression:

$$-\frac{\partial}{\partial x_e}\left(\frac{\omega_{\gamma+1}^2}{\omega_\gamma^2}\right) = -\left(\frac{1}{\omega_\gamma^2}\frac{\partial \omega_{\gamma+1}^2}{\partial x_e} - \frac{\omega_{\gamma+1}^2}{\omega_\gamma^4}\frac{\partial \omega_\gamma^2}{\partial x_e}\right) \tag{5.77}$$

Since, it was already shown in Equations 5.48 and 5.49 that, the sensitivities $\partial\omega_\gamma^2/\partial x_e$ and $\partial\omega_{\gamma+1}^2/\partial x_e$ are independent of $\partial \boldsymbol{u_\gamma}/\partial x_e$ or $\partial \boldsymbol{u_{\gamma+1}}/\partial x_e$ terms, the adjoint method [142] procedure followed in Section 5.2 can also be employed here. To that end, the necessary derivatives in Equation 5.76 can be obtained by utilizing Equations 5.37, 5.38, 5.39, 5.40, and 5.51. As a result, the necessary conditions for optimality are found as:

$$\frac{\partial \mathcal{L}}{\partial x_e} = 0 = -\frac{\partial}{\partial x_e}\left(\frac{\omega_{\gamma+1}^2}{\omega_\gamma^2}\right) + \lambda_0 \qquad \text{for } e=1,2,\ldots..,N \tag{5.78}$$

or equivalently:

$$\frac{\partial \mathcal{L}}{\partial x_e} = 0 = -\left(\frac{1}{\omega_\gamma^2}\frac{\partial \omega_{\gamma+1}^2}{\partial x_e} - \frac{\omega_{\gamma+1}^2}{\omega_\gamma^4}\frac{\partial \omega_\gamma^2}{\partial x_e}\right) + \lambda_0 \qquad \text{for } e=1,2,\ldots..,N \tag{5.79}$$

Hence, the B_e parameter for OC method is defined as:

$$B_e = \frac{\frac{\partial}{\partial x_e}\left(\frac{\omega_{\gamma+1}^2}{\omega_\gamma^2}\right)}{\lambda_0} \tag{5.80}$$

Similar to the natural frequency maximization problems, the sensitivities can take positive or negative values for the frequency gap maximization problems, as well. Thus, because of the reasoning mentioned in Section 5.2, B_e parameter is also modified here similar to Equation 5.63 as:

$$B_e = \frac{max\left(0, \frac{\partial}{\partial x_e}\left(\frac{\omega_{\gamma+1}^2}{\omega_\gamma^2}\right)\right)}{\lambda_0} \tag{5.81}$$

Since, the necessary sensitivity expressions and OC method update parameter are now available, the general procedure presented in Section 5.2 can be followed to obtain topologically optimized structures with maximized frequency gap. To that end, after the design sensitivities are calculated, they are modified with sensitivity filtering (see Section 5.1). Then, B_e parameters for each element are calculated with the filtered sensitivities in Equation 5.81 where the Lagrange multiplier for the mass constraint (λ_0) is found by a bisection algorithm [132,133]. Finally, the calculated B_e parameters are used in Equation 5.26 to calculate the new element densities attained at the end of that iteration. In the case of repeated eigenvalues, the procedure described at the end of the Section 5.2 is applied. The entire process is repeated until the convergence criterion is met.

On the other hand, to obtain topologically optimized structures that maximize frequency gap, alternative objective functions such as ($\omega_{\gamma+1}/\omega_\gamma$) or ($\omega_{\gamma+1}$-$\omega_\gamma$) maximization [53], can also be employed. In those cases, design sensitivities are determined by:

$$\frac{\partial}{\partial x_e}\left(\frac{\omega_{\gamma+1}}{\omega_\gamma}\right) = \frac{1}{2\omega_\gamma}\left(\frac{1}{\omega_{\gamma+1}}\frac{\partial\omega_{\gamma+1}^2}{\partial x_e} - \frac{\omega_{\gamma+1}}{\omega_\gamma^2}\frac{\partial\omega_\gamma^2}{\partial x_e}\right) \tag{5.82}$$

$$\frac{\partial}{\partial x_e}\left(\omega_{\gamma+1} - \omega_\gamma\right) = \frac{1}{2}\left(\frac{1}{\omega_{\gamma+1}}\frac{\partial\omega_{\gamma+1}^2}{\partial x_e} - \frac{1}{\omega_\gamma}\frac{\partial\omega_\gamma^2}{\partial x_e}\right) \tag{5.83}$$

where, the values for $\partial\omega_\gamma^2/\partial x_e$ and $\partial\omega_{\gamma+1}^2/\partial x_e$ derivatives are obtained from Equations 5.48 and 5.49. The same solution procedure, which is employed throughout Sections 5.2 and 5.3, is still valid for the topology optimization problems proposed with these alternative objective functions.

6. TOPOLOGY OPTIMIZATION OF INERTIAL AMPLIFICATION INDUCED PHONONIC BAND GAP STRUCTURES

So far, size and shape optimization is performed on inertial amplification mechanisms to enhance phononic band gap characteristics. This chapter addresses the improvements achieved in band gap limits by employing topology optimization on inertial amplification mechanisms. To that end, size and topology optimization studies are conducted on an inertial amplification mechanism and results are discussed.

6.1. Structural Optimization Problems

Previously [61] it was shown that, when beam elements are employed, the inertial amplification induced phononic band gap occurs between ω_s (see Equation 2.14) and the second natural frequency (ω_2) of the mechanism shown in Figure 2.3. However, it was also demonstrated in those studies that, the first and second natural frequencies (ω_1 and ω_2) closely resemble the band gap limits. Moreover, in the literature it is shown that the ω_2/ω_1 ratio maximization corresponds to a way of maximizing the band width [53]. In this study, band gap limits are considered as ω_2 and ω_1. Besides, ω_2/ω_1 ratio is maximized.

The structural optimizations are performed via finite elements method, therefore the distributed parameter mechanism shown in Figure 2.3 needs to be discretized accordingly. To that end, two dimensional four node eight degrees of freedom square plane stress finite elements are employed. The finite element models of the inertial amplification mechanism are constructed in a $nelx \times nely$ domain represented in Figure 6.1, where $nelx$ and $nely$ denote the total number of finite elements in the horizontal and vertical axes, respectively.

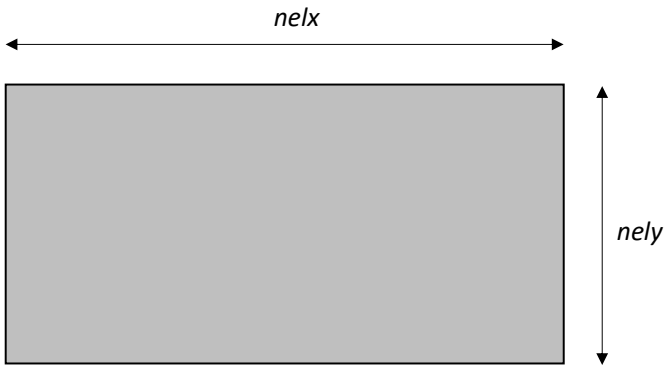


Figure 6.1. Finite element design space dimensions used in structural optimization studies. ($\max(nelx) = 100$ elements, $\max(nely) = 50$ elements.).

In the numerical studies, a workstation that has 24 GB RAM and 2 processors with 4 cores operating at 2.67 GHz is used. MATLAB is used to create finite element models and to perform the necessary optimization routines. In large dynamic problems, eigenvalue and eigenvector calculations require high memory allocations which in turn result in long run times. Balanced design domain dimensions should be selected to conclude optimization process in reasonable run times while capturing the details of the optimized mechanisms. For this reason, the maximum number of elements allowed in the horizontal and vertical axes are selected as 100 and 50, respectively.

A one dimensional inertial amplification induced phononic band gap structure can be obtained by using the mechanism shown in Figure 2.3 periodically. Herein, the beams enumerated as 1 are the connection parts of the periodic structure. Small but not very small dimensions (4 elements $\times$ 4 elements) can be assigned for these parts which yields a large effective design area while ensuring connectivity of the periodic structure. Therefore, beams enumerated as 1 are dismissed from the structural optimization procedure. Moreover, the thin compliant hinges that are enumerated as 2 and 4 are also omitted in the structural optimization since the proper length/thickness ratios, which lead large frequency gap without causing excessive stresses, are determined previously as 5 [61]. Thereof, the size and the topology optimization studies are performed only on the beams enumerated as 3 in Figure 2.3.

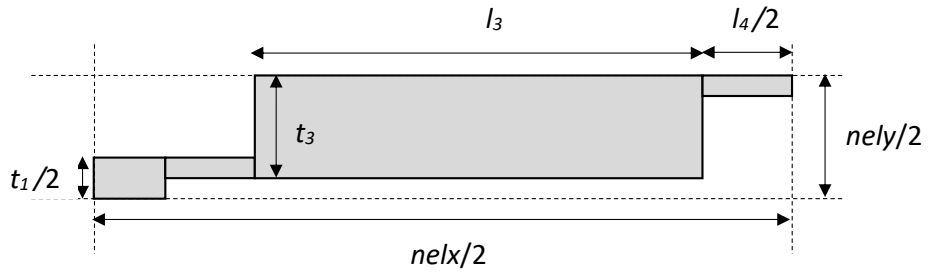


Figure 6.2. One quarter of the distributed parameter inertial amplification mechanism. Here, t_3 and l_3 are the design variables of the size optimization problem.

6.1.1. Size Optimization Problem

The primary design constraint for numerical studies is the mesh size which is allowed to be 100×50 at maximum. The finite element mesh consists of square finite elements with equal dimensions, thus an individual finite element can be regarded as a pixel. Therefore, the size optimization problem can be stated as the determination of the pixel numbers used to construct the 3rd beam where the design variables (l_3 and t_3) can be seen in Figure 6.2. Eventually, size optimization problem becomes a discrete optimization problem in which the optimum pixel numbers for l_3 and t_3 need to be determined. In the size optimization, minimum pixel number that l_3 and t_3 can take is determined as 2; whereas maximum pixel number for l_3 and t_3 depends on l_1, l_2, l_4, t_1, t_2 values. Herein, the size optimization problem that maximizes the band gap width is stated as:

$$
\begin{aligned}
\max._{\,l_3,t_3} \quad & \frac{\omega_2}{\omega_1} && (6.1)\\
\text{s.t.} \quad & \boldsymbol{K u_1} = \omega_1^2 \boldsymbol{M u_1} \\
& \boldsymbol{K u_2} = \omega_2^2 \boldsymbol{M u_2} \\
& 2 \leq t_3 \leq 25 - t_1/2 + t_2 \qquad t_3 \in \mathbb{Z}^+ \\
& 2 \leq l_3 \leq 50 - l_1 - l_2 - l_4/2 \qquad l_3 \in \mathbb{Z}^+
\end{aligned}
$$

where; $\boldsymbol{K}$ denotes the global stiffness matrix, $\boldsymbol{M}$ denotes the global mass matrix, $\boldsymbol{u_1}$ and $\boldsymbol{u_2}$ denote the 1st and 2nd mode shape vectors, ω_1 and ω_2 denote the 1st and 2nd natural frequencies of the structure.

6.1.2. Topology Optimization Problem

Topology optimization can be defined as finding the optimal material layout in the design space that minimizes (or maximizes) a certain objective function subject to some prescribed design constraints. In this study, modified SIMP [131] (Solid Isotropic Material with Penalization) method is used as the material interpolation scheme for topology optimization studies. In this method, an individual finite element's (i.e., a design variable's) stiffness property is given by Equation 5.1 and physical density is defined by Equation 5.64. Moreover, global stiffness ($\boldsymbol{K}$) and mass ($\boldsymbol{M}$) matrices are constructed by using Equations 5.32 and 5.33.

The objective of the topology optimization problem is maximization of the band gap width. To that end, $-\omega_2/\omega_1$ is minimized. Since the goal of this study is to observe the improvements achieved in the band gap width, a mass constraint is defined so that the size and topologically optimized mechanisms' masses are the same. The topology optimization problem with all constraints is defined as:

$$\begin{aligned} \text{min.}_{\ \boldsymbol{x}} \quad & f(\boldsymbol{x}) = -\frac{\omega_2(\boldsymbol{x})}{\omega_1(\boldsymbol{x})} \\ \text{s.t.} \quad & \boldsymbol{K}\boldsymbol{u_1} = \omega_1^2 \boldsymbol{M}\boldsymbol{u_1} \\ & \boldsymbol{K}\boldsymbol{u_2} = \omega_2^2 \boldsymbol{M}\boldsymbol{u_2} \\ & V(\boldsymbol{x}) = aV_0 \\ & 0 \leq x_e \leq 1 \qquad \text{for } e = 1, 2, ..., N \end{aligned} \tag{6.2}$$

where $\boldsymbol{x}$ is the vector which consists of individual element density values (x_es), V is the total isotropic solid material amount which is equal to the sum of all individual element density (x_e) values, V_0 denotes the total design space area, a denotes the volume fraction defined as the ratio of solid area over total area. Here, aV_0 value will

be declared by the size optimization study since the aim is to observe the band width improvements achieved with topology optimization under the same mass condition.

The topology optimization problem given in Equation 6.2 is solved with optimality criteria (OC) method by modifying an open source MATLAB code [132] which is provided for static topology optimization studies. To that end, a parameter (B_e) that is used in OC update scheme is defined by utilizing design sensitivities [86]:

$$B_e = \frac{max\left(0, \partial f(\boldsymbol{x})/\partial x_e\right)}{\lambda} \tag{6.3}$$

where; λ denotes the Lagrange multiplier for the mass constraint which can be found by a bisection algorithm [132]. The parameter B_e is used to update the element density values according to Equation 5.26.

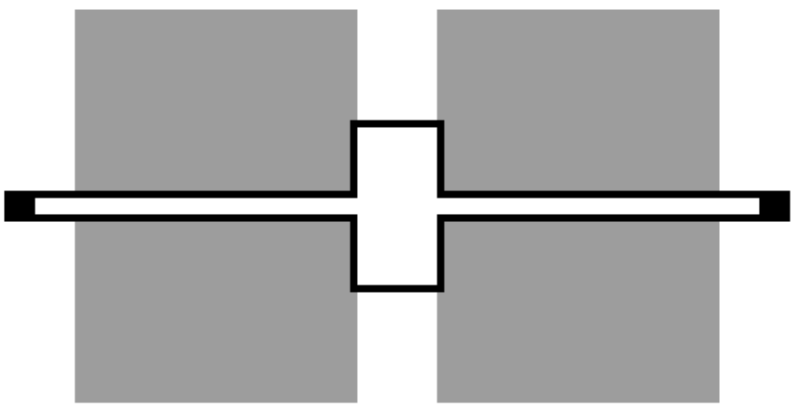


Figure 6.3. Topology optimization design space. Grey regions indicate the active region where the topology is allowed to change.

The topology optimization design space is shown in Figure 6.3. In this design domain, grey areas are the active areas where the topology is allowed to change. Black areas indicate fully solid parts, whereas white areas are void. On the periphery of the 3rd beams, passive fully solid supports are included to avoid one node connected hinges [131] at the end of the optimization procedure. To deal with checkerboard pattern formation and mesh dependency issues [121], sensitivity filtering technique

[128, 129] presented in Section 5.1 is employed. To tackle with the repeated eigenvalue problem [158], the procedure suggested in Section 5.2 [53] is utilized. At the end of the optimization procedure, the element densities are adjusted with a post processing filter [90], to ensure solid or void type of design.

6.2. Numerical Results

The isotropic material properties used in the numerical studies are provided in Table 6.1. In order to have a manufacturable design, minimum thickness of the beams is considered as 1 mm. Second and fourth beams' length/thickness ratios are determined via previous study [61] to take into account the trade off between the band gap maximization and excessive stress formation within the body. Finally, first beam dimensions are determined by noticing connectivity issues of a manufacturable periodic structure. An individual finite element's dimensions are determined as 1 mm by 1 mm. As a result of these considerations, the fixed parameters can be seen in Table 6.2.

Table 6.1. Isotropic material properties used in the numerical studies.

Elastic Modulus (E_0)	Density (ρ_0)	Poisson's Ratio (ν)
210 GPa	7800 kg/m^3	0.3

Table 6.2. Fixed beam parameters used in the numerical studies.

l_1	t_1	l_2	t_2	l_4	t_4
4 mm	4 mm	5 mm	1 mm	10 mm	1 mm

6.2.1. The Size Optimized Mechanism

The size optimization problem stated in Equation 6.1 is solved for the specified parameters and the design in Figure 6.4 is attained. The design variables are found

as: $l_3 = 36$ mm and $t_3 = 10$ mm. The size optimized mechanism's first three mode shapes are given in Figure 6.5. Accordingly the first natural frequency (f_1) is found at 368.7 Hz, the second natural frequency (f_2) is found at 1590.4 Hz and the third natural frequency (f_3) is found at 1641.4 Hz. With these results, ω_2/ω_1 ratio is calculated as 4.31.

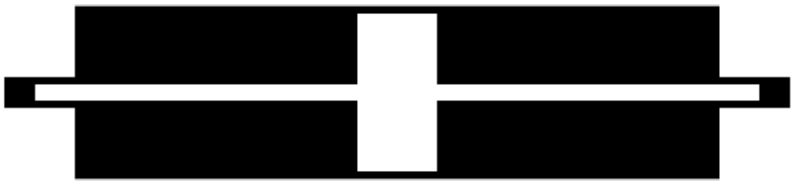


Figure 6.4. The size optimized inertial amplification mechanism. $l_3 = 36$ mm, $t_3 = 10$ mm, $\omega_2/\omega_1 = 4.31$.

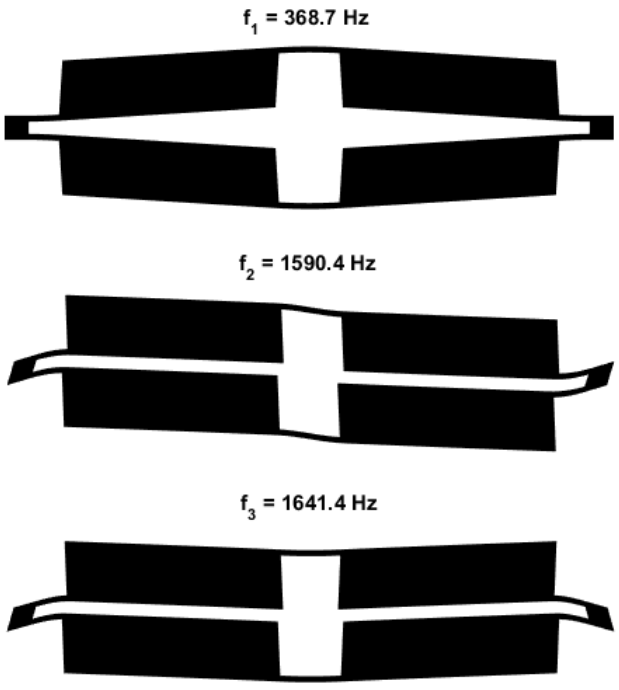


Figure 6.5. The first three mode shapes of the size optimized inertial amplification mechanism.

The size optimized mechanism is used as a unit cell in the finite periodic structure in order to reduce the transmitted vibration in the band gap frequency range. For that

purpose, several finite periodic structures are formed by using various number of unit cells to observe how number of mechanisms improves the achieved vibration isolation level. A representative one dimensional finite periodic structure that consists of three inertial amplification mechanisms is shown in Figure 6.6. The vibration transmissibilities of structures that consist of one, three and six size optimized mechanisms are provided in Figure 6.7. Accordingly, it is found that; when one unit cell is employed at least 14%, when three unit cells are employed at least 50%, and when six unit cells are employed at least 87% of input vibration cannot reach the output end. Moreover, the stop band occurs between 368.7 Hz and 1590.4 Hz, which are the first and second natural frequencies of the size optimized mechanism.



Figure 6.6. One dimensional periodic structure that consists of three size optimized inertial amplification mechanisms.

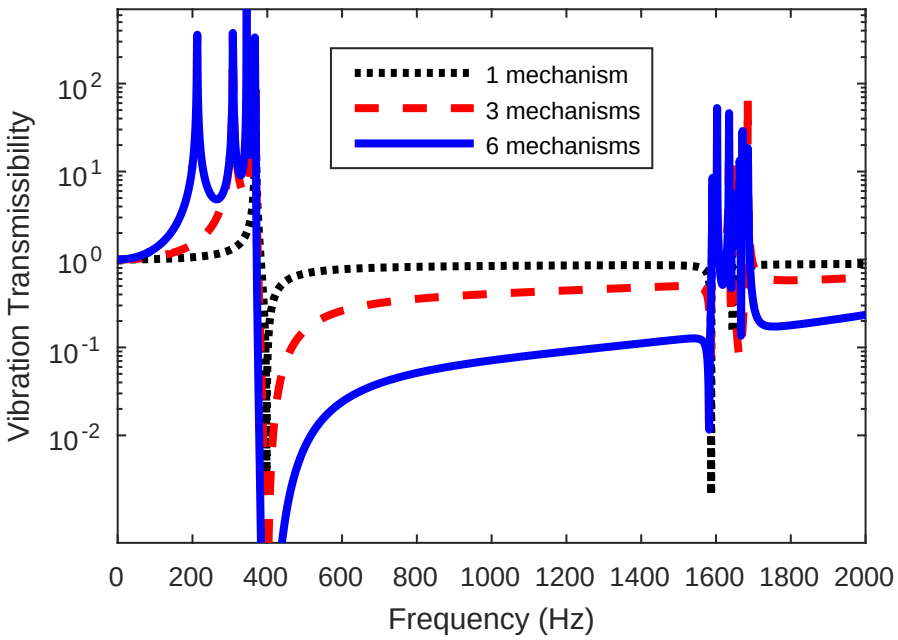


Figure 6.7. Vibration transmissibility of periodic structures consisting of several number of size optimized unit cells.

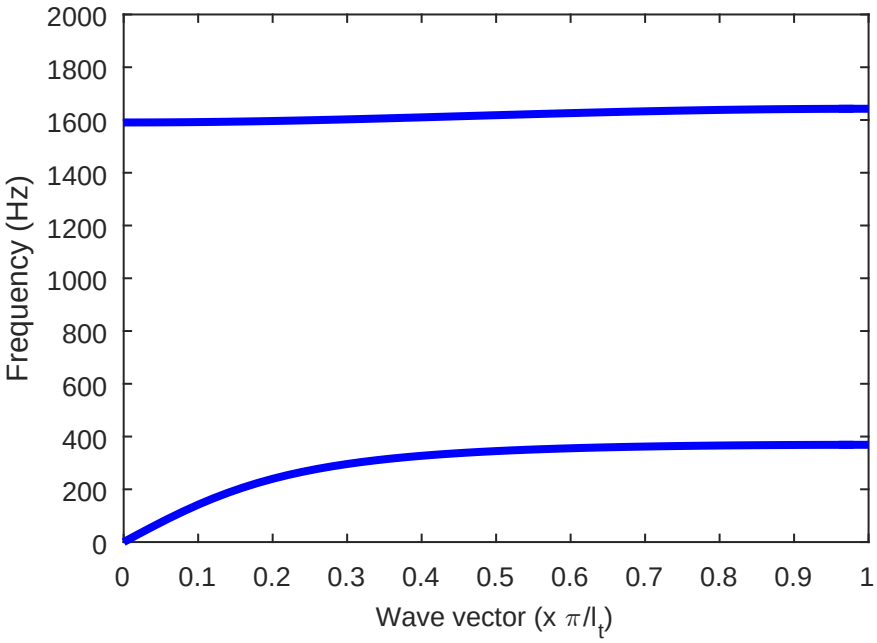


Figure 6.8. Band structure of the infinitely periodic size optimized unit cells.

When the size optimized mechanism is used to form an infinitely periodic one dimensional structure, there will be no vibration transmission to the output end [38]. In order to observe the phononic band gap limits for the infinitely periodic structure constructed with size optimized unit cell mechanisms, the band structure provided in Figure 6.8 is calculated by employing periodic boundary conditions on a unit cell mechanism [159]. These results also validate the previous findings, i.e., inertial amplification induced phononic band gap occurs between 368.7 Hz and 1590.4 Hz frequency range.

6.2.2. The Topologically Optimized Mechanism

In addition to provided fixed beam and material properties, more parameters need to be defined to solve the topology optimization problem stated in Equation 6.2: The penalty number for stiffness (p) presented in Equation 5.1 is taken as 3 [54]. Whereas, the penalty number for mass (d) given in Equation 5.64 is taken as 6 [54]. In Equation 5.1, E_{min} is taken as $E_0 \times 10^{-9}$ [132]. Same approach is employed in Equation 5.64, where ρ_{min} is taken as $\rho_0 \times 10^{-9}$. In Equation 5.26, η is taken as 1/2 [132]. As a result of performed dynamic topology optimization studies, the move limit (ml) in

Equation 5.26 is determined as 0.02. The sensitivity filter radius is selected as 3. If the difference between the 3rd and the 2nd natural frequencies of the structure is found to be smaller than a predetermined percentage, these are counted as repeated eigenvalues as suggested in [86]. According to numerical studies, this percentage is determined as 0.5%. The topology optimization design space dimensions are 100×50 elements. Optimization process starts from the initial design provided in Figure 6.3, where element densities (x_es) in grey regions all have the same initial density value which satisfies the mass constraint (i.e., the topologically optimized design has the same mass with the size optimized one). The fourth thin beam's connection location to the third beam is accepted to be the same as the size optimized mechanism. Iterations are concluded, if the difference between the ω_2/ω_1 values of the two successive designs are less than 0.1%.

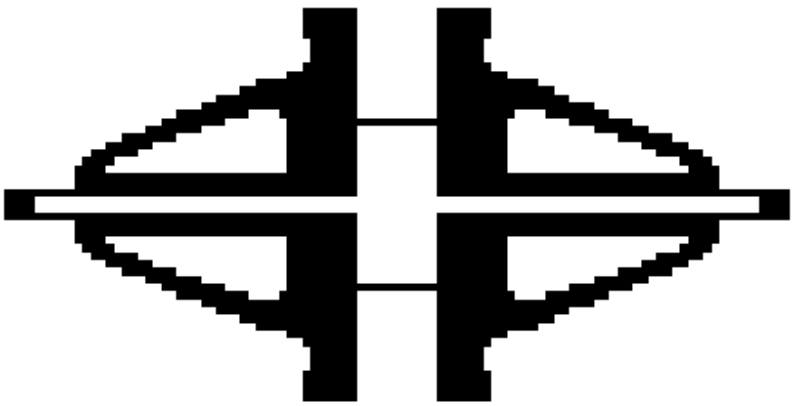


Figure 6.9. The topologically optimized inertial amplification mechanism. ($\omega_2/\omega_1 = 6.07$).

According to these specifications, topologically optimized mechanism shown in Figure 6.9 is obtained. The first three mode shapes of this topologically optimized inertial amplification mechanism are shown in Figure 6.10. Accordingly, the first natural frequency (f_1) is found at 304.4 Hz, the second natural frequency (f_2) is found at 1847.7 Hz and the third natural frequency (f_3) is found at 1865.3 Hz. With these results, ω_2/ω_1 ratio is calculated as 6.07, which is 41% larger than the value obtained through size optimization. Moreover, as a result of topology optimization, the first

natural frequency (i.e., band gap starting frequency) is lowered by 17% and the second natural frequency (i.e., band gap ending frequency) is increased by 16% for the same mass. The band gap limits of the size and the topologically optimized mechanisms are provided in Table 6.3.

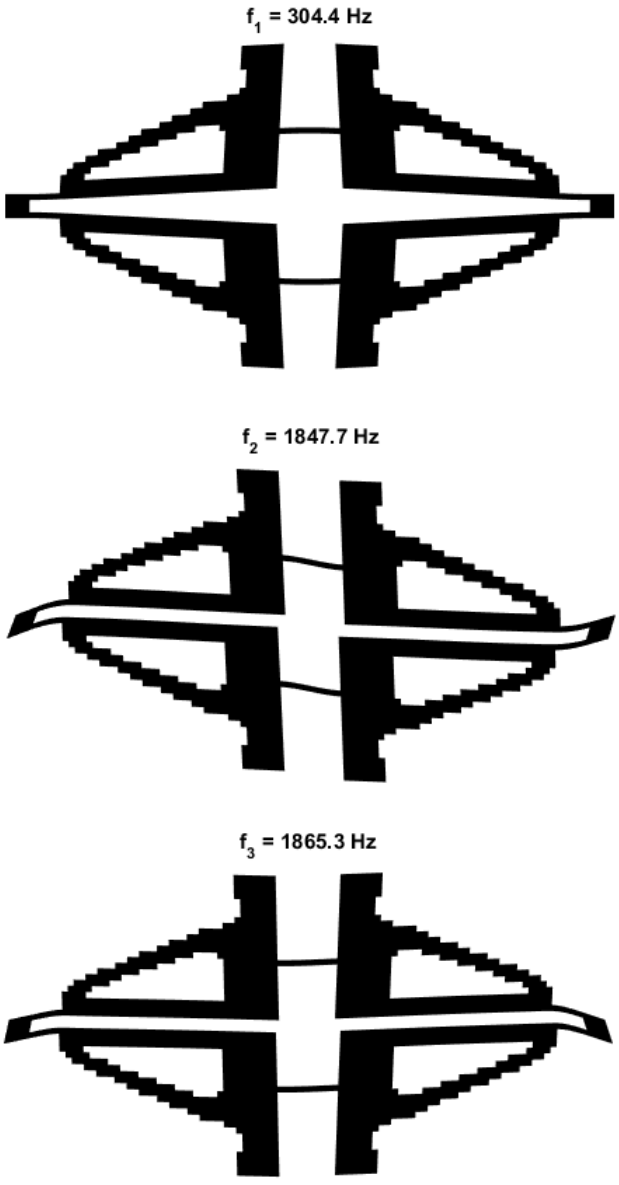


Figure 6.10. The first three mode shapes of the topologically optimized inertial amplification mechanism.

The topologically optimized mechanism is used as a unit cell in the finite periodic structure to inhibit the transmitted vibration amount in the band gap frequency range.

For this reason, several finite periodic structures are formed by using various number of unit cells to investigate how number of mechanisms used affects the attained vibration isolation amount. A representative one dimensional finite periodic structure that consists of three topologically optimized inertial amplification mechanisms is shown in Figure 6.11. The vibration transmissibilities of structures that consist of one, three and six topologically optimized mechanisms are provided in Figure 6.12. Accordingly it is found that; when one unit cell is employed at least 10%, when three unit cells are employed at least 28%, and when six unit cells are employed at least 63% of input vibration cannot reach the output end.

Table 6.3. Comparison of band gap limits of size and topologically optimized mechanisms which have the same mass.

Design	f_1	f_2	f_2/f_1
Size Opt. (Figure 6.4)	368.7 Hz	1590.4 Hz	4.31
Top. Opt. (Figure 6.9)	304.4 Hz	1847.7 Hz	6.07



Figure 6.11. One dimensional periodic structure that consists of three topologically optimized inertial amplification mechanisms.

These values are lower than the achieved vibration isolation levels for the size optimized mechanism since the primary concern of this study is to maximize the phononic band gap frequency range, and band depth constraint is not taken into account when formulating the optimization problems. Yet, high amount of vibration isolation is still achieved within a large frequency range when the topologically optimized inertial

amplification mechanism shown in Figure 6.9 is used as the building block of a finite periodic structure. The band gap occurs between 304.4 Hz and 1847.7 Hz, which are the first and second natural frequencies of the topologically optimized mechanism.

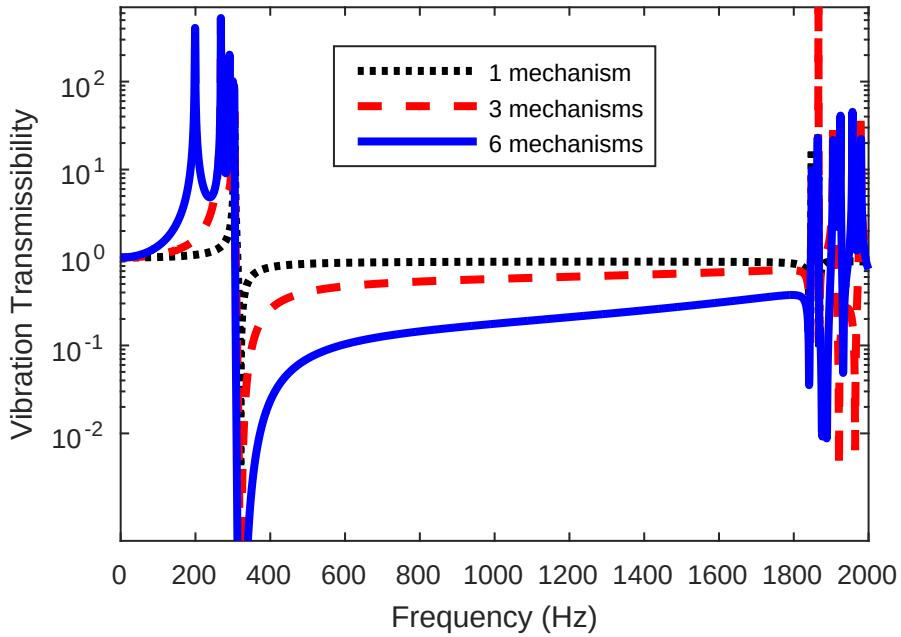


Figure 6.12. Vibration transmissibility of periodic structures consisting of several number of topologically optimized unit cells.

The phononic band gap limits for the infinitely periodic structure formed by the topologically optimized unit cell building blocks can be seen in the band structure shown in Figure 6.13. These results are in accordance with the previous ones, i.e., inertial amplification induced phononic band gap occurs between 304.4 Hz and 1847.7 Hz.

6.2.3. The Influence of Topology Optimization Design Space Volume Fraction on Band Gap Limits

In this section, a parametric study is conducted, in which the topology optimization design space volume fraction's influence on attained band gap limits is investigated. Since the topology optimization is performed on the 3rd beams, different volume

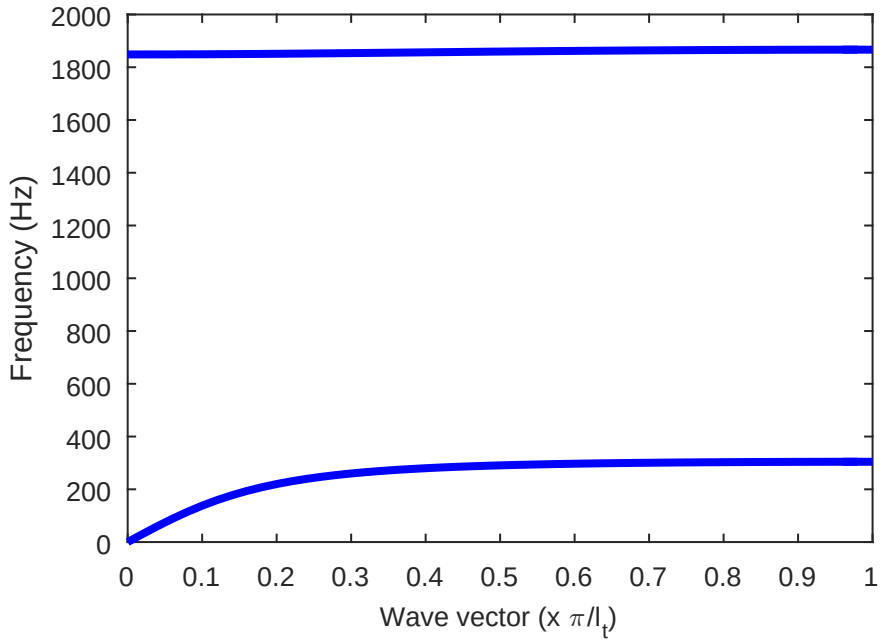


Figure 6.13. Band structure of the infinitely periodic topologically optimized unit cells.

fraction values can be obtained by changing the topology optimization design space dimensions for the 3rd beam. In both size and topology optimization problems, maximum allowable length (100 elements) is used. Although the maximum allowable width is 50 elements, the size optimization problem yielded a width of 22 elements. In order to have a fair comparison, as the width of the design domain in the topology optimization problem is varied between 22 and 50 elements, the volume fraction is also varied to keep the mass constant. That is to say, the case that the active design area's volume fraction is equal to 0.385 (i.e., the case with the maximum design space width, which is 50 elements) results with the topologically optimized design given in Figure 6.9, whereas the case that the active design area's volume fraction is equal to 1 corresponds to the size optimized design provided in Figure 6.4.

With these descriptions, the aforementioned parametric study is conducted, then Figure 6.14 and Figure 6.15 are obtained. In Figure 6.14, f_2/f_1 vs active volume fraction data is presented. The top left asterisk represents the topologically optimized mechanism, whereas the cross at the bottom right represents the size optimized

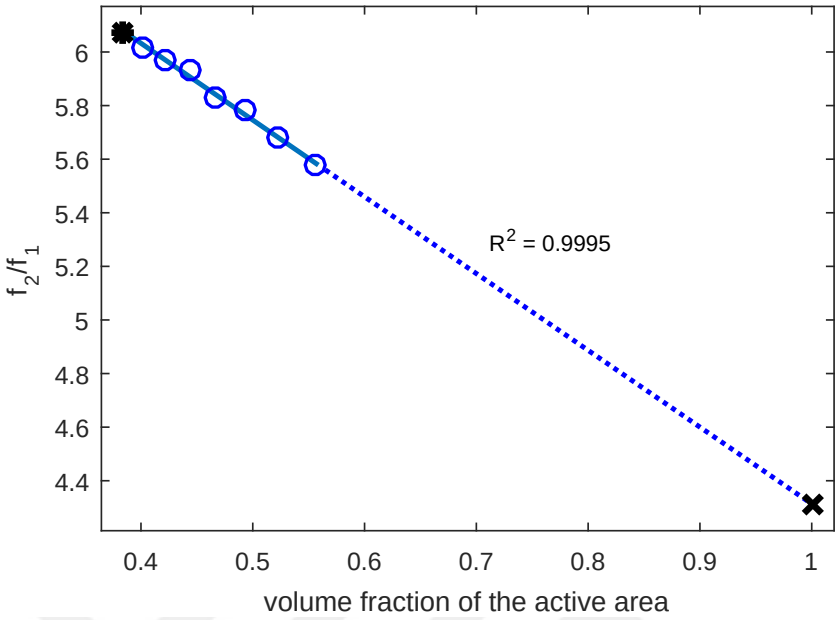


Figure 6.14. f_2/f_1 ratio vs active volume fraction graph. Top left asterisk: The topologically optimized design, Bottom right cross: The size optimized design, Circles: The intermediate data points, Solid line: The least squares line within achievable design space, Dashed line: The extension of the least squares line.

mechanism. The circles that lie between these two data points are the f_2/f_1 values obtained from the topologically optimized designs that correspond to associated active area volume fraction values. All the data points represented are used to construct the least squares line shown in Figure 6.14. It can be seen that, the f_2/f_1 variation with respect to the volume fraction of the active area is linear.

In Figure 6.15, the band gap limits' (f_2 and f_1) variation with volume fraction of the active area is provided. The asterisks that lie in the leftmost part of the figure show the topologically optimized design's (Figure 6.9) f_2 and f_1 values, whereas the rightmost crosses indicate the size optimized design's (Figure 6.4). The circles that lie between these two data points are the f_2 and f_1 values obtained from the topologically optimized designs that correspond to associated active area volume fraction values. All the data points represented are used to construct the least squares line shown in Figure 6.15. Again, a linear variation between the band gap limits and the volume fraction of

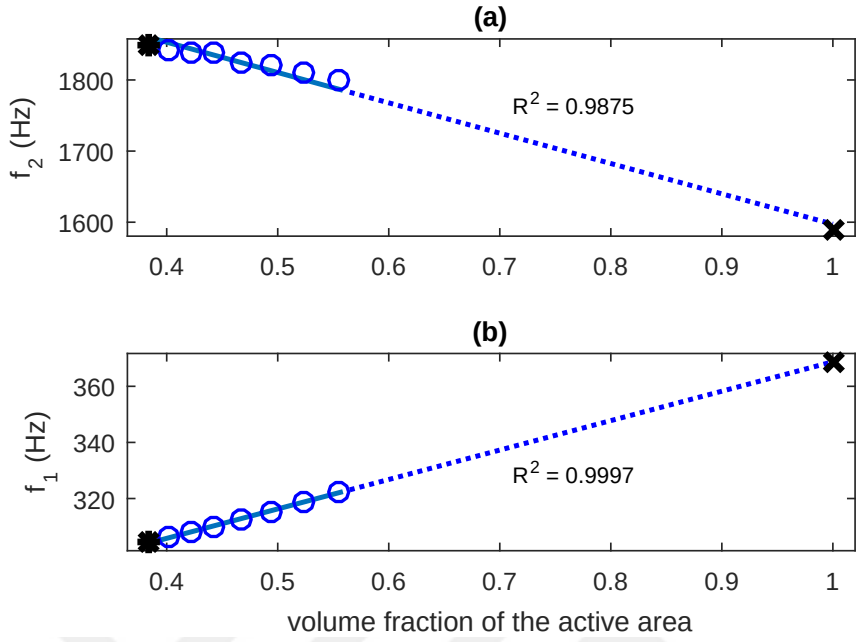


Figure 6.15. Band gap limits vs active volume fraction graph. a) Upper band gap limit. b) Lower band gap limit. (The descriptions for asterisks, crosses, circles and lines are the same as in Figure 6.14.).

the active area is observed.

In the parametric study, for some higher volume fraction values, proper designs cannot be obtained. This issue stems from the fact that, to maximize the band gap frequency range, the structure has a tendency to lose material. As a result, overall stiffness is lowered, which in turn results with lowered first natural frequency and higher band width for the constant mass condition. Therefore, it is natural to expect large numbers of elements with negative design sensitivity values in the active topology optimization domain. When element sensitivities become negative, the heuristic OC update scheme presented in Equation 5.26 decreases the corresponding element densities at the maximum move limit ml according to Equation 6.3. This situation causes OC algorithm to fail at high volume fraction values, since a high percentage of elements have negative sensitivity values. To this end, the maximum active area volume fraction achieved with OC algorithm, which is resulted with a proper design is found as 0.555. In Figure 6.14 and Figure 6.15, the solid lines indicate the region of

achievable design space with the current topology optimization problem formulation. This convergence problem can be prevented for some higher volume fraction values by employing mathematical programming optimizers [160–165] that determine both the search direction and appropriate step length, with a cost of increased run times. However, readily available open source implementations and ease of applicability with some modifications make the OC algorithm advantageous to use for lower volume fraction values and provides satisfactory topologically optimized designs subject to a mass constraint.

7. A NOVEL EFFICIENT TOPOLOGY OPTIMIZATION ALGORITHM FOR FUNDAMENTAL FREQUENCY MAXIMIZATION

The work performed in this chapter describes in detail an efficient novel topology optimization algorithm for fundamental frequency maximization which is based on design-dependent inertial loads and Rayleigh's principle.

7.1. The Motivation

Mechanical resonance is a situation that structural or mechanical engineers usually try to avoid. Thus, in the design stage, the natural frequencies of a structure should be taken into account. To that end, maximization of the fundamental natural frequency of any structure becomes an important design task. For instance, some of the real life excitations such as earthquakes are in the low frequency range. Hence, fundamental natural frequency maximization is beneficial in mitigating the effect of these excitations. Together with achieving maximized fundamental natural frequency, a designer intuitively considers the cost of the structure, as well. Therefore, obtaining a structure with maximum fundamental natural frequency and minimum weight is a natural target for a designer. To achieve this goal, the most general type of structural optimization, i.e., topology optimization should be performed. Although initially being developed for static problems [100,101,166], topology optimization techniques are readily utilized to solve various dynamic structural optimization problems, as well [155–157, 167–178].

In the literature, there are many studies that consider the fundamental eigenfrequency maximization of structures by utilizing topology optimization techniques. Among them, topology optimization problem of maximizing a beam's fundamental natural frequency with various boundary conditions is studied extensively [54, 64–80]. In all of these studies, first a dynamic analysis is performed, then element design sensitivities are calculated and ultimately elements are updated with an optimization

algorithm. Topology optimization problems usually involve high number of design variables. Thus, computational costs of eigenvalue, eigenvector and sensitivity calculations are high, as well. Therefore, if the topology of the structure with maximum fundamental natural frequency is obtained while avoiding the time consuming eigenfrequency and sensitivity calculations in every iteration step, topology optimization procedure becomes much more efficient.

On the other hand, as a static topology optimization problem, compliance minimization (stiffness maximization) subject to a mass constraint, is a well-posed problem and it is already proven to be solved efficiently [132]. It is well-known that the fundamental natural frequency of a beam is proportional to its stiffness. Therefore, if a proper topology optimization procedure is suggested, compliance minimization (stiffness maximization) algorithm can be utilized to obtain the optimum topology of the beam, which maximizes the fundamental natural frequency.

In this chapter, a time efficient method is proposed to obtain optimum beam topologies with maximum fundamental frequency. To that end, the mentioned free vibration problem is converted into two sequential static topology optimization problems in which eigenvalue calculations are omitted during the optimization process. The method utilizes the Rayleigh's principle [179]: 'if the lowest frequency mode shape of a vibrating structure can be estimated, then the corresponding natural frequency can be closely estimated'. In the proposed method, once a proper fundamental mode shape estimate is found, it is gradually improved in every iteration step by using a design-dependent inertial load vector, which changes due to the evolving topology. So far, design-dependent loads such as self-weight or fluid pressure have been utilized in various static topology optimization problems [143, 144, 180–188]. However, solution of a free vibration topology optimization problem without calculating eigenvalues in every iteration step by defining a design-dependent inertial load vector has not yet been studied in the literature.

In order to implement the method, an open source compliance minimization topology optimization code supplied in [132] is modified. As a verification of the method,

obtained optimum beam topologies are compared with the results found in the literature.

7.2. The Proposed Method

The proposed method aims to obtain optimum beam topologies, which maximize the fundamental natural frequency of the structure for a given mass constraint. For this purpose, the topology optimization code provided in [132] is modified. In that study, modified SIMP method [131] is used, which is derived from the original SIMP idea [103, 104]. The compliance minimization problem with a mass constraint is solved with optimality criteria (OC) [86] algorithm. Although several filtering techniques are provided in [132], here only sensitivity filter [128] is used to prevent checkerboard patterns.

The method proposed in this chapter utilizes the Rayleigh's principle [179], i.e., if an estimate of the vibration mode is found, then its natural frequency can be closely approximated. In a static topology optimization problem, the aim is to maximize the stiffness of a structure (i.e., minimize the compliance). When stiffness is increased and mass is held constant (i.e., employing a mass constraint), the natural frequency is increased, as well. Therefore, if a successful estimate of the first mode shape of a beam structure is found, then this information can be used to obtain the topologies, which maximizes stiffness and in turn the first natural frequency.

The static and dynamic structural problems are solved by the finite element method. In the solution of the static problem, nodal displacements are given by Equations 7.1 and 7.2:

$$\boldsymbol{f_s} = \boldsymbol{K}\boldsymbol{u_s} \tag{7.1}$$

$$\boldsymbol{u_s} = \boldsymbol{K}^{-1}\boldsymbol{f_s} \tag{7.2}$$

Here, $\boldsymbol{f_s}$ denotes static load vector, $\boldsymbol{K}$ denotes global stiffness matrix, $\boldsymbol{u_s}$ denotes displacements for this static problem.

Stiffness maximization topology optimization problem, which uses Equation 7.2 can be solved efficiently [132]. Therefore, if a free vibration problem is expressed as in the form given in Equation 7.2, then this formulation can be used to obtain topologically optimized structures with maximized fundamental natural frequency. To that end, the following derivations are provided.

For an eigenvalue problem, nodal displacements are obtained as in Equations 7.3 and 7.4:

$$\boldsymbol{K}\boldsymbol{u_n} = \omega^2 \boldsymbol{M}\boldsymbol{u_n} \tag{7.3}$$

$$\boldsymbol{u_n} = \boldsymbol{K}^{-1}\boldsymbol{M}\omega^2\boldsymbol{u_n} \tag{7.4}$$

Here, $\boldsymbol{K}$ denotes global stiffness matrix, $\boldsymbol{M}$ denotes global mass matrix, $\boldsymbol{u_n}$ denotes displacement vector, ω denotes the natural frequency.

In Equation 7.4, $\boldsymbol{M}\omega^2\boldsymbol{u_n}$ term represents the inertial forces. Moreover, $\omega^2\boldsymbol{u_n}$ term is the acceleration vector. In Rayleigh's principle if the eigenvector estimate is scaled, it does not change the eigenvalue calculation (see [179]). Here, the acceleration vector is normalized by dividing both sides of Equation 7.4 by $\omega^2\|\boldsymbol{u_n}\|$, where $\|\boldsymbol{u_n}\|$ indicates the norm of the displacement vector $\boldsymbol{u_n}$. As a result, the following expression is obtained:

$$\frac{\hat{\boldsymbol{u}}_{\boldsymbol{n}}}{\omega^2} = \boldsymbol{K}^{-1}\boldsymbol{M}\hat{\boldsymbol{u}}_{\boldsymbol{n}} \tag{7.5}$$

where $\hat{\boldsymbol{u}}_{\boldsymbol{n}}$ denotes the unit vector along $\boldsymbol{u_n}$.

A new vector $\boldsymbol{u_d}$ is defined using Equation 7.5 such that:

$$\boldsymbol{u_d} = \frac{\hat{\boldsymbol{u}}_{\boldsymbol{n}}}{\omega^2} \tag{7.6}$$

Then, Equation 7.5 becomes:

$$\boldsymbol{u_d} = \boldsymbol{K}^{-1}\boldsymbol{M}\hat{\boldsymbol{u}}_{\boldsymbol{n}} \tag{7.7}$$

$\boldsymbol{u_d}$ in Equation 7.6 is normalized:

$$\hat{\boldsymbol{u}}_{\boldsymbol{d}} = \frac{\boldsymbol{u_d}}{\|\boldsymbol{u_d}\|} = \frac{\hat{\boldsymbol{u}}_{\boldsymbol{n}}}{\omega^2}\frac{\omega^2}{\|\hat{\boldsymbol{u}}_{\boldsymbol{n}}\|} = \hat{\boldsymbol{u}}_{\boldsymbol{n}} \tag{7.8}$$

where $\hat{\boldsymbol{u}}_{\boldsymbol{d}}$ denotes the unit vector along $\boldsymbol{u_d}$.

According to Equation 7.8, $\hat{\boldsymbol{u}}_{\boldsymbol{d}}$ is equal to $\hat{\boldsymbol{u}}_{\boldsymbol{n}}$. Therefore, Equation 7.7 can be rewritten as:

$$\boldsymbol{u_d} = \boldsymbol{K}^{-1}\boldsymbol{M}\hat{\boldsymbol{u}}_{\boldsymbol{d}} \tag{7.9}$$

Inertial load vector ($\boldsymbol{f_d}$) is defined as:

$$\boldsymbol{f_d} = \boldsymbol{M}\hat{\boldsymbol{u}}_{\boldsymbol{d}} \tag{7.10}$$

Hence by using Equation 7.10 in Equation 7.9, the following expression is obtained:

$$\boldsymbol{u_d} = \boldsymbol{K}^{-1}\boldsymbol{f_d} \tag{7.11}$$

Please note that, Equations 7.2 and 7.11 have exactly the same form. Thus, a dynamic problem can be converted into a static one using the above procedure. Also note that, in Equation 7.11, ω^2 is eliminated. Hence, eigenvalue calculation is not required.

Compliance minimization topology optimization problems obtained by solving Equation 7.2 are well-defined and their convergence speed is high [132]. It has been shown that an eigenvalue problem can be converted into a static one (see Equations 7.2 and 7.11). Here, the proposed method uses the advantages of static topology optimization programming techniques to solve the dynamic topology optimization problem. Towards this goal, the following procedure is proposed:

(i) Set design domain, boundary conditions and optimization parameters.
(ii) Define an appropriate static point load vector ($\boldsymbol{f_s}$).
(iii) Solve the first static topology optimization problem:

$$\begin{aligned} \text{minimize:} \quad & \boldsymbol{u_s}^T \boldsymbol{K} \boldsymbol{u_s} \\ \text{subject to:} \quad & \boldsymbol{u_s} = \boldsymbol{K}^{-1} \boldsymbol{f_s} \\ & V(\boldsymbol{x}) = aV_0 \quad \text{(mass constraint)} \\ & 1 \geq x_e \geq 0 \qquad \text{for } e = 1, 2, ..., N \end{aligned} \tag{7.12}$$

(iv) To employ the Rayleigh's principle, set optimized structure's nodal displacement vector as the initial eigenvector estimate ($\boldsymbol{u_d} = \boldsymbol{u_s}$).
(v) Normalize $\boldsymbol{u_d}$ and thus obtain $\hat{\boldsymbol{u}}_{\boldsymbol{d}}$.
(vi) Set design-dependent inertial load vector ($\boldsymbol{f_d} = \boldsymbol{M}\hat{\boldsymbol{u}}_{\boldsymbol{d}}$).
(vii) Solve the following second static topology optimization problem, whose nodal displacement vector is a better estimate for the first eigenvector, for one iteration step and repeat steps 5-7 until convergence [187] criterion is met:

$$
\begin{aligned}
\text{minimize:} \quad & \boldsymbol{u_d^T K u_d} \\
\text{subject to:} \quad & \boldsymbol{u_d = K^{-1} f_d} \\
& V(\boldsymbol{x}) = aV_0 \quad \text{(mass constraint)} \\
& 1 \geq x_e \geq 0 \qquad \text{for } e = 1, 2, ..., N
\end{aligned}
\tag{7.13}
$$

(viii) Once the second static topology optimization problem converges, employ a post-processing step suggested by [90] to obtain a complete solid-void type of design.

(ix) Calculate the first natural frequency of the final structure.

To sum up, in the proposed method, two successive static topology optimizations are performed to closely estimate the solution of the eigenvalue maximization topology optimization problem. The first optimization is used to obtain a proper first eigenvector estimate. The second optimization is used to enhance the first eigenvector estimate. When the eigenvector is closely estimated, the topology obtained through the second static optimization problem closely resembles the optimum topology with maximized fundamental natural frequency.

In the second static topology optimization, design-dependent inertial loads are employed to imitate the dynamic forces of the free vibration problem as demonstrated in Equation 7.10. According to Rayleigh's principle, the eigenvalue is insensitive to small variations in the eigenvector [179]. Thus, gradual changes in inertial loads do not disrupt the eigenvalue convergence. So, it is reasonable to update inertial loads in every iteration step with evolving topology, to better estimate the fundamental mode of the structure. This kind of convergence through changing loads in topology optimization process is reported in the literature [187], as well.

The flowchart of the proposed method is shown in Figure 7.1. By employing this method, one can easily obtain topologically optimized structures, which has the maximum first natural frequency for a given mass without solving time consuming

eigenvalue problems in each iteration step. Large scale eigenvalue problems are not computationally economical. In addition, symmetry conditions cannot be utilized in problem size reduction since asymmetric eigenmodes can occur for any structure [86]. Considering these fundamental difficulties encountered with the large scale eigenvalue topology optimization problems, the method proposed in this section becomes a valuable tool to obtain the topologies, which maximizes the first natural frequency of the structure.

Finding a suitable first eigenvector estimate of the structure is very crucial for the proposed method's success. Here, two different estimation schemes are provided to get the proper eigenvectors for symmetric and asymmetric boundary conditions (BCs).

7.2.1. Symmetric Boundary Conditions

Consider the topology optimization design space with symmetric BCs such as with fixed-fixed (see Figure 7.2a) and pinned-pinned (see Figure 7.2b) ends. For dynamic problems, maximum deflections of the first mode shapes of these structures occur at the center. Similarly, for static problems, when a vertically downward point load is applied at the center of these beams, highest deflections occur at the center, as well. Thus, for the symmetric BC cases, it is natural to expect to obtain proper first eigenvector estimates by solving the compliance minimization problems with unit loads applied vertically downwards in the middle of the beams shown in Figures 7.2(a) and 7.2(b).

7.2.2. Asymmetric Boundary Conditions

For a beam with asymmetric BCs, a proper location for the unit static load needs to be determined. Consider the beam with fixed-pinned boundary conditions shown in Figure 7.2(c). When a unit point load is applied vertically downwards at the center, as done for the pinned-pinned and fixed-fixed end cases, the maximum deflection will not occur at the center. Therefore, using the same static load vector as in symmetric BC cases would be erroneous and can yield improper first eigenmode estimates.

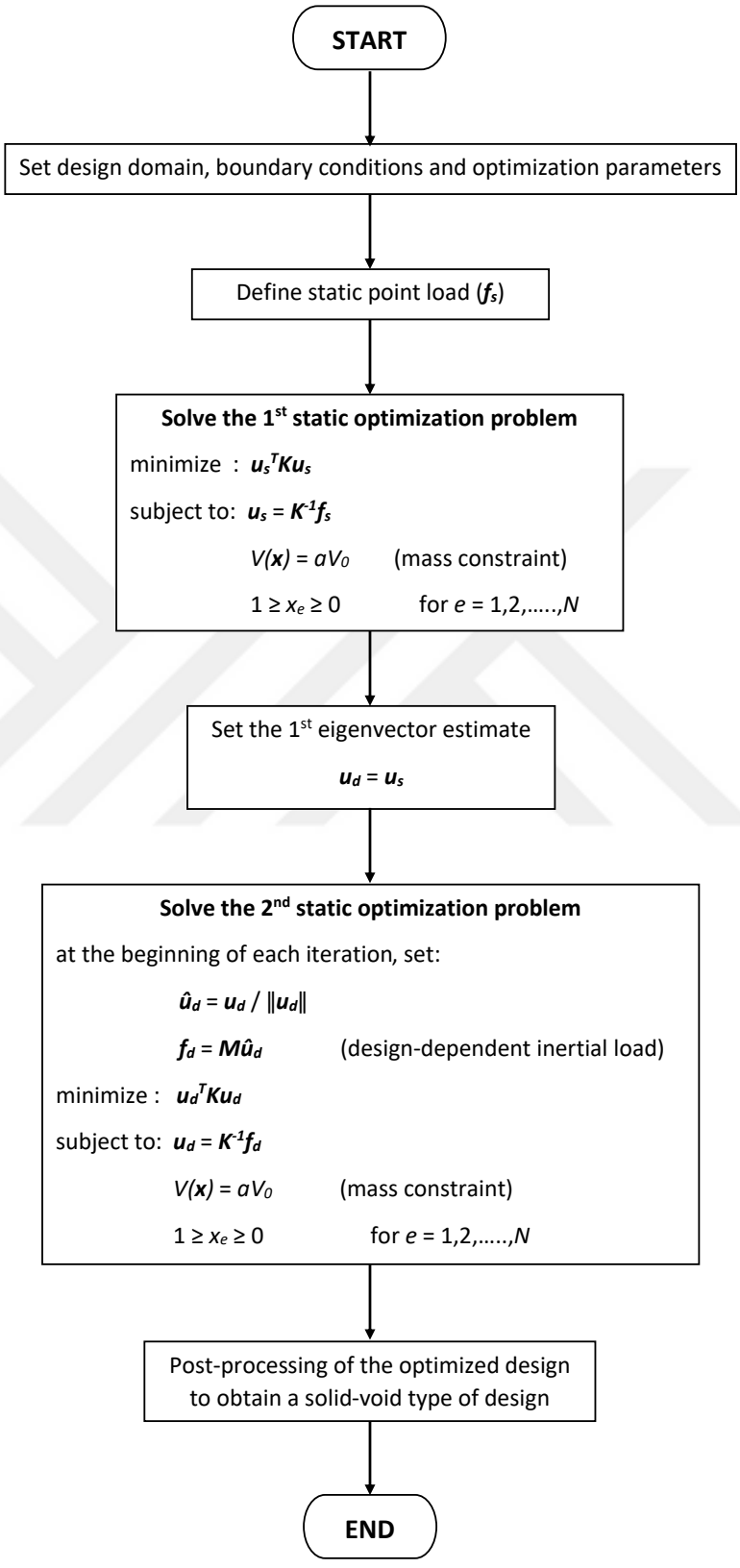


Figure 7.1. The flowchart of the proposed method.

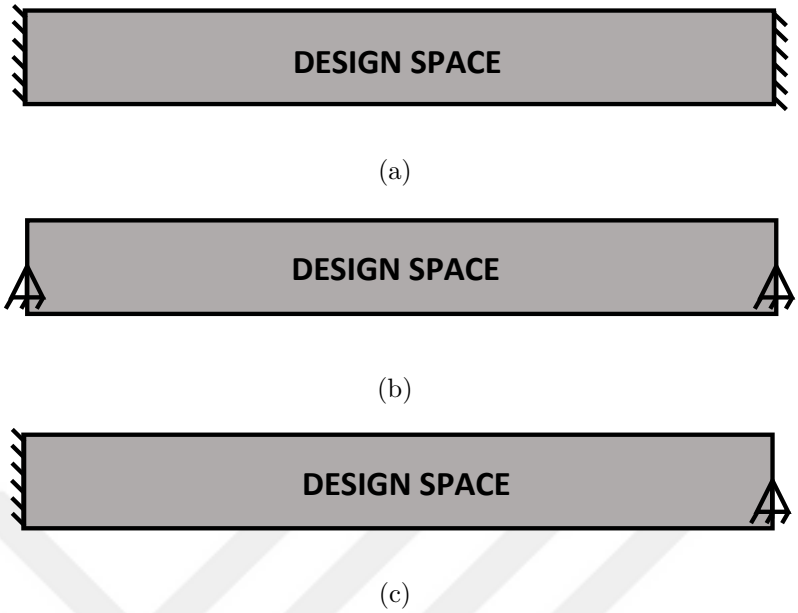


Figure 7.2. Topology optimization design spaces with symmetric and asymmetric boundary conditions. (a) Fixed-fixed beam, (b) Simply supported beam, (c) Fixed-pinned beam.

In order to overcome this shortcoming, a procedure is suggested. Firstly, the design space shown in Figure 7.2(c) is considered as fully solid. Then, just one eigenvalue problem is solved in the usual manner (modal analysis) to get the first eigenvector of this structure. Then, the node that has the maximum deflection is determined. Consequently, vertically downwards unit static load ($\boldsymbol{f_s}$) is applied at that node of the original design space with asymmetric BCs given in Figure 7.2(c). At the end, by solving the compliance minimization topology optimization problem for this load, a proper nodal displacement vector to estimate the first eigenmode of the structure is obtained.

7.3. The Hybrid Method

In this section, a hybrid method, which utilizes both the proposed method given in Section 7.2 and the standard dynamic topology optimization method mentioned in Section 5.2, is proposed. Again, the aim is to obtain topologically optimized structures, which maximize the fundamental natural frequency with a given mass constraint. By using the proposed method given in Section 7.2, optimum structures can be obtained

very quickly. In other words, the convergence speed is the most important feature of the proposed method. On the other hand, by using the dynamic topology optimization procedure mentioned in Section 5.2, structures with slightly better performance can be obtained at the expense of time consuming eigenvalue-eigenvector calculations in every iteration step. Here, the hybrid method is suggested to balance the trade off between speed and accuracy.

The algorithm for the hybrid method is as follows: Firstly, by using the proposed method given in Section 7.2, topologically optimized structure whose fundamental eigenfrequency is maximized for a given mass constraint is obtained. Then, this structure is supplied as an initial guess to the dynamic topology optimization problem mentioned in Section 5.2 to get the final improved design. As a result of this process, the slightly better topology of the dynamic optimization method is obtained in less time. The flowchart of the hybrid method is provided in Figure 7.3.

7.4. Numerical Results

In this section, the proposed method will be tested numerically. In Section 7.4.1, the proposed method will be verified via the comparison of the results that are found in the literature. In Section 7.4.2, the proposed method's claim, the better performance through changing (design-dependent) inertial loads, will be verified.

For all of the topology optimization problems considered here, design spaces are discretized by using four-node, quadrilateral, square, plane stress finite elements. Moreover, the maximum density change of an individual element in an iteration is selected as 0.2 as in the original source code [132]. In each successive static topology optimization problem, the iterations are stopped if the maximum change of the elements are less than 0.01 [132]. The modified SIMP interpolation scheme's stiffness penalty factor (p) is taken as 3, as frequently encountered in the literature [54, 86, 90, 156]. In addition, for dynamic calculations the interpolation scheme provided in Equation 5.64 is utilized with a mass penalization factor of $d = 6$, as in [54, 156]. For all the problems, optimization starts at the point where all of the element densities are equal

to the volume fraction (i.e., initial $x_e = a$ for all e) [54, 86, 132, 139]. Moreover, E_{min} is defined as $10^{-9}E_0$ as in [132]. The definition of ρ_{min} is similar, i.e., $\rho_{min} = 10^{-9}\rho_0$.

The numerical calculations are conducted in the same computer, which has 4 processors. Each processor has 16 cores and each processor's operating frequency is 2.29 GHz. Installed memory (RAM) of the computer is 128 GB. The computer runs a 64-bit operating system.

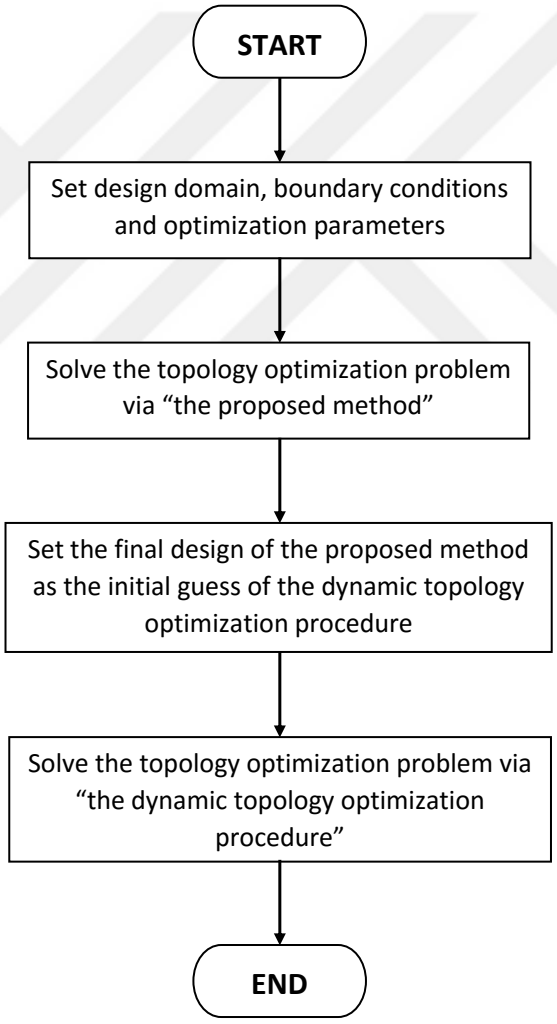


Figure 7.3. The flowchart of the hybrid method.

7.4.1. The Benchmark Problems for Numerical Verification

For numerical verification, the proposed method in Section 7.2 is utilized to obtain topologically optimized beam structures whose first natural frequencies are maximized under a mass constraint for pinned-pinned (see Figure 7.2b) and fixed-pinned (see Figure 7.2c) boundary conditions. In addition to these, a cantilever beam problem with a concentrated mass at the free end (see Figure 7.4) is also considered. Recently, in [139] a benchmark library for static topology optimization problems is suggested. However, for dynamic topology optimization problems no such benchmark library exists. Therefore, these three problems, which are frequently encountered in the literature, are chosen as the benchmark problems for numerical verification.

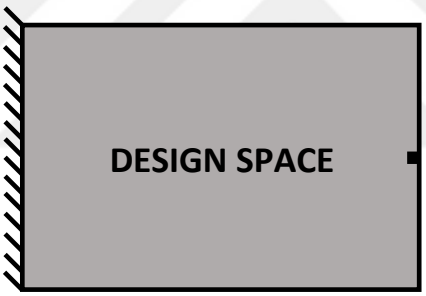


Figure 7.4. Topology optimization design space of the cantilever beam that has a concentrated mass in the middle of the right end.

7.4.1.1. Simply Supported Beam. As the first benchmark example, the problem found in [54,71,79] is considered. This problem aims to find the optimum topology of a simply supported beam, which maximizes the first natural frequency under a mass constraint. Material parameters are given as follows: Elastic modulus, $E_0 = 10^7$ Pa; Poisson ratio, $\nu = 0.3$; density, $\rho_0 = 1\text{kg/m}^3$. The design domain (see Figure 7.2b) has the following dimensions: length = 8 m, height = 1 m. Finally volume fraction (a) is considered to be 0.5, i.e., at the end of the optimization process only half of the design space will be occupied by material and the remaining half will be empty. This topology optimization problem is solved via the proposed method with a design space discretization of 320 by

40 finite elements. Sensitivity filtering is applied with a filter radius of 2.5 to prevent checkerboarding and mesh dependency.

In the proposed method, two successive static topology optimization problems are solved as described in Figure 7.1. The first static topology optimization problem finds the stiffest structure with 0.5 volume fraction (mass constraint) for which a point load is applied in the middle of the beam as discussed for the symmetric BC case. When this problem, shown in Figure 7.5, is solved using the static topology optimization procedure (see the 1st static optimization problem box in the flowchart given in Figure 7.1), the structure shown in Figure 7.6 is obtained. Here, the first natural frequency is calculated as 150.9 rad/s. As proposed by the method, the static displacement vector of this structure is supplied as an initial eigenvector estimate (see Figure 7.1) of the final structure that maximizes the first natural frequency. Doing so and applying the procedure mentioned in the 2nd static optimization problem box in the flowchart given in Figure 7.1, the topology shown in Figure 7.7 is obtained with a first natural frequency value of 162.5 rad/s. Please note that, by the second optimization loop, the natural frequency is increased by 7.7% and the topology is changed especially in the middle portion where the load was applied in the first optimization loop.

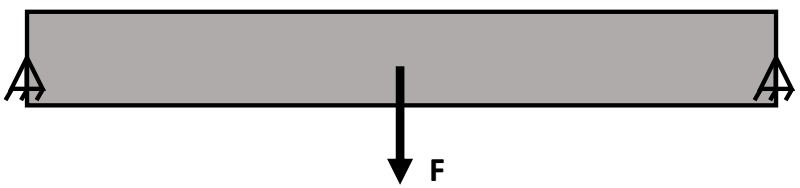


Figure 7.5. Static topology optimization problem of simply supported beam with a point load in the middle.

In order to show the accuracy and efficiency of the proposed method, the same topology optimization problem, i.e., the maximization of the simply supported beam's first natural frequency under mass constraint, is solved with the dynamic topology optimization procedure mentioned in Section 5.2. For the dynamic problem formulation, again sensitivity filtering is applied with a filter radius of 2.5. As in the static code, the

maximum density change of an individual element in one iteration is initially selected as 0.2. However, this resulted with convergence problems. In order to prevent convergence problems, the maximum density change of an individual element in one iteration is determined as 0.01 for the dynamic code. Moreover, optimization is halted after 200 iterations. In every iteration, the first three eigenvalues and eigenvectors of the structure are efficiently calculated by using MATLAB®'s built-in function 'eigs' which uses implicitly restarted Arnoldi/Lanczos methods [189] provided in ARPACK [190] software package. Discretization of the design domain is again chosen as 320 by 40 elements. In order to calculate the proper sensitivities for the repeated eigenvalues the procedure mentioned in Section 5.2 is followed. If the difference between the first and the second natural frequencies of the beam structure becomes less than 4%, these two eigenfrequencies are assumed to be multiple (repeated). This 4% value is determined via the numerical studies performed. As the result of the dynamic topology optimization, the structure shown in Figure 7.8 is obtained, which has the same topology with the design obtained in Figure 7.7. Although both methods yielded the same topology, there exists a 4.6% discrepancy between the first natural frequencies, which stems from the minor differences in between these two structures. Moreover, the convergence history of the dynamic code results is provided in Figure 7.9. This convergence history behavior is similar with the one that is supplied in [54].

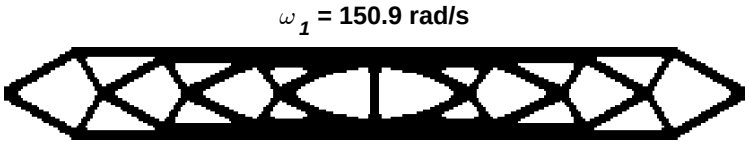


Figure 7.6. Topologically optimized simply supported beam whose stiffness is maximized for a point load applied at the middle of the structure. $E_0 = 10^7$ Pa, $\rho_0 = 1$ kg/m^3, $\nu = 0.3$, beam dimensions are 8 m by 1 m, volume fraction is 0.5, mesh size is 320 by 40 elements.

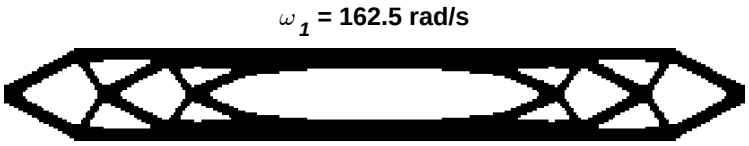


Figure 7.7. Topologically optimized simply supported beam whose first natural frequency is maximized by the proposed method. $E_0 = 10^7$ Pa, $\rho_0 = 1$ kg/m^3, $\nu = 0.3$, beam dimensions are 8 m by 1 m, volume fraction is 0.5, mesh size is 320 by 40 elements.

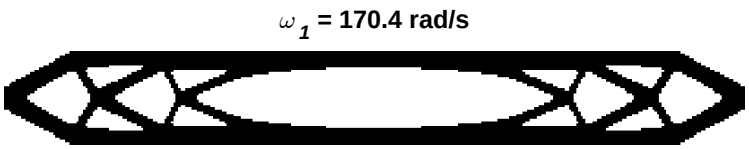


Figure 7.8. Topologically optimized simply supported beam whose first natural frequency is maximized by using the dynamic code. $E_0 = 10^7$ Pa, $\rho_0 = 1$ kg/m^3, $\nu = 0.3$, beam dimensions are 8 m by 1 m, volume fraction is 0.5, mesh size is 320 by 40 elements.

The displacement vector of the design, which is obtained as a result of the first static topology optimization problem, is supplied to the successive optimization loop as the first eigenvector estimate of the desired structure that maximizes the first natural frequency for the specified BCs and mass constraint. In order to check the validity of this assumption, modal assurance criteria (MAC) [191, 192] number comparisons are done and the following results are obtained for this problem:

The MAC number between the first static code displacement vector, i.e., the displacement vector of the structure shown in Figure 7.6 and the first mode shape of the final design shown in Figure 7.7 is 0.99996. This result indicates that updating the design-dependent inertial load vector in every iteration provides well tracking of the estimated fundamental mode. On the other hand, the MAC number between the

first mode shape of the final design shown in Figure 7.7 and the first mode shape of the dynamic topology optimization result given in Figure 7.8 is 0.99951. This also indicates that, these two final optimized designs have nearly the same fundamental mode, and through successive updating of the design-dependent inertial load vector in every iteration, the topology is evolved into the optimum via the proposed method. Since these two MAC numbers are very close to 1, the proposed claim is verified.

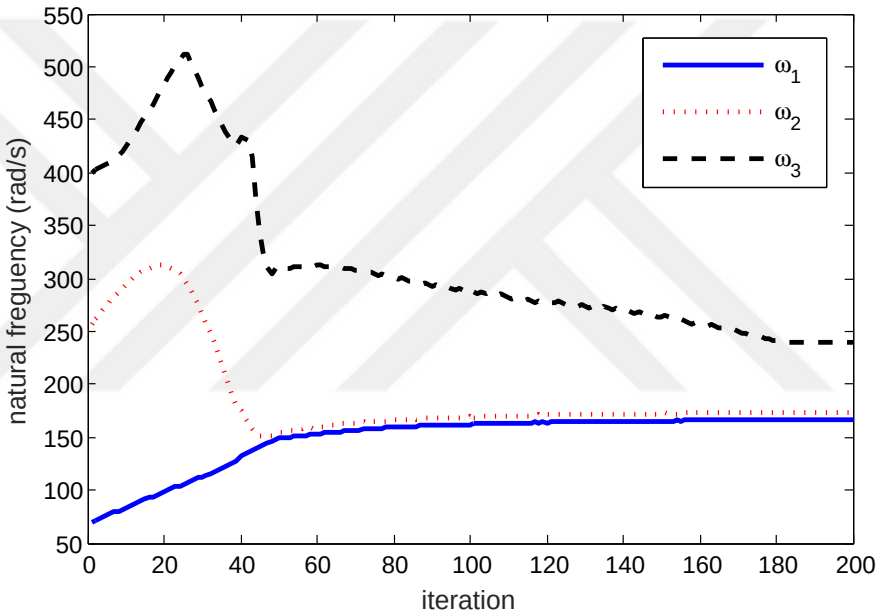


Figure 7.9. Convergence history of the topology optimized simply supported design whose first natural frequency is maximized by using the dynamic code.

The most important feature of the proposed method can be observed when Table 7.1 is examined in which run time comparisons of the proposed method and the standard dynamic topology optimization method is given for the current problem for several mesh sizes. It is clearly seen that the proposed method is far superior than the dynamic method both with respect to total elapsed times and run times per iteration basis. According to maximum memory usage, the dynamic topology optimization code is very sensitive to the mesh size while the proposed method is not. In the dynamic code,

when the mesh size increases, the memory usage also increases tremendously. This increase in the memory results in excessive execution times, i.e., slow convergence. However, the proposed method results in the same topology with orders of magnitude decreased execution time as computationally costly eigenvalue-eigenvector calculations are avoided in each iteration step.

Table 7.1. Run time comparison of the proposed method and standard dynamic topology optimization code results obtained for the problem in which simply supported beam's first natural frequency is maximized.

METHOD USED	MESH SIZE	RUN TIME (TOTAL)	RUN TIME (ITER.)	MAX RAM USED (ITER.)
Proposed Method	160 by 20	104.4 s + (43.1 s)*	0.4 s/iter	905 MB
Dynamic Code	160 by 20	8767.8 s	43.8 s/iter	4072 MB
Proposed Method	240 by 30	166.2 s + (277.5 s)*	0.8 s/iter	912 MB
Dynamic Code	240 by 30	55801.8 s	279.0 s/iter	18376 MB
Proposed Method	320 by 40	252.2 s + (1040.6 s)*	1.4 s/iter	950 MB
Dynamic Code	320 by 40	208604.1 s	1043.0 s/iter	54934 MB

* In the proposed method, eigenvalue calculation is only conducted at the end of the optimization process.

As described in Section 7.3, a balance between accuracy and speed can be achieved by using the hybrid method. To that end, the topology optimization problem is solved by using the hybrid method (see Figure 7.3). Firstly, by employing the proposed method, the structure shown in Figure 7.7 is obtained. Then, by supplying this structure to the dynamic topology optimization code as an initial guess and solving the optimization problem, the final design given in Figure 7.10 is obtained. The dynamic topology optimization iterations have been terminated when 100 iterations were completed. Please note that, the structures obtained via the dynamic code (see Figure 7.8) and the hybrid method (see Figure 7.10) are the same, with negligible discrepancy in

the first natural frequencies (0.4%). Therefore, as suggested in Section 7.3, the same structure is obtained by employing the hybrid method instead of using the standard dynamic code that starts from a totally gray design domain. In Table 7.2, the run time details for the hybrid method result given in Figure 7.10 is shown. When investigating Table 7.1 and Table 7.2 together, hybrid method's time advantage with respect to dynamic code can be seen. Hence, two different conclusions can be drawn here. First of all, if a designer's primary concern is speed, then usage of the proposed method will be the proper choice. On the other hand, if a designer's primary concern is to get the design with the highest possible first natural frequency, then the hybrid method can be used instead of the standard dynamic topology optimization routine.

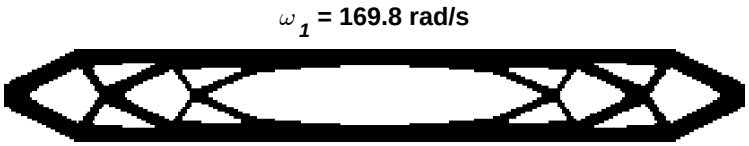


Figure 7.10. Topologically optimized simply supported beam whose first natural frequency is maximized by using the hybrid method. $E_0 = 10^7$ Pa, $\rho_0 = 1$ kg/m^3, $\nu = 0.3$, beam dimensions are 8 m by 1 m, volume fraction is 0.5, mesh size is 320 by 40 elements.

Table 7.2. Run time for the hybrid method result shown in Figure 7.10 in which simply supported beam's first natural frequency is maximized.

MESH SIZE	RUN TIME PER ITERATION (FOR STATIC PART)	RUN TIME PER ITERATION (FOR DYNAMIC PART)	TOTAL RUN TIME
320 by 40	1.3 s/iter	888.3 s/iter	89064.9 s

Moreover, the topology shown in Figure 7.7 is the same with the topologies found in [54,71,79]. As seen in Table 7.3, the proposed method provides nearly the same first

natural frequency when compared with the results found in the literature [54, 71]. The precise first natural frequency is not indicated in [79], however, it is seen from their natural frequency convergence figure that the corresponding natural frequency value lies between 160 and 170 rad/s. This benchmark example shows that, the proposed method's output is in accordance with the literature results [54, 71, 79].

Table 7.3. First natural frequency comparisons of the beams found in the literature, which have the same topology with the beam shown in Figure 7.7.

SOURCE OF THE RESULT	THE FIRST NATURAL FREQUENCY (rad/s)
The Proposed Method	162.5
The Dynamic Code	170.4
The Hybrid Method	169.8
Ref. [54]	174.7
Ref. [71]	171.5
Ref. [79]	160-170

7.4.1.2. Fixed-Pinned Beam. As the second benchmark example, a beam with asymmetric BCs (fixed-pinned) is considered. In order to determine the proper unit point load application node, the procedure given in Section 7.2.2 is followed. The proposed method's first static problem is shown in Figure 7.11 where the load is applied at the node, which has the maximum deflection according to the first eigenvector of the fully solid beam. For this problem, parameters given by [54] are used: Elastic modulus, $E_0 = 10^7$ Pa; Poisson ratio, $\nu = 0.3$; density, $\rho_0 = 1\text{kg/m}^3$. beam length = 8 m, beam height = 1 m, volume fraction, $a = 0.5$.

For the proposed method, the design space discretization is 320 by 40 finite elements. Sensitivity filtering is applied with a filter radius of 2. The first static

topology optimization problem with the above specifications is solved as the first part of the proposed method. As a result, the topologically optimized structure given in Figure 7.12 is obtained, which has its first natural frequency at 224.6 rad/s.

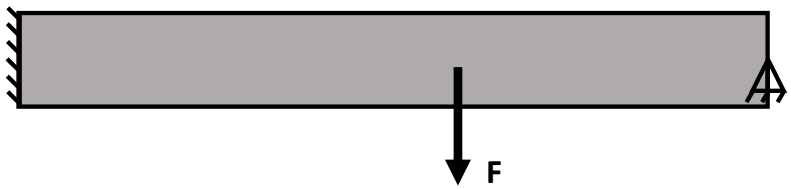


Figure 7.11. Static topology optimization problem of fixed-pinned beam with a point load at the maximum deflection node of the first eigenvector of the structure that consists of fully solid finite elements.

After solving the second static optimization loop given by the proposed method, the topology shown in Figure 7.13 is obtained, which has its first natural frequency at 255.6 rad/s. Here, 13.8% increase in the first natural frequency is observed as a result of the successive second static topology optimization loop within the proposed method. The topology given in [54] is similar and that structure has the first natural frequency at 288.7 rad/s.

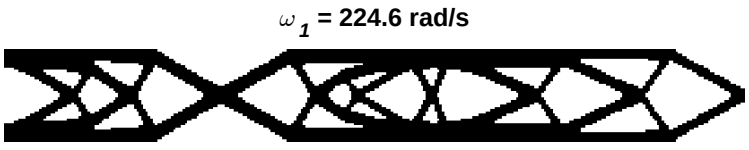


Figure 7.12. Topologically optimized fixed-pinned beam whose stiffness is maximized for a point load applied at the node, which has the maximum deflection according to the first eigenvector of the fully solid beam.

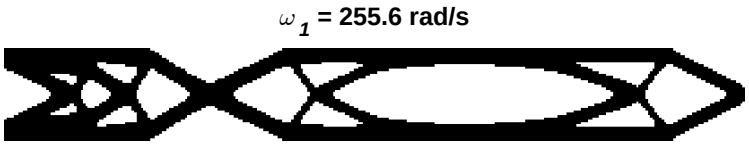


Figure 7.13. Topologically optimized beam with fixed-pinned ends whose first natural frequency is maximized by the proposed method.

7.4.1.3. Cantilever Beam. As the last benchmark example, a cantilever beam with a concentrated mass attached at the free end is considered (see Figure 7.4). Although being a problem with asymmetric BCs, the maximum deflection in the first vibration mode occurs at the free end for this beam. Therefore, the proper application node of the unit point load is selected intuitively as the middle point of the right end. This topology optimization problem is solved for the parameters given in [79], which are: Elastic modulus, $E_0 = 10^7$ Pa; Poisson ratio, $\nu = 0.3$; density, $\rho_0 = 1\text{kg/m}^3$; beam length = 15 m, beam height = 10 m, beam thickness = 1 m; volume fraction, $a = 0.5$; and the concentrated mass at the middle of the right free edge contains 20% of the total mass of the permitted material.

For this problem, a finite element model that consists of 150 by 100 elements are used. Sensitivity filter radius is selected as 2.3. The first static topology optimization problem shown in Figure 7.14 is solved as the first part of the proposed method and the structure given in Figure 7.15, with the first natural frequency at 94.1 rad/s is obtained. Then, the second static optimization problem is solved to get the design with maximized fundamental natural frequency. As a result, the design given in Figure 7.16 is obtained with the first natural frequency at 101.5 rad/s. That is to say, by employing the second static optimization procedure as suggested in Figure 7.1, the fundamental natural frequency of the beam is increased by 7.9%. Meanwhile, the topology given in [79] is similar to the one shown in Figure 7.16. Furthermore, when the convergence graph in [79] is examined, it is seen that the first natural frequency occurs approximately at 100 rad/s.



Figure 7.14. Static topology optimization problem of cantilever beam with a point load applied at the middle of the right edge.

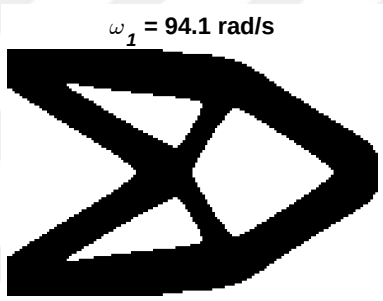


Figure 7.15. Topologically optimized cantilever beam whose stiffness is maximized for a point load applied at the middle of the right edge.

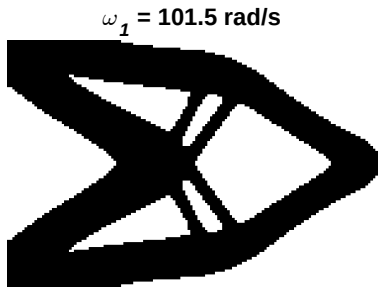


Figure 7.16. Topologically optimized cantilever beam whose first natural frequency is maximized by the proposed method.

7.4.2. Comparison of Design-Dependent Inertial Loading and Fixed Inertial Loading

In this section, the advantage of using design-dependent inertial loads instead of utilizing constant loading in the 2nd static optimization problem of the proposed method (see Figure 7.1) is demonstrated on a sample numerical study. To that end, the optimum beam topology, that maximizes the fundamental natural frequency under a mass constraint, is sought with two different approaches in the design space shown in Figure 7.2(a).

In the first approach, once an eigenvalue estimate is found via the 1st static optimization, an inertial load vector is formed by Equation 7.10, and is used in the 2nd static optimization like done in the proposed method. However, in contrast to the proposed method, this inertial loading vector remains constant during the optimization process. On the other hand, the second approach is the proposed method itself, i.e., in the 2nd static optimization, inertial loading is design-dependent, so that it gradually changes with the evolving topology during the optimization process.

For numerical calculations, the fixed-fixed beam parameters are provided as follows: Elastic modulus, $E_0 = 10^7$ Pa; Poisson ratio, $\nu = 0.3$; density, $\rho_0 = 1\text{kg/m}^3$, design domain (see Figure 7.2a) dimensions: length = 3 m, height = 1 m, volume fraction, $a = 0.5$. This topology optimization problem is solved in a design space which is discretized with 150 by 50 finite elements. Sensitivity filter radius is selected as 3 for this problem. Since the BCs are symmetric, the unit point load is applied in the middle of the structure (see Figure 7.17) as described in Section 7.2.1.

The results of the 1st static optimization loop are given in Figure 7.18. The post-processed topologically optimized design has the first natural frequency at 1356.3 rad/s. Using the displacement vector of the post-processed structure as the first eigenvector estimate, the 2nd static optimization loop is performed for each of the two approaches mentioned above. For the first approach, in which a constant inertial load vector is used, the post processed design given in Figure 7.19(b) is obtained, with the first natural

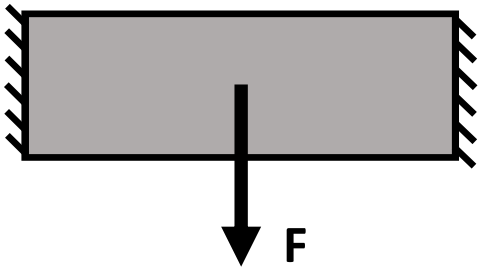


Figure 7.17. Static topology optimization problem of fixed-fixed beam with a point load in the middle.



(a) (b)

Figure 7.18. Topologically optimized fixed-fixed beam whose stiffness is maximized for a point load applied at the middle of the structure. (a) Topologically optimized design, (b) Post processed design.

frequency at 1684.2 rad/s. Thus, as a result of the first approach, the first natural frequency is increased by 24.2%. Whereas, for the second approach, in which design-dependent inertial loading is utilized, the post-processed design provided in Figure 7.20(b), with the first natural frequency at 1840.0 rad/s, is obtained. Therefore, a much more increase (35.7%) in the first natural frequency is achieved by the proposed method. Furthermore, the topologically optimized design shown in Figure 7.19(a) displays significant grey areas with intermediate density values which cause the post-processed design (Figure 7.19(b)) to have worse performance compared to the design given in Figure 7.20(b).



(a) (b)

Figure 7.19. Topologically optimized beam with fixed-fixed ends whose first natural frequency is maximized under constant inertial loading. (a) Topologically optimized design, (b) Post processed design.



(a) (b)

Figure 7.20. Topologically optimized beam with fixed-fixed ends whose first natural frequency is maximized under design-dependent inertial loads as suggested in the proposed method. (a) Topologically optimized design, (b) Post processed design.

In all of the numerical studies performed with various design parameters and BCs, similar results are obtained. Thus, the effectiveness of using design-dependent inertial loads in the proposed method is justified.

8. NOTES ON TOPOLOGY OPTIMIZATION STUDIES

In this chapter, various notes on numerical topology optimization studies performed during this graduate study are presented.

The initial designs for topology optimization studies conducted via SIMP method are chosen commonly as the vector in which all of the element density values are taken equal to the volume fraction (i.e., initial $x_e = a$ for all e) [54, 86, 132, 133, 139]. In this thesis, this approach has been adopted and satisfactory results were obtained.

Among the two most popular optimizers utilized in structural topology optimization field, in this study, OC based optimizer [132] provided faster convergence rates compared to the MMA [160] optimizer.

In the proposed method (Section 7.2), move limit (ml) value of 0.2 provided satisfactory results with fast convergence. Whereas, for dynamic topology optimization studies, this value resulted in non-converged designs. It was observed that, maximum density change of an individual element in one iteration should be lower than or equal to 0.02 for dynamic topology optimization problems considered here (Sections 6.2.2 and 7.4.1.1).

Sensitivity filtering [128] radius values were determined according to conducted numerical studies for each topology optimization problem independently (Sections 6.2.2, 7.4.1 and 7.4.2). Usage of density filtering [130] or projection filtering [131] did not improve the final designs. Instead, their employment resulted with increased computational cost. Employment of sensitivity filtering [128,129] in topology optimizations and post-processing of the optimized designs with a filter [90] resulted in satisfactory structures for this study.

In topology optimization studies, different stiffness penalty numbers (p) were tested. Consequently, the best results were obtained when p was taken as 3. Stiffness

penalization values other than 3, either resulted in non-converged or poor performance designs having large regions with intermediate densities (grey areas). In addition, the continuation approach (Section 4.3.1 [90, 96, 111]) was tested, however, it also suffered from the same problem.

In this thesis, spurious modes were observed in dynamic topology optimization problems when mass penalization was not utilized for elements with low density values. Spurious modes have been eliminated via employment of a mass penalty number (d) value of 6 for elements with $x_e \leq 0.1$ (Equation 5.64). This choice indeed makes physical density function non-differentiable at $x_e = 0.1$, but any numerical problem has not been encountered in our studies, since non-differentiability with respect to design variable x_e only exists at a single point for the whole domain. The same behaviour is also reported in the literature [54].

Repeated eigenvalue issue was observed in our dynamic topology optimization studies. To overcome this problem, the procedure presented in Section 5.2 was employed. The eigenvalues were considered as repeated if the difference of their values were less than a small tolerance percentage [54, 86, 158]. This percentage was problem dependent, i.e., it was determined for each problem separately via performed numerical studies (Sections 6.2.2 and 7.4.1). Among the two possible eigenvalue sensitivities available in Equation 5.72, the one that had maximum value was chosen, since the other choice resulted in non-converged designs.

In this thesis, the proper E_{min} value given in Equation 5.1 was determined as $10^{-9}E_0$ as in [132]. Other values that were in the range 10^6 times larger or smaller than this, were also tested. However, these choices resulted with numerical errors and instability. For determination of ρ_{min} value in Equation 5.30, the same approach was adopted (i.e., $\rho_{min} = 10^{-9}\rho_0$).

In fundamental natural frequency maximization of a cantilever beam, it is a common practice to use concentrated mass at the free end of the structure [67, 68, 72, 74, 79]. If concentrated mass is not involved, all the material will be moved towards

the fixed end to maximize the fundamental natural frequency. Whereas, concentrated mass located at the free end acts as a constraint to prevent this. To that end, in this study, concentrated mass is utilized to maximize the fundamental natural frequency of a cantilever beam (Section 7.4.1.3).

In topology optimization, compliance minimization problems for multiple load case are handled via superposition of individual compliance values obtained for each load separately [132,133]. Consequently, for multiple load case, there exists a matrix of displacements instead of a displacement vector $\boldsymbol{u}$. Therefore, for the proposed method (Section 7.2) distributed loads cannot be utilized to find the initial eigenvector estimate $\boldsymbol{u_d}$. On the other hand, it was observed that, when we have used a distributed load vector in the first static optimization part of the proposed method, the same topologies were obtained as for the case in which a point load vector is utilized. However, the resulting designs of the first static optimization part were not solid or void type, i.e., they had excessive grey regions around the nodes where the distributed loads were applied. In fact, these grey regions are the reason why superposition is utilized for multiple loads in compliance minimization problems. In the proposed method, if a designer is only interested with the final topology in which fundamental natural frequency is maximized, then he/she can utilize a distributed load vector to find a proper initial eigenvector estimate that is to be used for the second static optimization part. On the contrary, if a point load vector is utilized in the proposed method, the results of the two static optimizations both have physical meaning. Consequently, it is suggested to use a point load vector for the first static optimization part of the proposed method.

9. CONCLUSIONS

Inertial amplification is a unique phononic band gap generation method for low frequency region without sacrificing structure's stiffness and increasing its mass. By employing structural optimization methods on a compliant inertial amplification mechanism, this special property is further improved. Size, shape and topology optimization methods are utilized and compared with each other. The primary focus is given to the topology optimization since it is the most general type of structural optimization. Additionally, as a result of topology optimization, for fine finite element meshes, not only the structural topology but also the shape and the size of the structural members are also determined simultaneously. Consequently, in this study, a comprehensive review on topology optimization methods and detailed problem formulation derivations are provided for the researchers interested in the subject. Furthermore, the following conclusions are drawn as the results of the conducted researches:

First of all, a two-dimensional periodic structure, which has a wide and deep stop band at low frequencies is designed via inertial amplification method. Size and shape optimizations are performed on the one-dimensional beam element model of the building block mechanism to achieve wide and deep stop bands. For the same stiffness and mass values, the shape optimized design provides a wider and deeper stop band compared to the size optimized one. Besides, the relationship between band width and band depth is shown in Pareto studies in which shape optimization procedure provides better designs than that can be obtained by size optimization. Moreover, a shell element model of the building block mechanism is formed and this model shows similar stop band characteristics as the beam element model, indicating that the one-dimensional finite element model is valid for a fast optimization procedure. Using the shell element model, a two-dimensional periodic structure is formed. It is shown that the stop band limits of this periodic structure are nearly the same with its building block mechanism. Moreover, the two-dimensional phononic band gap structure is manufactured with a suitable out-of-plane thickness to prevent any out-of-plane vibration modes to occur within the stop band. Frequency response of the phononic band gap

structure is obtained numerically and experimentally and it is found that they are close to each other. Experimental results show that, a wide and deep phononic gap is created for in-plane excitations in both longitudinal and transverse directions. It is also shown via experiments that, out-of-plane vibration modes do not occur within the phononic gap due to the proper selection of the out-of-plane thickness of the periodic structure.

Then, size and topology optimization studies are conducted on an inertial amplification mechanism with the purpose of maximizing the achieved band gap width. As a result of the topology optimization, a much wider band gap is achieved compared to the size optimized design for the same mass. The vibration transmissibility calculations confirm that the topology optimized design has a wider stop band. A parametric study is conducted, in which linear variation of band gap width and band gap limits are observed with respect to the topology optimization design space volume fraction, i.e., band gap limits and width improve with decreasing volume fraction. In further topology optimization studies, to obtain wider as well as deeper inertial amplification induced phononic band gaps, band depth constraint can be taken into account within a mathematical programming algorithm.

Besides, a fast algorithm is proposed to obtain topologically optimized beams with maximized fundamental natural frequency. Beams with both symmetric and asymmetric boundary conditions are analyzed. It is found that, the proposed method provides great reduction in run times compared to the standard dynamic topology optimization methods, in which computationally costly eigenvalue-eigenvector calculations are involved in each iteration step. Orders of magnitude reduction in elapsed times per iterations are achieved via the proposed method, for large size meshes. Therewithal, orders of magnitude reduction in computer memory allocation is also observed when the proposed method is utilized. However, the proposed method yields beam topologies that have slightly lower performance than that can be obtained by the dynamic topology optimization procedure. Therefore, if a designer's primary concern is to minimize the computational effort, thus in turn the execution time while obtaining satisfactory designs (like most of the engineers desire), then the proposed method can be used instead of the standard dynamic topology optimization methods that involve

eigenvalue-eigenvector calculations. For some designers, obtaining the highest possible natural frequency may be crucial in the expense of large computational effort. In order to balance the trade off between computational speed and accuracy, a hybrid method is suggested to get the best results in less time. The proposed method is not limited to sensitivity filtering and optimality criteria based optimizer considered in this study, but also can be used together with the other filtering and optimization techniques utilized in the topology optimization literature.

Finally, as a result of this thesis, a journal article [193] and three conference papers [194–196] have been published so far. Regarding the author's M.Sc. study, a journal article [197] has also been published during this graduate study. Moreover, with the studies performed in Chapter 7, a journal article has been prepared and submitted to one of the prominent journals of the structural optimization field. The evaluation process for the submitted manuscript continues. As a post-doc study, in the near future, the research performed for topology optimization of inertial amplification induced phononic band gap structures will further be improved to create a journal article.

REFERENCES

1. Brillouin, L., *Wave Propagation in Periodic Structures*, McGrawHill-NewYork, 1946.

2. Gorishnyy, T., M. Maldovan, C. Ullal and E. Thomas, "Sound ideas", *Physics World*, Vol. 18, No. 12, pp. 24–29, 2005.

3. Lu, M. H., L. Feng and Y. F. Chen, "Phononic crystals and acoustic metamaterials", *Materials Today*, Vol. 12, No. 12, pp. 34–42, 2009.

4. Armenise, M. N., C. E. Campanella, C. Ciminelli, F. Dell'Olio and V. M. N. Passaro, "Phononic and photonic band gap structures: Modelling and applications", *Physics Procedia*, Vol. 3, No. 1, pp. 357–364, 2010.

5. Hussein, M. I., M. J. Leamy and M. Ruzzene, "Dynamics of phononic materials and structures: Historical origins, recent progress, and future outlook", *Applied Mechanics Reviews*, Vol. 66, No. 4, p. 040802, 2014.

6. Sigalas, M. M. and E. N. Economou, "Elastic and acoustic wave band structure", *Journal of Sound and Vibration*, Vol. 158, No. 2, pp. 377–382, 1992.

7. Sigalas, M. and E. N. Economou, "Band structure of elastic waves in two dimensional systems", *Solid State Communications*, Vol. 86, pp. 141–143, 1993.

8. Kushwaha, M. S., P. Halevi, L. Dobrzynski and B. Djafari-Rouhani, "Acoustic band structure of periodic elastic composites", *Physical Review Letters*, Vol. 71, No. 13, p. 2022, 1993.

9. Kushwaha, M. S., P. Halevi, G. Martinez, L. Dobrzynski and B. Djafari-Rouhani, "Theory of acoustic band structure of periodic elastic composites", *Physical Review B*, Vol. 49, No. 4, pp. 2313–2322, 1994.

10. Kafesaki, M., M. M. Sigalas and E. N. Economou, "Elastic wave band gaps in 3-D periodic polymer matrix composites", *Solid State Communications*, Vol. 96, No. 5, pp. 285–289, 1995.

11. Kushwaha, M. S., "Classical band structure of periodic elastic composites", *International Journal of Modern Physics B*, Vol. 10, No. 09, pp. 977–1094, 1996.

12. Kushwaha, M. S., B. Djafari-Rouhani, L. Dobrzynski and J. O. Vasseur, "Sonic stop-bands for cubic arrays of rigid inclusions in air", *The European Physical Journal B-Condensed Matter and Complex Systems*, Vol. 3, No. 2, pp. 155–161, 1998.

13. Kushwaha, M. S., B. Djafari-Rouhani and L. Dobrzynski, "Sound isolation from cubic arrays of air bubbles in water", *Physics Letters A*, Vol. 248, No. 2, pp. 252–256, 1998.

14. Psarobas, I. E., N. Stefanou and A. Modinos, "Scattering of elastic waves by periodic arrays of spherical bodies", *Physical Review B*, Vol. 62, No. 1, pp. 278–291, 2000.

15. Vasseur, J. O., P. A. Deymier, B. Chenni, B. Djafari-Rouhani, L. Dobrzynski and D. Prevost, "Experimental and theoretical evidence for the existence of absolute acoustic band gaps in two-dimensional solid phononic crystals", *Physical Review Letters*, Vol. 86, No. 14, p. 3012, 2001.

16. Yang, S., J. H. Page, Z. Liu, M. L. Cowan, C. T. Chan and P. Sheng, "Focusing of sound in a 3D phononic crystal", *Physical Review Letters*, Vol. 93, No. 2, p. 024301, 2004.

17. Cheng, W., J. Wang, U. Jonas, G. Fytas and N. Stefanou, "Observation and tuning of hypersonic bandgaps in colloidal crystals", *Nature Materials*, Vol. 5, No. 10, pp. 830–836, 2006.

18. Khelif, A., B. Aoubiza, S. Mohammadi, A. Adibi and V. Laude, "Complete band gaps in two-dimensional phononic crystal slabs", *Physical Review E*, Vol. 74, No. 4, p. 046610, 2006.

19. Bilal, O. R. and M. I. Hussein, "Ultrawide phononic band gap for combined in-plane and out-of-plane waves", *Physical Review E*, Vol. 84, No. 6, p. 065701, 2011.

20. Xu, Y. L., X. G. Tian and C. Q. Chen, "Band structures of two dimensional solid/air hierarchical phononic crystals", *Physica B: Condensed Matter*, Vol. 407, No. 12, pp. 1995–2001, 2012.

21. Liu, Z., X. Zhang, Y. Mao, Y. Y. Zhu, Z. Yang, C. T. Chan and P. Sheng, "Locally resonant sonic materials", *Science*, Vol. 289, No. 5485, pp. 1734–1736, 2000.

22. Goffaux, C. and J. Sanchez-Dehesa, "Two-dimensional phononic crystals studied using a variational method: Application to lattices of locally resonant materials", *Physical Review B*, Vol. 67, No. 14, p. 144301, 2003.

23. Hirsekorn, M., P. P. Delsanto, N. K. Batra and P. Matic, "Modelling and simulation of acoustic wave propagation in locally resonant sonic materials", *Ultrasonics*, Vol. 42, No. 1, pp. 231–235, 2004.

24. Wang, G., D. Yu, J. Wen, Y. Liu and X. Wen, "One-dimensional phononic crystals with locally resonant structures", *Physics Letters A*, Vol. 327, No. 5, pp. 512–521, 2004.

25. Oudich, M., Y. Li, B. M. Assouar and Z. Hou, "A sonic band gap based on the locally resonant phononic plates with stubs", *New Journal of Physics*, Vol. 12, No. 8, p. 083049, 2010.

26. Xu, Z., F. Wu and Z. Guo, "Low frequency phononic band structures in two-dimensional arc-shaped phononic crystals", *Physics Letters A*, Vol. 376, No. 33,

pp. 2256–2263, 2012.

27. Claeys, C. C., K. Vergote, P. Sas and W. Desmet, "On the potential of tuned resonators to obtain low-frequency vibrational stop bands in periodic panels", *Journal of Sound and Vibration*, Vol. 332, No. 6, pp. 1418–1436, 2013.

28. Zhou, X. and C. Chen, "Tuning the locally resonant phononic band structures of two-dimensional periodic electroactive composites", *Physica B: Condensed Matter*, Vol. 431, pp. 23–31, 2013.

29. Baravelli, E. and M. Ruzzene, "Internally resonating lattices for bandgap generation and low-frequency vibration control", *Journal of Sound and Vibration*, Vol. 332, No. 25, pp. 6562–6579, 2013.

30. Wang, P., F. Casadei, S. H. Kang and K. Bertoldi, "Locally resonant band gaps in periodic beam lattices by tuning connectivity", *Physical Review B*, Vol. 91, No. 2, p. 020103, 2015.

31. Li, Y., T. Chen, X. Wang, Y. Xi and Q. Liang, "Enlargement of locally resonant sonic band gap by using composite plate-type acoustic metamaterial", *Physics Letters A*, Vol. 379, No. 5, pp. 412–416, 2015.

32. Ozkaya, E. and C. Yilmaz, "Effect of eddy current damping on phononic band gaps generated by locally resonant periodic structures", *Journal of Sound and Vibration*, Vol. 389, pp. 250–265, 2017.

33. Liu, Z., C. T. Chan and P. Sheng, "Three-component elastic wave band-gap material", *Physical Review B*, Vol. 65, No. 16, p. 165116, 2002.

34. Jensen, J. S., "Phononic band gaps and vibrations in one-and two-dimensional mass–spring structures", *Journal of Sound and Vibration*, Vol. 266, No. 5, pp. 1053–1078, 2003.

35. Assouar, M. B., J. H. Sun, F. S. Lin and J. C. Hsu, "Hybrid phononic crystal plates for lowering and widening acoustic band gaps", *Ultrasonics*, Vol. 54, No. 8, pp. 2159–2164, 2014.

36. Coffy, E., T. Lavergne, M. Addouche, S. Euphrasie, P. Vairac and A. Khelif, "Ultra-wide acoustic band gaps in pillar-based phononic crystal strips", *Journal of Applied Physics*, Vol. 118, No. 21, p. 214902, 2015.

37. Alonso-Redondo, E., M. Schmitt, Z. Urbach, C. M. Hui, R. Sainidou, P. Rembert, K. Matyjaszewski, M. R. Bockstaller and G. Fytas, "A new class of tunable hypersonic phononic crystals based on polymer-tethered colloids", *Nature Communications*, Vol. 6, No. 8309, pp. 1–8, 2015.

38. Yilmaz, C., G. M. Hulbert and N. Kikuchi, "Phononic band gaps induced by inertial amplification in periodic media", *Physical Review B*, Vol. 76, No. 5, p. 054309, 2007.

39. Yilmaz, C. and G. M. Hulbert, "Theory of phononic gaps induced by inertial amplification in finite structures", *Physics Letters A*, Vol. 374, No. 34, pp. 3576–3584, 2010.

40. Christensen, P. W. and A. Klarbring, *An Introduction to Structural Optimization*, Springer Netherlands, 2009.

41. Bendsoe, M. P., *Optimization of Structural Topology, Shape, and Material*, Springer, Berlin, Heidelberg, 1995.

42. Halkjær, S., O. Sigmund and J. S. Jensen, "Inverse design of phononic crystals by topology optimization", *Zeitschrift für Kristallographie-Crystalline Materials*, Vol. 220, No. 9-10, pp. 895–905, 2005.

43. Rupp, C. J., A. Evgrafov, K. Maute and M. L. Dunn, "Design of phononic materials/structures for surface wave devices using topology optimization", *Structural*

and Multidisciplinary Optimization, Vol. 34, No. 2, pp. 111–121, 2007.

44. Dahl, J., J. S. Jensen and O. Sigmund, "Topology optimization for transient wave propagation problems in one dimension", *Structural and Multidisciplinary Optimization*, Vol. 36, No. 6, pp. 585–595, 2008.

45. El-Sabbagh, A., W. Akl and A. Baz, "Topology optimization of periodic Mindlin plates", *Finite Elements in Analysis and Design*, Vol. 44, No. 8, pp. 439–449, 2008.

46. Dede, E. M. and G. M. Hulbert, "Topology optimization of structures with integral compliant mechanisms for mid-frequency response", *Structural and Multidisciplinary Optimization*, Vol. 39, No. 1, pp. 29–45, 2009.

47. Søe-Knudsen, A., "Design of stop-band filter by use of curved pipe segments and shape optimization", *Structural and Multidisciplinary Optimization*, Vol. 44, No. 6, pp. 863–874, 2011.

48. Olhoff, N., B. Niu and G. Cheng, "Optimum design of band-gap beam structures", *International Journal of Solids and Structures*, Vol. 49, No. 22, pp. 3158–3169, 2012.

49. Huang, Y., S. Liu and J. Zhao, "Optimal design of two-dimensional band-gap materials for uni-directional wave propagation", *Structural and Multidisciplinary Optimization*, Vol. 48, No. 3, pp. 487–499, 2013.

50. Hashimoto, H., M. G. Kim, K. Abe and S. Cho, "A level set-based shape optimization method for periodic sound barriers composed of elastic scatterers", *Journal of Sound and Vibration*, Vol. 332, No. 21, pp. 5283–5301, 2013.

51. Sigmund, O. and J. S. Jensen, "Systematic design of phononic band–gap materials and structures by topology optimization", *Philosophical Transactions of the Royal Society of London A: Mathematical, Physical and Engineering Sciences*, Vol. 361,

No. 1806, pp. 1001–1019, 2003.

52. Halkjær, S., O. Sigmund and J. S. Jensen, "Maximizing band gaps in plate structures", *Structural and Multidisciplinary Optimization*, Vol. 32, No. 4, pp. 263–275, 2006.

53. Jensen, J. S. and N. L. Pedersen, "On maximal eigenfrequency separation in two-material structures: the 1D and 2D scalar cases", *Journal of Sound and Vibration*, Vol. 289, No. 4-5, pp. 967–986, 2006.

54. Du, J. and N. Olhoff, "Topological design of freely vibrating continuum structures for maximum values of simple and multiple eigenfrequencies and frequency gaps", *Structural and Multidisciplinary Optimization*, Vol. 34, No. 2, pp. 91–110, 2007.

55. Vatanabe, S. L., G. H. Paulino and E. C. N. Silva, "Maximizing phononic band gaps in piezocomposite materials by means of topology optimization", *The Journal of the Acoustical Society of America*, Vol. 136, No. 2, pp. 494–501, 2014.

56. Yilmaz, C. and G. M. Hulbert, "Dynamics of Locally Resonant and Inertially Amplified Lattice Materials", *Dynamics of Lattice Materials*, pp. 233–258, 2017.

57. Taniker, S. and C. Yilmaz, "Inertial amplification induced phononic band gaps in sc and bcc lattices", *Proceedings of the ASME International Mechanical Engineering Congress and Exposition, San Diego, CA, USA*, IMECE2013-62674, p. V014T15A046, 2013.

58. Taniker, S. and C. Yilmaz, "Phononic gaps induced by inertial amplification in BCC and FCC lattices", *Physics Letters A*, Vol. 377, No. 31, pp. 1930–1936, 2013.

59. Frandsen, N. M. M., O. R. Bilal, J. S. Jensen and M. I. Hussein, "Inertial amplification of continuous structures: Large band gaps from small masses", *Journal of Applied Physics*, Vol. 119, No. 12, p. 124902, 2016.

60. Yilmaz, C. and A. H. Orta, "Wide band gaps at low frequencies using inerters", *Proceedings of the 4th International Conference on Phononic Crystals/Metamaterials, Phonon Transport/Coupling and Topological Phononics, Changsha, China*, pp. 198–199, 2017.

61. Acar, G. and C. Yilmaz, "Experimental and numerical evidence for the existence of wide and deep phononic gaps induced by inertial amplification in two-dimensional solid structures", *Journal of Sound and Vibration*, Vol. 332, No. 24, pp. 6389–6404, 2013.

62. Taniker, S. and C. Yilmaz, "Design, analysis and experimental investigation of three-dimensional structures with inertial amplification induced vibration stop bands", *International Journal of Solids and Structures*, Vol. 72, pp. 88–97, 2015.

63. Taniker, S. and C. Yilmaz, "Generating ultra wide vibration stop bands by a novel inertial amplification mechanism topology with flexure hinges", *International Journal of Solids and Structures*, Vol. 106, pp. 129–138, 2017.

64. Ma, Z. D., N. Kikuchi and H. C. Cheng, "Topological design for vibrating structures", *Computer Methods in Applied Mechanics and Engineering*, Vol. 121, No. 1, pp. 259–280, 1995.

65. Kim, T. S. and Y. Y. Kim, "Mac-based mode-tracking in structural topology optimization", *Computers & Structures*, Vol. 74, No. 3, pp. 375–383, 2000.

66. Belblidia, F. and S. Bulman, "Constrained adaptive topology optimization for vibrating shell structures", *Structural and Multidisciplinary Optimization*, Vol. 22, No. 2, pp. 167–176, 2001.

67. Allaire, G. and F. Jouve, "A level-set method for vibration and multiple loads structural optimization", *Computer Methods in Applied Mechanics and Engineering*, Vol. 194, No. 30, pp. 3269–3290, 2005.

68. De Gournay, F., "Velocity extension for the level-set method and multiple eigenvalues in shape optimization", *SIAM Journal on Control and Optimization*, Vol. 45, No. 1, pp. 343–367, 2006.

69. Niu, B., J. Yan and G. Cheng, "Optimum structure with homogeneous optimum cellular material for maximum fundamental frequency", *Structural and Multidisciplinary Optimization*, Vol. 39, No. 2, pp. 115–132, 2009.

70. Takezawa, A., S. Nishiwaki and M. Kitamura, "Shape and topology optimization based on the phase field method and sensitivity analysis", *Journal of Computational Physics*, Vol. 229, No. 7, pp. 2697–2718, 2010.

71. Huang, X., Z. H. Zuo and Y. M. Xie, "Evolutionary topological optimization of vibrating continuum structures for natural frequencies", *Computers & Structures*, Vol. 88, No. 5, pp. 357–364, 2010.

72. Xia, Q., T. Shi and M. Y. Wang, "A level set based shape and topology optimization method for maximizing the simple or repeated first eigenvalue of structure vibration", *Structural and Multidisciplinary Optimization*, Vol. 43, No. 4, pp. 473–485, 2011.

73. Bruggi, M. and A. Taliercio, "Maximization of the fundamental eigenfrequency of micropolar solids through topology optimization", *Structural and Multidisciplinary Optimization*, Vol. 46, No. 4, pp. 549–560, 2012.

74. Zheng, J., S. Long and G. Li, "Topology optimization of free vibrating continuum structures based on the element free Galerkin method", *Structural and Multidisciplinary Optimization*, Vol. 45, No. 1, pp. 119–127, 2012.

75. Tsai, T. D. and C. C. Cheng, "Structural design for desired eigenfrequencies and mode shapes using topology optimization", *Structural and Multidisciplinary Optimization*, Vol. 47, No. 5, pp. 673–686, 2013.

76. Zhou, K., "Topology optimization of truss-like continuum structures for natural frequencies", *Structural and Multidisciplinary Optimization*, Vol. 47, No. 4, pp. 613–619, 2013.

77. Kim, H. G., S. H. Park and M. Cho, "Structural topology optimization based on system condensation", *Finite Elements in Analysis and Design*, Vol. 92, pp. 26–35, 2014.

78. Liu, T., B. Li, S. Wang and L. Gao, "Eigenvalue topology optimization of structures using a parameterized level set method", *Structural and Multidisciplinary Optimization*, Vol. 50, No. 4, pp. 573–591, 2014.

79. Su, W. and S. Liu, "Topology design for maximization of fundamental frequency of couple-stress continuum", *Structural and Multidisciplinary Optimization*, Vol. 53, No. 3, pp. 395–408, 2016.

80. Yang, Y., M. Zhu, M. D. Shields and J. K. Guest, "Topology optimization of continuum structures subjected to filtered white noise stochastic excitations", *Computer Methods in Applied Mechanics and Engineering*, Vol. 324, pp. 438–456, 2017.

81. Yilmaz, C. and N. Kikuchi, "Analysis and design of passive low-pass filter-type vibration isolators considering stiffness and mass limitations", *Journal of Sound and Vibration*, Vol. 293, No. 1–2, pp. 171–195, 2006.

82. Yilmaz, C. and N. Kikuchi, "Analysis and design of passive band-stop filter-type vibration isolators for low-frequency applications", *Journal of Sound and Vibration*, Vol. 291, No. 3–5, pp. 1004–1028, 2006.

83. Miller, R. E., "Dynamic aspects of the error in eccentric beam modelling", *International Journal for Numerical Methods in Engineering*, Vol. 15, No. 10, pp. 1447–1455, 1980.

84. Petyt, M., *Introduction to Finite Element Vibration Analysis*, Cambridge University Press, 2010.

85. McConnell, K. G., *Vibration Testing: Theory and Practice*, John Wiley & Sons, 1995.

86. Bendsøe, M. P. and O. Sigmund, *Topology Optimization: Theory, Methods, and Applications*, Springer Berlin Heidelberg, 2004.

87. Rozvany, G. I. N., *Topology Optimization in Structural Mechanics*, Springer, 2014.

88. Eschenauer, H. A. and N. Olhoff, "Topology optimization of continuum structures: A review", *Applied Mechanics Reviews*, Vol. 54, No. 4, pp. 331–390, 2001.

89. Rozvany, G. I. N., M. P. Bendsoe and U. Kirsch, "Layout optimization of structures", *Applied Mechanics Reviews*, Vol. 48, No. 2, pp. 41–119, 1995.

90. Sigmund, O. and K. Maute, "Topology optimization approaches", *Structural and Multidisciplinary Optimization*, Vol. 48, No. 6, pp. 1031–1055, 2013.

91. Michell, A. G. M., "LVIII. The limits of economy of material in frame-structures", *The London, Edinburgh, and Dublin Philosophical Magazine and Journal of Science*, Vol. 8, No. 47, pp. 589–597, 1904.

92. Hemp, W. S., *Optimum Structures*, Clarendon Press, 1973.

93. Munk, D. J., G. A. Vio and G. P. Steven, "Topology and shape optimization methods using evolutionary algorithms: a review", *Structural and Multidisciplinary Optimization*, Vol. 52, No. 3, pp. 613–631, 2015.

94. Kirsch, U., *Optimum Structural Design: Concepts, Methods, and Applications*, McGraw-Hill Companies, 1981.

95. Kirsch, U., "Optimal topologies of structures", *Applied Mechanics Reviews*,

Vol. 42, No. 8, pp. 223–239, 1989.

96. Rozvany, G. I. N., "Aims, scope, methods, history and unified terminology of computer-aided topology optimization in structural mechanics", *Structural and Multidisciplinary Optimization*, Vol. 21, No. 2, pp. 90–108, 2001.

97. Deaton, J. D. and R. V. Grandhi, "A survey of structural and multidisciplinary continuum topology optimization: Post 2000", *Structural and Multidisciplinary Optimization*, Vol. 49, No. 1, pp. 1–38, 2014.

98. Hassani, B. and E. Hinton, "A review of homogenization and topology opimization II — Analytical and numerical solution of homogenization equations", *Computers & Structures*, Vol. 69, No. 6, pp. 719–738, 1998.

99. Hassani, B. and E. Hinton, "A review of homogenization and topology optimization I — Homogenization theory for media with periodic structure", *Computers & Structures*, Vol. 69, No. 6, pp. 707–717, 1998.

100. Bendsøe, M. P. and N. Kikuchi, "Generating optimal topologies in structural design using a homogenization method", *Computer Methods in Applied Mechanics and Engineering*, Vol. 71, No. 2, pp. 197–224, 1988.

101. Suzuki, K. and N. Kikuchi, "A homogenization method for shape and topology optimization", *Computer Methods in Applied Mechanics and Engineering*, Vol. 93, No. 3, pp. 291–318, 1991.

102. Hassani, B. and E. Hinton, *Homogenization and Structural Topology Optimization*, Springer-Verlag London, 1999.

103. Bendsøe, M. P., "Optimal shape design as a material distribution problem", *Structural Optimization*, Vol. 1, No. 4, pp. 193–202, 1989.

104. Rozvany, G. I. N., M. Zhou and T. Birker, "Generalized shape optimization

without homogenization", *Structural Optimization*, Vol. 4, No. 3, pp. 250–252, 1992.

105. Stolpe, M. and K. Svanberg, "An alternative interpolation scheme for minimum compliance topology optimization", *Structural and Multidisciplinary Optimization*, Vol. 22, No. 2, pp. 116–124, 2001.

106. Schittkowski, K., C. Zillober and R. Zotemantel, "Numerical comparison of nonlinear programming algorithms for structural optimization", *Structural Optimization*, Vol. 7, No. 1-2, pp. 1–19, 1994.

107. Sigmund, O., "On the usefulness of non-gradient approaches in topology optimization", *Structural and Multidisciplinary Optimization*, Vol. 43, No. 5, pp. 589–596, 2011.

108. Huang, X. and M. Xie, *Evolutionary Topology Optimization of Continuum Structures: Methods and Applications*, John Wiley & Sons, 2010.

109. Xie, Y. M. and G. P. Steven, "A simple evolutionary procedure for structural optimization", *Computers & Structures*, Vol. 49, No. 5, pp. 885–896, 1993.

110. Querin, O. M., G. P. Steven and Y. M. Xie, "Evolutionary structural optimisation (ESO) using a bidirectional algorithm", *Engineering Computations*, Vol. 15, No. 8, pp. 1031–1048, 1998.

111. Rozvany, G. I. N., "A critical review of established methods of structural topology optimization", *Structural and Multidisciplinary Optimization*, Vol. 37, No. 3, pp. 217–237, 2009.

112. Rozvany, G. I. N., "Stress ratio and compliance based methods in topology optimization–a critical review", *Structural and Multidisciplinary Optimization*, Vol. 21, No. 2, pp. 109–119, 2001.

113. Zhou, M. and G. I. N. Rozvany, "On the validity of ESO type methods in topology optimization", *Structural and Multidisciplinary Optimization*, Vol. 21, No. 1, pp. 80–83, 2001.

114. Huang, X. and Y. M. Xie, "Bi-directional evolutionary topology optimization of continuum structures with one or multiple materials", *Computational Mechanics*, Vol. 43, No. 3, pp. 393–401, 2009.

115. Huang, X. and Y. M. Xie, "A further review of ESO type methods for topology optimization", *Structural and Multidisciplinary Optimization*, Vol. 41, No. 5, pp. 671–683, 2010.

116. Sethian, J. A., *Level Set Methods and Fast Marching Methods: Evolving Interfaces in Computational Geometry, Fluid Mechanics, Computer Vision, and Materials Science*, Vol. 3, Cambridge University Press, 1999.

117. Wang, M. Y., X. Wang and D. Guo, "A level set method for structural topology optimization", *Computer Methods in Applied Mechanics and Engineering*, Vol. 192, No. 1, pp. 227–246, 2003.

118. Allaire, G., F. Jouve and A. M. Toader, "Structural optimization using sensitivity analysis and a level-set method", *Journal of Computational Physics*, Vol. 194, No. 1, pp. 363–393, 2004.

119. Van Dijk, N. P., K. Maute, M. Langelaar and F. Van Keulen, "Level-set methods for structural topology optimization: a review", *Structural and Multidisciplinary Optimization*, Vol. 48, No. 3, pp. 437–472, 2013.

120. Bendsøe, M. P. and O. Sigmund, "Material interpolation schemes in topology optimization", *Archive of Applied Mechanics*, Vol. 69, No. 9-10, pp. 635–654, 1999.

121. Sigmund, O. and J. Petersson, "Numerical instabilities in topology optimization:

a survey on procedures dealing with checkerboards, mesh-dependencies and local minima", *Structural Optimization*, Vol. 16, No. 1, pp. 68–75, 1998.

122. Diaz, A. and O. Sigmund, "Checkerboard patterns in layout optimization", *Structural Optimization*, Vol. 10, No. 1, pp. 40–45, 1995.

123. Sigmund, O., "Manufacturing tolerant topology optimization", *Acta Mechanica Sinica*, Vol. 25, No. 2, pp. 227–239, 2009.

124. Xu, S., Y. Cai and G. Cheng, "Volume preserving nonlinear density filter based on heaviside functions", *Structural and Multidisciplinary Optimization*, Vol. 41, No. 4, pp. 495–505, 2010.

125. Lazarov, B. S. and O. Sigmund, "Filters in topology optimization based on Helmholtz-type differential equations", *International Journal for Numerical Methods in Engineering*, Vol. 86, No. 6, pp. 765–781, 2011.

126. Wang, F., B. S. Lazarov and O. Sigmund, "On projection methods, convergence and robust formulations in topology optimization", *Structural and Multidisciplinary Optimization*, Vol. 43, No. 6, pp. 767–784, 2011.

127. Schevenels, M., B. S. Lazarov and O. Sigmund, "Robust topology optimization accounting for spatially varying manufacturing errors", *Computer Methods in Applied Mechanics and Engineering*, Vol. 200, No. 49, pp. 3613–3627, 2011.

128. Sigmund, O., "On the design of compliant mechanisms using topology optimization", *Mechanics of Structures and Machines*, Vol. 25, No. 4, pp. 493–524, 1997.

129. Sigmund, O. and K. Maute, "Sensitivity filtering from a continuum mechanics perspective", *Structural and Multidisciplinary Optimization*, Vol. 46, No. 4, pp. 471–475, 2012.

130. Bourdin, B., "Filters in topology optimization", *International Journal for Nu-*

merical Methods in Engineering, Vol. 50, No. 9, pp. 2143–2158, 2001.

131. Sigmund, O., "Morphology-based black and white filters for topology optimization", *Structural and Multidisciplinary Optimization*, Vol. 33, No. 4, pp. 401–424, 2007.

132. Andreassen, E., A. Clausen, M. Schevenels, B. S. Lazarov and O. Sigmund, "Efficient topology optimization in MATLAB using 88 lines of code", *Structural and Multidisciplinary Optimization*, Vol. 43, No. 1, pp. 1–16, 2011.

133. Sigmund, O., "A 99 line topology optimization code written in MATLAB", *Structural and Multidisciplinary Optimization*, Vol. 21, No. 2, pp. 120–127, 2001.

134. Liu, K. and A. Tovar, "An efficient 3D topology optimization code written in Matlab", *Structural and Multidisciplinary Optimization*, Vol. 50, No. 6, pp. 1175–1196, 2014.

135. Tcherniak, D. and O. Sigmund, "A web-based topology optimization program", *Structural and Multidisciplinary Optimization*, Vol. 22, No. 3, pp. 179–187, 2001.

136. Aage, N., M. Nobel-Jørgensen, C. S. Andreasen and O. Sigmund, "Interactive topology optimization on hand-held devices", *Structural and Multidisciplinary Optimization*, Vol. 47, No. 1, pp. 1–6, 2013.

137. Nobel-Jørgensen, M., N. Aage, A. N. Christiansen, T. Igarashi, J. A. Bærentzen and O. Sigmund, "3D interactive topology optimization on hand-held devices", *Structural and Multidisciplinary Optimization*, Vol. 51, No. 6, pp. 1385–1391, 2015.

138. Zargham, S., T. A. Ward, R. Ramli and I. A. Badruddin, "Topology optimization: A review for structural designs under vibration problems", *Structural and Multidisciplinary Optimization*, Vol. 53, No. 6, pp. 1157–1177, 2016.

139. Rojas-Labanda, S. and M. Stolpe, "Benchmarking optimization solvers for structural topology optimization", *Structural and Multidisciplinary Optimization*, Vol. 52, No. 3, pp. 527–547, 2015.

140. Bendsoe, M., E. Lund, N. Olhoff and O. Sigmund, "Topology optimization-broadening the areas of application", *Control and Cybernetics*, Vol. 34, No. 1, p. 7, 2005.

141. Hassani, B. and E. Hinton, "A review of homogenization and topology optimization III - Topology optimization using optimality criteria", *Computers & Structures*, Vol. 69, No. 6, pp. 739–756, 1998.

142. Tortorelli, D. A. and P. Michaleris, "Design sensitivity analysis: Overview and review", *Inverse Problems in Engineering*, Vol. 1, No. 1, pp. 71–105, 1994.

143. Hammer, V. B. and N. Olhoff, "Topology optimization of continuum structures subjected to pressure loading", *Structural and Multidisciplinary Optimization*, Vol. 19, No. 2, pp. 85–92, 2000.

144. Du, J. and N. Olhoff, "Topological optimization of continuum structures with design-dependent surface loading–Part I: New computational approach for 2D problems", *Structural and Multidisciplinary Optimization*, Vol. 27, No. 3, pp. 151–165, 2004.

145. Venkayya, V. B., "Optimality criteria: A basis for multidisciplinary design optimization", *Computational Mechanics*, Vol. 5, No. 1, pp. 1–21, 1989.

146. Zhou, M. and G. I. N. Rozvany, "The COC algorithm, Part II: Topological, geometrical and generalized shape optimization", *Computer Methods in Applied Mechanics and Engineering*, Vol. 89, No. 1-3, pp. 309–336, 1991.

147. Patnaik, S. N., J. D. Guptill and L. Berke, "Merits and limitations of optimality criteria method for structural optimization", *International Journal for Numerical*

Methods in Engineering, Vol. 38, No. 18, pp. 3087–3120, 1995.

148. Vemaganti, K. and W. E. Lawrence, "Parallel methods for optimality criteria-based topology optimization", *Computer Methods in Applied Mechanics and Engineering*, Vol. 194, No. 34, pp. 3637–3667, 2005.

149. Belegundu, A. D., "A general optimality criteria algorithm for a class of engineering optimization problems", *Engineering Optimization*, Vol. 47, No. 5, pp. 674–688, 2015.

150. Shang, L. and G. Zhao, "Optimality criteria-based topology optimization of a bi-material model for acoustic–structural coupled systems", *Engineering Optimization*, Vol. 48, No. 6, pp. 1060–1079, 2016.

151. Li, H., L. Gao and P. Li, "Topology optimization of structures under multiple loading cases with a new compliance–volume product", *Engineering Optimization*, Vol. 46, No. 6, pp. 725–744, 2014.

152. Cai, K., Z. Gao and J. Shi, "Topology optimization of continuum structures with bi-modulus materials", *Engineering Optimization*, Vol. 46, No. 2, pp. 244–260, 2014.

153. Venkayya, V. B., "Structural optimization: A review and some recommendations", *International Journal for Numerical Methods in Engineering*, Vol. 13, No. 2, pp. 203–228, 1978.

154. Haftka, R. T. and Z. Gurdal, *Elements of Structural Optimization*, Springer Netherlands, 1992.

155. Ma, Z. D., N. Kikuchi and I. Hagiwara, "Structural topology and shape optimization for a frequency response problem", *Computational Mechanics*, Vol. 13, No. 3, pp. 157–174, 1993.

156. Pedersen, N. L., "Maximization of eigenvalues using topology optimization", *Structural and Multidisciplinary Optimization*, Vol. 20, No. 1, pp. 2–11, 2000.

157. Tcherniak, D., "Topology optimization of resonating structures using SIMP method", *International Journal for Numerical Methods in Engineering*, Vol. 54, No. 11, pp. 1605–1622, 2002.

158. Seyranian, A. P., E. Lund and N. Olhoff, "Multiple eigenvalues in structural optimization problems", *Structural Optimization*, Vol. 8, No. 4, pp. 207–227, 1994.

159. Deymier, P. A., *Acoustic Metamaterials and Phononic Crystals*, Springer Berlin Heidelberg, 2013.

160. Svanberg, K., "The method of moving asymptotes – A new method for structural optimization", *International Journal for Numerical Methods in Engineering*, Vol. 24, No. 2, pp. 359–373, 1987.

161. Fleury, C., "CONLIN: An efficient dual optimizer based on convex approximation concepts", *Structural Optimization*, Vol. 1, No. 2, pp. 81–89, 1989.

162. Svanberg, K., "A class of globally convergent optimization methods based on conservative convex separable approximations", *SIAM Journal on Optimization*, Vol. 12, No. 2, pp. 555–573, 2002.

163. Kočvara, M. and M. Stingl, "PENNON: A code for convex nonlinear and semidefinite programming", *Optimization Methods and Software*, Vol. 18, No. 3, pp. 317–333, 2003.

164. Gill, P. E., W. Murray and M. A. Saunders, "SNOPT: An SQP algorithm for large-scale constrained optimization", *SIAM Review*, Vol. 47, No. 1, pp. 99–131, 2005.

165. Wächter, A. and L. T. Biegler, "On the implementation of an interior-point fil-

ter line-search algorithm for large-scale nonlinear programming", *Mathematical Programming*, Vol. 106, No. 1, pp. 25–57, 2006.

166. Olhoff, N., M. P. Bendsøe and J. Rasmussen, "On CAD-integrated structural topology and design optimization", *Computer Methods in Applied Mechanics and Engineering*, Vol. 89, No. 1-3, pp. 259–279, 1991.

167. Díaz, A. R. and N. Kikuchi, "Solutions to shape and topology eigenvalue optimization problems using a homogenization method", *International Journal for Numerical Methods in Engineering*, Vol. 35, No. 7, pp. 1487–1502, 1992.

168. Ma, Z. D., H. C. Cheng and N. Kikuchi, "Structural design for obtaining desired eigenfrequencies by using the topology and shape optimization method", *Computing Systems in Engineering*, Vol. 5, No. 1, pp. 77–89, 1994.

169. Xie, Y. M. and G. P. Steven, "A simple approach to structural frequency optimization", *Computers & Structures*, Vol. 53, No. 6, pp. 1487–1491, 1994.

170. Jog, C. S., "Topology design of structures subjected to periodic loading", *Journal of Sound and Vibration*, Vol. 253, No. 3, pp. 687–709, 2002.

171. Achtziger, W. and M. Kočvara, "On the maximization of the fundamental eigenvalue in topology optimization", *Structural and Multidisciplinary Optimization*, Vol. 34, No. 3, pp. 181–195, 2007.

172. Dühring, M. B., J. S. Jensen and O. Sigmund, "Acoustic design by topology optimization", *Journal of Sound and Vibration*, Vol. 317, No. 3, pp. 557–575, 2008.

173. Jensen, J. S., "Space–time topology optimization for one-dimensional wave propagation", *Computer Methods in Applied Mechanics and Engineering*, Vol. 198, No. 5, pp. 705–715, 2009.

174. Yamamoto, T., S. Maruyama, S. Nishiwaki and M. Yoshimura, "Topology design of multi-material soundproof structures including poroelastic media to minimize sound pressure levels", *Computer Methods in Applied Mechanics and Engineering*, Vol. 198, No. 17, pp. 1439–1455, 2009.

175. Zuo, Z. H., Y. M. Xie and X. Huang, "Optimal topological design of periodic structures for natural frequencies", *Journal of Structural Engineering*, Vol. 137, No. 10, pp. 1229–1240, 2011.

176. Shu, L., M. Y. Wang and Z. Ma, "Level set based topology optimization of vibrating structures for coupled acoustic–structural dynamics", *Computers & Structures*, Vol. 132, pp. 34–42, 2014.

177. Jung, J., J. Hyun, S. Goo and S. Wang, "An efficient design sensitivity analysis using element energies for topology optimization of a frequency response problem", *Computer Methods in Applied Mechanics and Engineering*, Vol. 296, pp. 196–210, 2015.

178. Lee, H. A. and G. J. Park, "Nonlinear dynamic response topology optimization using the equivalent static loads method", *Computer Methods in Applied Mechanics and Engineering*, Vol. 283, pp. 956–970, 2015.

179. Meirovitch, L., *Fundamentals of Vibrations*, McGraw-Hill, 2001.

180. Chen, B. C. and N. Kikuchi, "Topology optimization with design-dependent loads", *Finite Elements in Analysis and Design*, Vol. 37, No. 1, pp. 57–70, 2001.

181. Bruns, T. E., "Topology optimization by penalty (TOP) method", *Computer Methods in Applied Mechanics and Engineering*, Vol. 196, No. 45, pp. 4430–4443, 2007.

182. Zhang, H., X. Zhang and S. Liu, "A new boundary search scheme for topology optimization of continuum structures with design-dependent loads", *Structural*

and Multidisciplinary Optimization, Vol. 37, No. 2, pp. 121–129, 2008.

183. Huang, X. and Y. M. Xie, "Evolutionary topology optimization of continuum structures including design-dependent self-weight loads", *Finite Elements in Analysis and Design*, Vol. 47, No. 8, pp. 942–948, 2011.

184. Lee, E. and J. R. R. A. Martins, "Structural topology optimization with design-dependent pressure loads", *Computer Methods in Applied Mechanics and Engineering*, Vol. 233–236, pp. 40–48, 2012.

185. Lee, E., K. A. James and J. R. R. A. Martins, "Stress-constrained topology optimization with design-dependent loading", *Structural and Multidisciplinary Optimization*, Vol. 46, No. 5, pp. 647–661, 2012.

186. Picelli, R., W. M. Vicente and R. Pavanello, "Bi-directional evolutionary structural optimization for design-dependent fluid pressure loading problems", *Engineering Optimization*, Vol. 47, No. 10, pp. 1324–1342, 2015.

187. Wang, C., M. Zhao and T. Ge, "Structural topology optimization with design-dependent pressure loads", *Structural and Multidisciplinary Optimization*, Vol. 53, No. 5, pp. 1005–1018, 2016.

188. Zhang, W., L. Zhao and T. Gao, "CBS-based topology optimization including design-dependent body loads", *Computer Methods in Applied Mechanics and Engineering*, Vol. 322, pp. 1–22, 2017.

189. Sorensen, D. C., "Implicitly restarted Arnoldi/Lanczos methods for large scale eigenvalue calculations", *Parallel Numerical Algorithms*, pp. 119–165, 1997.

190. Lehoucq, R. B., D. C. Sorensen and C. Yang, *ARPACK Users' Guide: Solution of Large-Scale Eigenvalue Problems With Implicitly Restarted Arnoldi Methods*, Society for Industrial and Applied Mathematics, 1998.

191. Allemang, R. J. and D. L. Brown, "A correlation coefficient for modal vector analysis", *Proceedings of the 1st International Modal Analysis Conference*, Vol. 1, pp. 110–116, SEM, Orlando, 1982.

192. Allemang, R. J., "The modal assurance criterion–twenty years of use and abuse", *Sound and Vibration*, Vol. 37, No. 8, pp. 14–23, 2003.

193. Yuksel, O. and C. Yilmaz, "Shape optimization of phononic band gap structures incorporating inertial amplification mechanisms", *Journal of Sound and Vibration*, Vol. 355, pp. 232–245, 2015.

194. Yuksel, O. and C. Yilmaz, "Obtaining inertial amplification induced phononic gaps via structural optimization of a compliant mechanism", *11th International Conference on Vibration Problems, Lisbon, Portugal*, pp. 1–10, 2013.

195. Yüksel, O. and Ç. Yılmaz, "Esnek bağlantılı atalet artırımı mekanizmasının titreşim yalıtımı frekans aralığının topoloji eniyilemesi ile genişletilmesi", *18. Ulusal Makina Teorisi Sempozyumu, Trabzon, Türkiye*, pp. 343–349, 2017.

196. Yuksel, O. and C. Yilmaz, "Size and topology optimization of inertial amplification induced phononic band gap structures", *Proceedings of the ASME International Mechanical Engineering Congress and Exposition, Tampa, Florida, USA*, IMECE2017-71342, p. V013T01A007, 2017.

197. Yuksel, O. and C. Yilmaz, "Active noise control in a duct with flow", *Journal of Dynamic Systems, Measurement, and Control*, Vol. 136, No. 3, p. 031014, 2014.